



Sergey Fedosov
Alexandra Sergeeva

Formation and relaxation of polarized state in ferroelectric polymers

Physical properties of polymer dielectrics

 **LAMBERT**
Academic Publishing

Sergey Fedosov
Alexandra Sergeeva

Formation and relaxation of the polarized state in ferroelectric polymers

2020

CONTENT

Introduction

Chapter 1. Important characteristics of ferroelectric polymers

- 1.1 Structure and physical properties of PVDF and its copolymers
- 1.2 Brief description of the studied materials
- 1.3 Effective conductivity of PVDF films
- 1.4 Calculation of the dielectric permittivity in PVDF
- 1.5 Methods of ferroelectric polymer films poling
- 1.6 Application of ferroelectric polymers

Chapter 2. Formation of polarized state in ferroelectric polymers

- 2.1 Transfer of charge and formation of polarization in FPs
- 2.2 Method of quasi-stationary volt-ampere characteristics measuring
- 2.3 Volt-ampere characteristics of PVDF films
- 2.4 Electric displacement during constant voltage poling
- 2.5 Isothermal kinetics of the electret potential in PVDF films
- 2.6 Phenomenological model of constant charge poling of FPs

Chapter 3. Switching of polarization in ferroelectric polymers

- 3.1 Method of studying the ferroelectric polarization switching
- 3.2 Switching of the ferroelectric polarization in PVDF
- 3.3 Features of polarization switching in copolymers
- 3.4 Model of the polarization switching in PVDF at a constant voltage

Chapter 4. Polarization profiles in ferroelectric polymers

- 4.1 Distribution of polarization along the thickness of FPs films
- 4.2 Methodology for studying polarization profiles in FPs
- 4.3 Spatial distribution of polarization in PVDF films
 - 4.3.1 Polarization profile dynamics: poling and switching in middle fields
 - 4.3.2 Impossibility to completely switch non-uniformly polarized FPs
 - 4.3.3 Polarization profile dynamics: poling and switching in high fields
- 4.4 Model of the polarization profile formation at constant voltage poling
- 4.5 Polarization profiles in P(VDF-TFE) films poled in corona discharge
- 4.6 Thermal stability of polarization in P(VDF-TFE) copolymer

Chapter 5. Thermally stimulated processes in ferropolymers

- 5.1 Thermally stimulated depolarization (TSD) of ferropolymers
- 5.2 Thermally stimulated depolarization current spectroscopy
- 5.3 Homocharge and heterocharge relaxation and TSD currents
- 5.4 Thermoelectret poling of PVDF and P(VDF-TFE) films
- 5.5 Thermally stimulated depolarization currents in PVDF
- 5.6 Separation of TSD current components in PVDF
- 5.7 Isothermal and thermally stimulated processes in composites

Chapter 6. Pyroelectric effect in ferroelectric polymers

- 6.1 Nature of the pyroelectricity in ferroelectric polymers
- 6.2 Method for measuring the pyroelectric coefficient
- 6.3 Pyroelectric activity of PVDF and switching of polarization
- 6.4 Pyroelectric activity of composites based on PVDF

Conclusion

References

Introduction

Ferroelectric polymers and composites on their basis have prospects of widespread application in electronic devices such as electroacoustic transducers, pressure and temperature sensors, and various detectors. Despite the fact that many devices based on ferroelectric polymers have already been implemented, there are questions that remain unanswered. For introduction of the ferroelectric polymers into industrial technology it is necessary to increase the reliability and stability of the electrophysical properties of these materials. Namely to these questions this book is devoted.

Typical ferroelectric polymers are polyvinylidene fluoride (PVDF) and its copolymers with tetrafluoroethylene P(VDF-TFE) and trifluoroethylene P(VDF-TrFE), which exhibit ferroelectric, piezoelectric and pyroelectric properties after a certain processing. Among the main advantages of such materials is the high value of piezoelectric and pyroelectric modules, which makes it possible for their practical application. Another valuable quality that is difficult to implement in inorganic materials is the wide range of frequencies, in which the active element created on the basis of PVDF can work. The possibility of using large areas and relatively simple methods of making thin films included PVDF into a category of promising materials for creation of new classes of recording devices. The flexibility of PVDF films and their acoustic impedance, close to the impedance of biological tissue and water, put PVDF and its copolymers out of competition in comparison with other materials in the development of various kinds of medical sensors.

In contrast to conventional polymers and crystalline ferroelectrics, the properties of ferroelectric polymers differ substantially due to the presence of the amorphous phase along with crystallites. Despite a fairly large number of papers, the question of the interrelation between polarization in ferroelectric polymers and space charge is still open and requires additional research.

The distribution of polarization in the thickness direction of polymer films with ferroelectric properties plays an important role in their behavior when they used in pyro and piezoelectric converters, but despite the large amount of actual material, this phenomenon has not been systematically studied. There are still unexplained reasons for appearance of heterogeneous polarization and reliable ways to increase it is not known. Very little is known about the dynamics of the polarization profile formation, which can

be studied only with the use of measurements directly in the process of films poling.

The thermally stimulated depolarization (TSD) of ferroelectric polymers, as shown by the analysis of numerical published data, can give important information about the relaxation of the polarized state, but because of the absence of the TSD currents theory for ferroelectric polymers, the interpretation of the obtained data is very arbitrary. In addition, the possibilities of the TSD method are not fully utilized. In particular, such modification as using of the dielectric insert is rarely applied. There is no reliable method for allocating the contribution of the homocharge and heterocharge relaxation to the measured TSD current. Modes of thermoelectret poling and the method of thermal windows are rarely used. Practically there are no papers on the separate effect of crystalline and amorphous phases on the TSD currents.

The analysis of available literature shows that the study of the pyroelectric effect in ferroelectric polymers, besides the important for practical application of data on the magnitude and stability of pyrocoefficients, provides an opportunity to study the important characteristics of the polarized state. Particularly promising is the study of pyroelectricity in parallel with the study of the formation and relaxation of the polarized state, as well as with other isothermal and thermally stimulated processes. These possibilities are not fully utilized.

Regarding the pyroactivity of composites based on PVDF, there are very few literature data on this subject, despite its scientific and practical importance, since the main promising field for using of such composites is just pyro- and piezoelectric converters. Unfortunately, very little attention was paid to the study of the commonality of the physical nature of many phenomena in ferroelectric polymers and in composites. This is related in the first place to the influence of the non-ferroelectric phase in these groups of materials on formation and relaxation of the polarized state, on the mechanism of the depolarizing field appearance during poling and the possibility of its effective neutralization.

It is known that application of ferroelectric polymers and composites is already extremely wide. At the same time, their wider application in production of new types of sensors and transducers is hampered by insufficient knowledge of the potential capabilities of these materials, which can become clearer only after understanding the mechanism of formation and relaxation of the polarized state. It is this knowledge that allows predicting and obtaining high values of the ferroelectric polarization needed for

production of pyro- and piezoelectric devices with high temporal and temperature stability and the expanded range of operating frequencies and temperatures.

At present, along with detailed research on the structure of ferroelectric polymers and their widespread use, there is no clarity in the understanding of important processes of the polarized state formation and its electrical relaxation, as well as the relationship between this relaxation and pyro- and piezoelectric effects. Peculiarities of the thermoelectret poling and depolarization of ferroelectric polymers and composites, in particular poled in a corona discharge, are insufficiently studied. This applies both to the measurement methodology and to the interpretation of the results.

The purpose of the research, which formed the basis of this book, was to establish mechanisms of the polarized state formation, as well as its relaxation in PVDF and its copolymer with tetrafluoroethylene P(VDF-TFE) and in composites based on them. The regularities of the polarization formation processes and its relaxation were studied by measuring the electret potential kinetics during poling of the films and after its completion, as well as by measuring the absorption and thermoelectret poling and depolarization currents.

The method of volt-ampere characteristics was used to detect the charge transfer mechanism. Parameters of relaxation processes were studied by carrying out fractional poling followed by the thermally stimulated depolarization. To study the pyroactivity, quasistatic and dynamic methods were used. The distribution of polarization and space charge over the film thickness was studied mainly by the piezoelectrically generated pressure step (PPS) method.

The main experimental studies were carried out on PVDF films, as the most typical ferroelectric polymer, and two types of the films were investigated: uniaxially and biaxially oriented.

Part of the research was carried out on films of a copolymer of vinylidene fluoride with tetrafluoroethylene P(VDF-TFE). As a charging method, a corona triode with a vibrating control grid was mainly used. Samples of PVDF-PZT and PVDF-BaTiO₃ composites were also prepared and investigated.

The obtained scientific results allow formulating practical recommendations on optimal parameters of ferroelectric polymer films poling, which provide for high and stable residual polarization.

Chapter 1. Important characteristics of ferroelectric polymers

1.1. Structure and physical properties of PVDF and its copolymers

Polyvinylidene fluoride (PVDF) is a linear polymer having the chemical formula $(\text{CH}_2\text{-CF}_2)_n$. The PVDF molecules consist of 10^3 - 10^4 repeating elementary $(-\text{CH}_2\text{-CF}_2-)$ cells corresponding to the molecular weight of 10^5 - 10^6 amu.

PVDF and copolymers are semi-crystalline materials, that is, they contain an amorphous phase and scattered crystallites in it. The amorphous phase at room temperature is in the liquid-viscous state, since the glass transition temperature T_g is about minus 40-50 °C. When the melt is cooled, some molecular chains formed crystals (lamellae), in which the macromolecular chains are zigzag-shaped, since the chains are repeatedly composed with one macromolecule passing through both the crystalline and the amorphous phase [121].

Crystallites are brick-like blocks located parallel to the direction of mechanical drawing (1) having 5.9-7.6 nm in the length, 2.5 nm in height and 3.7 nm in thickness. The crystallites are separated by layers (0.4-0.7 nm) of amorphous phases (Fig. 1.1) consisting of 1-3 polymer chains [122].

The macroscopic structure of PVDF is shown in Fig. 1.2 [121]. The polymer chain consists of monomer units $-\text{CH}_2\text{-CF}_2-$, each having a rather large dipole moment $\mu = 7 \cdot 10^{-30}$ C·m (2.1 D) due to the spatially symmetric arrangement of positively charged H atoms and negatively charged F atoms. PVDF is characterized by polymorphism with two basic crystalline α and β phases, which correspond to two types of the polymer chain conformations. In crystallites of the α -phase formed during the crystallization of PVDF from the melt under normal conditions, the chains in the crystallites are stacked antiparallel, so that the total dipole moment of the volume unit is zero, that is, the α -phase is nonpolar.

After the orientational stretching of PVDF or under the influence of a high electric field [27], the nonpolar α -phase is transformed into polar β -phase, in which the polymer chains are in the shape of a flat zigzag (Fig. 1.2). All molecular dipoles along the chain are oriented in one direction, and the chains in the crystallites are stacked parallel to each other. As a result, a highly polar β -phase with spontaneous ferroelectric polarization is formed, so that the direction of polarization can be changed under the

action of the external electric field. The calculation shows that the magnitude of spontaneous polarization in the β -phase of PVDF is $P_o = 130 \text{ mC/m}^2$.

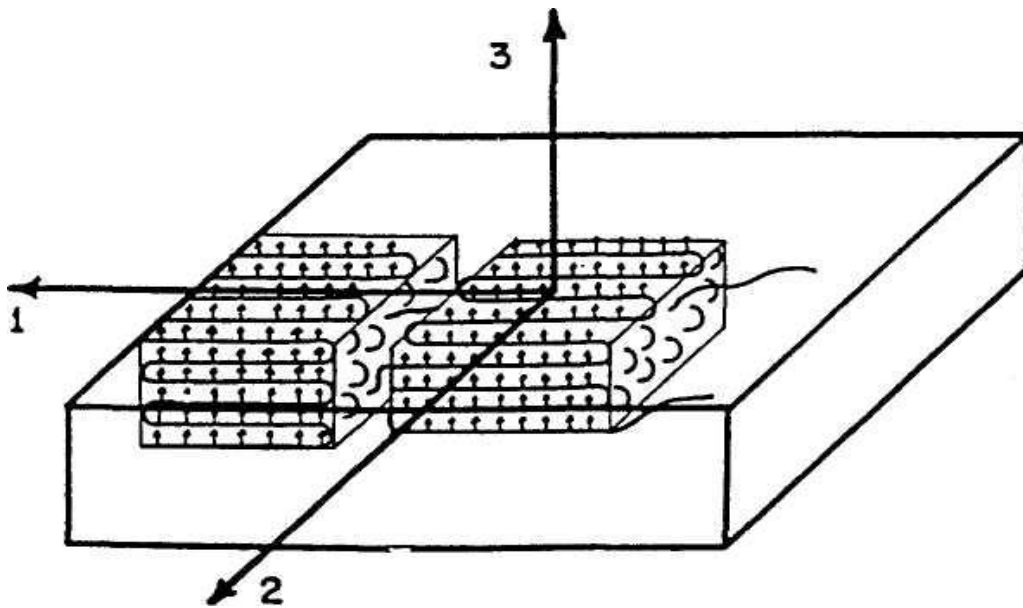


Fig.1.1 The layout of crystallites in a PVDF film. 1 – direction of the orientational stretching, 2 – lateral direction, 3 – axis of the polarization vector

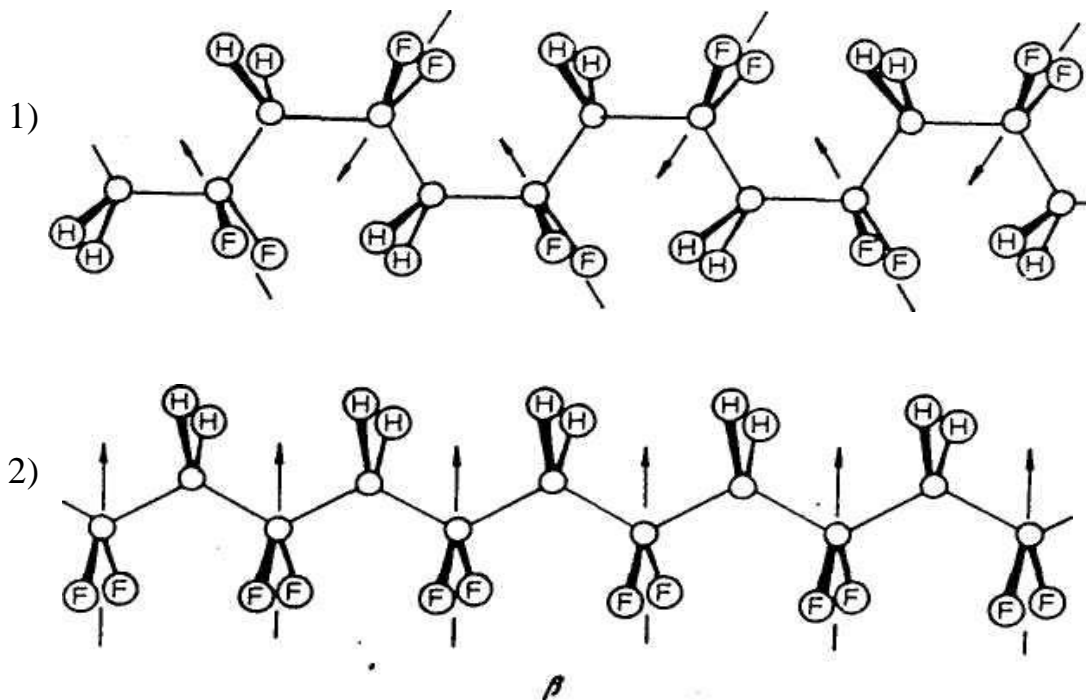


Fig. 1.2 Arrangement of atoms in crystallites α - and β -phases of PVDF

The crystal lattice of the β -phase in the PVDF is orthorhombic but close to the hexagonal [68] with lattice periods $a = 0.885$ nm, $b = 0.791$ nm and $c = 0.256$ nm. In PVDF films, the ratio between α - and β -phases depends on mechanical stretching and heat treatment, as well as on the action of the electric field [188].

Ferroelectric properties of PVDF copolymers with trifluoroethylene P(VDF-TrFE) and tetrafluoroethylene P(VDF-TFE) appear immediately during crystallization from the melt in the polar β -phase, so the requirement in orientation stretching is eliminated.

Some physical properties of PVDF and P(VDF-TFE) are shown in Table. 1.1 [102].

Table 1.1

Physical properties of ferroelectric polymers and crystalline ferroelectrics [102]

Properties	PVDF	P(VDF-TFE)	PZT	BaTiO ₃
Density, kg/m ³	1800	1900	7800	5700
Melting point of crystals, °C	178	134-155		
The modulus of elasticity, GPa	1.3-2.0	1.5-2.5	80	110
Specific heat capacity, kJ/kg·K	1.38	-	0.4	0.5
Specific resistance, 10 ¹¹ Ω·m	0.1-100	1-10 ³	1-10	0.1
Dielectric constant (1 kHz)	8-14	9-11	200-2000	1600
Electrical strength, MW/m	130	100	1-10	10
The dielectric loss tangent (1 kHz)	0.02	0.02	0.005	0.005
Piezocoefficient:				
d_{33} , pC/N	20-40	15-30	-	-
d_{31} , pC/N	60	25	100-300	80
g_{31} , V·m/N	0.18	0.16	-	-
e_{33} , C/m ²	0.16	0.23	15	-
g_{33} , V·m/N	0.32	0.38	0.017	-
Pyrocoefficient μC/(m ² ·K)	30-40	30-50	50-300	200
Coercive field, MV/m	35-100	40	0.1	0.1
Electromechanical coupling, %	10-15	10-15	30	21
Sound velocity, km/s	2,25	2,5	4,6	-
Acoustic impedance 10 ⁶ kg/m ² s	4	4,5	40	-

For comparison, the properties of such inorganic ferroelectrics, as lead zirconate-titanate (PZT) and barium titanate (BaTiO_3) are shown in the Table 1.1, which were used by us as fillers in PVDF-PZT and PVDF- BaTiO_3 composites. As can be seen from the Table 1.1, ferroelectric polymers have better mechanical properties than inorganic ferroelectrics. At the same time, they have lower piezoelectric and pyroelectric coefficients. Therefore, further research is needed for improving these important parameters.

1.2. Brief description of the studied materials

We studied thin films of ferroelectric polymers, such as PVDF, its copolymer with tetrafluoroethylene P(VDF-TFE), as well as PVDF-PZT and PVDF- BaTiO_3 composite materials. Samples of PVDF and P(VDF-TFE) films having thickness of 20-30 μm were obtained from the experimental batches of "Plastpolymer", St. Petersburg, produced by the method of extrusion, followed by uniaxial orientation (stretching) in the ratio 1:4 at the temperature of 100 °C followed by annealing at 120 °C for 1 hour. The degree of crystallinity of PVDF and P(VDF-TFE) films according to the manufacturer was (47 ± 3) %. The crystallites sizes according to the results of X-ray analysis have the following values: $L_\alpha = 96 \pm 6 \text{ \AA}$, $L_\beta = 70 \pm 8 \text{ \AA}$.

The percentage of tetrafluoroethylene in P(VDF-TFE) was 5-10%. Biaxially oriented PVDF films of the Kureha Co. had a thickness of 12.5 microns. In order to determine the relation between non-polar α -phase and ferroelectric β -phase, transmission and reflection spectra of all types of films in the range of 400-650 cm^{-1} were studied using the IR spectrometer FT-IR Perkin-Elmer 1750 with Fourier transform. Judging by the magnitude of 535 and 510 cm^{-1} peaks, it was found that the ratio 43:57 was between α and β in PVDF (Plastpolymer) films, 30:70 in Kureha Co. films, and 5: 95 in P(VDF-TFE) films.

Samples of PVDF-PZT and PVDF- BaTiO_3 composites were prepared by hot pressing of a powders mixture of ferro-ceramic PZT or BaTiO_3 and PVDF with a volume fraction of ceramics, respectively, 40% and 70%, and the average particle size of about 10 μm [63]. In preparing of composites, two types of polymer PVDF were used, which differed in concentration of ionogenic end groups and had a different specific resistance at a temperature of 20 °C, namely $10^{10} \text{ Ohm}\cdot\text{m}$ and $10^{12} \text{ Ohm}\cdot\text{m}$. These composites were

chosen as modeling ones, so that in case of PZT the Curie point of the filler (290 °C) was significantly higher than the melting point of the polymer (160-170 °C), and in the other (BaTiO₃) the Curie point (120 °C) was lower than the melting point. Both inorganic ferroelectrics in the form of ceramics are widely used for production of piezoelectric and pyroelectric converters.

1.3. Effective conductivity of PVDF films

Von Seggern and Fedosov [174] have found that conductivity plays an essential role in the formation and relaxation of the ferroelectric polarization in PVDF. Therefore, its experimental definition is very important. In this regard, two methods for determining the conductivity of PVDF were developed, namely, 1) by using the residual voltage on the measuring capacitor after repeated polings of the polarized sample and the following short circuiting and 2) by measuring the inclination of the displacement curves with prolonged poling.

If a constant voltage V is applied to the specimen of thickness d and area A for the time t , and then the sample is short-circuited for a sufficiently long time, then the following residual voltage ΔV_o remains on the measuring capacitor C_o

$$\Delta V_o = \frac{V \cdot t \cdot A}{C_o \cdot d} g \quad (1.1)$$

It should be noted that this does not postulate the applicability of the Ohm law, which implies the constancy of the specific conductivity and the proportionality between current and voltage.

$$g = \frac{C_o \cdot d \cdot \Delta V_o}{V \cdot t \cdot A} \quad (1.2)$$

The $g(E)$ dependence is shown in Fig. 1.3. Despite the scattering of experimental points, the dependence of conductivity on the field strength is close to the linear one, which confirms the quadratic dependence of the current on the voltage characteristic of the injection currents, limited by the volume charge.

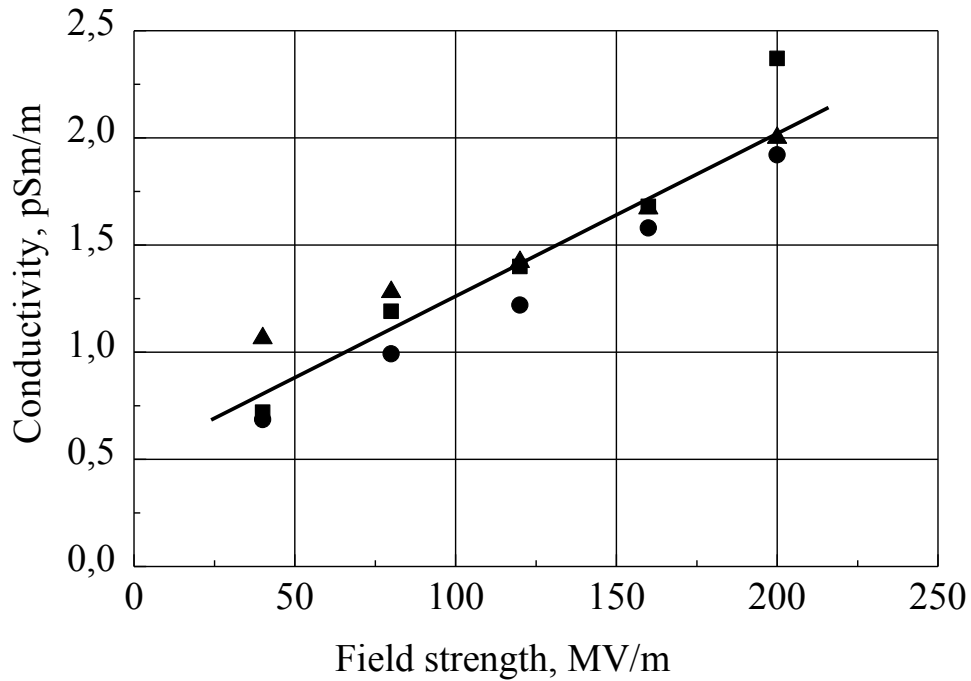


Fig. 1.3. Effective conductivity of PVDF calculated on the basis of experimental kinetics of displacement under influence of different voltages applied during 50 and 150 sec by the method of residual voltage on the measuring capacitor and by the displacement slope method.

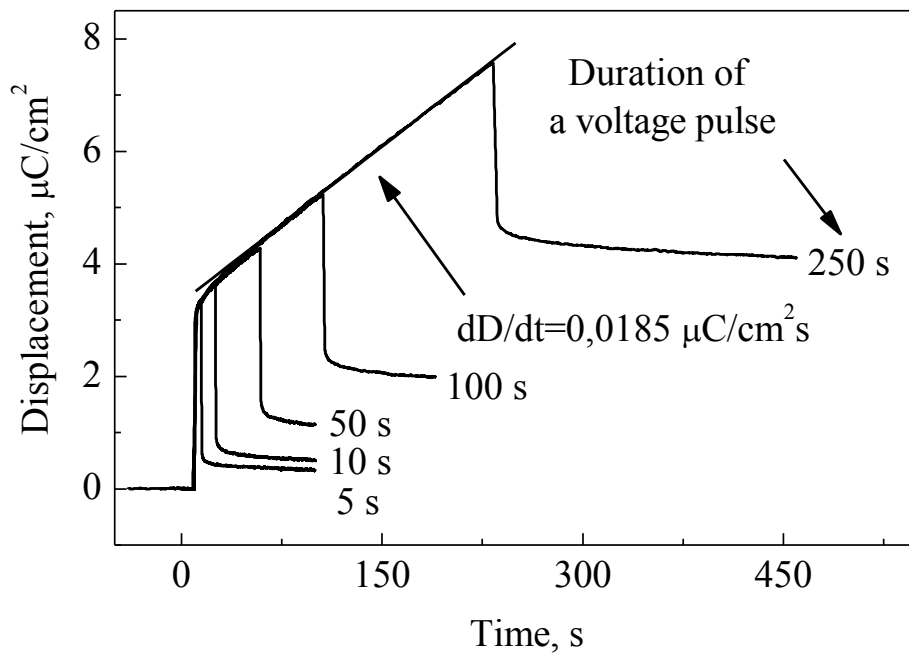


Fig. 1.4. Influence of conductivity on the form of the electric response at different duration of 2 kV polarizing pulses. The voltage of the same polarity was applied to already polarized films.

As follows from Fig. 1.3, the value of the PVDF conductivity is in the range of $(1-2) \cdot 10^{-12}$ Sm/m that corresponds to the specific resistivity of $(0.5-1.0) \cdot 10^{12}$ $\Omega \cdot \text{m}$ independently on the applied measuring method.

In the second method of determining the effective conductivity, we used linear sections of the kinetics displacement graphs obtained during prolonged application of DC voltage to already completely polarized samples (forward poling). It is supposed that the growth of the measured displacement D was caused by accumulation of charges on the measuring capacitor due to the conductivity current

$$I = gAE = A \frac{dD}{dt} = \frac{gAV}{d} \quad (1.3)$$

where

$$g = \left(\frac{dD}{dt} \right) \frac{d}{V} \quad (1.4)$$

Experimental $D(t)$ curves obtained at a voltage of 2 kV over different time intervals are shown in Fig 1.4. It is convincingly evident that the slope of the displacement curves remains constant ($dD/dt=0.0185$ $\mu\text{C}/\text{cm}^2 \cdot \text{s}$) irrespective of the voltage application duration in the range from 5 to 250 s. This indicates the constancy of effective conductivity and its dependence only on the voltage (field strength). By substituting numerical values in (1.4) we obtain the conductivity $g = 1.16 \cdot 10^{-12}$ Sm/m, being very close to the data shown in Fig. 1.3 at the same conditions.

1.4 Calculation of the dielectric permittivity in PVDF

Despite numerous studies, the exact value of the dielectric permittivity ε of PVDF is unknown, because the reported values of ε are in the range of 2 to 30 depending on the method of measurement or the calculation methodology, as well as the technology of obtaining, structure and composition of samples. For example, different authors report the following values for ε for semi-crystalline (50%) PVDF at room temperature: 6.2 [104], 7.3-9.3 [144], 10 [87], 12-13 [18], 12-16 [156], 13 [161,184], 15 [158], 16 [70]. In [100], the dielectric permittivity of amorphous α and crystalline β phases of PVDF

were calculated, and the values of $\varepsilon_a = 8-13$, $\varepsilon_c = 2.2-3.5$ were obtained. Furukawa [67] has found that ε is a function of the applied field, namely $\varepsilon = 19$ in a zero field, $\varepsilon = 9$ when the ferroelectric polarization reaches saturation and $\varepsilon = 30$ when the polarization is zero near the coercive field.

All components of the polarization in the non-ferroelectric phase of PVDF are linear, whereas, the ferroelectric nonlinear component P_F in the ferroelectric phase consists of electron and dipole components. The polarization P in linear dielectrics is proportional to the applied field strength E

$$P = \varepsilon_o (\varepsilon - 1) E, \quad (1.5)$$

where ε_o is the permittivity of a vacuum; ε is the dielectric permittivity of the sample.

It is known from the theory of dielectrics that ε depends on the concentration of the atoms n_a and that of dipoles n_d , the atomic polarizability α , the static dipole moment p , and the temperature T [54]

$$\varepsilon = 1 + \frac{1}{\varepsilon_o} \left(n_a \alpha + \frac{n_d p^2}{3kT} \right), \quad (1.6)$$

where k is Boltzmann's constant.

It is also known [109] that the dipole moment p of the $-\text{CF}_2\text{-CH}_2-$ unit in PVDF is $p = 7.6 \cdot 10^{-30}$ C·m, while $m_d = 9 \cdot 10^{-26}$ kg (dipole mass). It is also known that the densities of amorphous ρ_a and crystalline ρ_c phases in PVDF are different ($\rho_a = 1.68$ g/cm³, $\rho_c = 1.93$ g/cm³), and therefore the concentrations of dipoles are also different ($n_{cr} = 2.1 \cdot 10^{28}$ m⁻³ and $n_{am} = 1.8 \cdot 10^{28}$ m⁻³). The concentration of atoms in the crystalline and amorphous phases is easy to calculate as $n_{cr}' = 1.26 \cdot 10^{29}$ m⁻³ and $n_{am}' = 1.08 \cdot 10^{29}$ m⁻³. Atomic polarization is usually calculated as $\alpha = 2\pi\varepsilon_o r^3$, where $r \approx 10^{-10}$ m is the average radius of the atom.

Substituting the above values into (1.6), we obtain the value of the dielectric constant in amorphous and in crystalline phases at room temperature $\varepsilon_a = 11.3$, $\varepsilon_c = 12.9$. The obtained values are in good agreement with the values of the dielectric constant in PVDF given in literature [104,144].

In the amorphous phase of PVDF, there are dipoles $-\text{CF}_2-\text{CH}_2-$ oriented to some degree under action of the external field creating some additional polarization P' , proportional to the field strength E . Polarization P' is reversible, that is, it completely disappears at zero field similarly to the electronic and dipole components of the full polarization. von Seggern and Fedosov [178] have found that there is a reversible component of polarization in PVDF equal to $1.6 \mu\text{C}/\text{cm}^2$ at $E = 160 \text{ MV}/\text{m}$. Assuming that the polarization P' is responsible for this polarization component, its influence can be taken into account as an additional part of the dielectric constant in the amorphous phase equal to 8.3. Thus, it seems that the dielectric constant of the amorphous phase is actually equal to $\epsilon_a = 19.6$. However, it should be noted that contributions of electronic and dipole components to polarization P' are different. This follows from the experimental data that P' is formed in about $50 \mu\text{s}$ at $E = 160 \text{ MV}/\text{m}$ and it disappears during the same time during the short circuiting. Consequently, the constant time of this relaxation process is of the order of $1 \mu\text{s}$, while the electronic and dipole polarization components follow the field almost instantaneously.

Considering above calculated data and discussions we will use in our subsequent calculations the following numerical values of the PVDF dielectric constant: $\epsilon_c = 12.9$ and $\epsilon_a = 19.6$.

1.5. Methods of ferroelectric polymer films poling

We studied three methods of poling, namely: the thermoelectret method, the high field method, and corona discharge poling (Fig. 1.5). In the first and the second methods, 150 nm thick Al electrodes were deposited on both surfaces of the sample by thermal evaporation and condensation in vacuum. In case of corona poling, the electrode was deposited only on the rear side of the sample leaving non-metallized another side subjected to the action of a corona discharge.

The thermoelectret method consisted in poling at $90-100 \text{ }^\circ\text{C}$ for one hour and subsequent cooling to room temperature without switching off the poling voltage. It is assumed in the theory of thermoelectrets that the residual polarization is "thermally frozen". Since PVDF is a ferroelectric, it is possible to obtain high residual polarization at room temperature without heating, if a sufficiently high poling field is used (the high field method) [159].

For poling in a corona discharge and for conducting a series of experimental studies, a specialized set-up (a corona triode) was designed [63,150], the block diagram of which is shown in Fig. 1.5. Samples metallised in vacuum from one side with a bare working surface of 4 cm^2 area were fixed on a massive metal table, inside of which there was an electric heater.

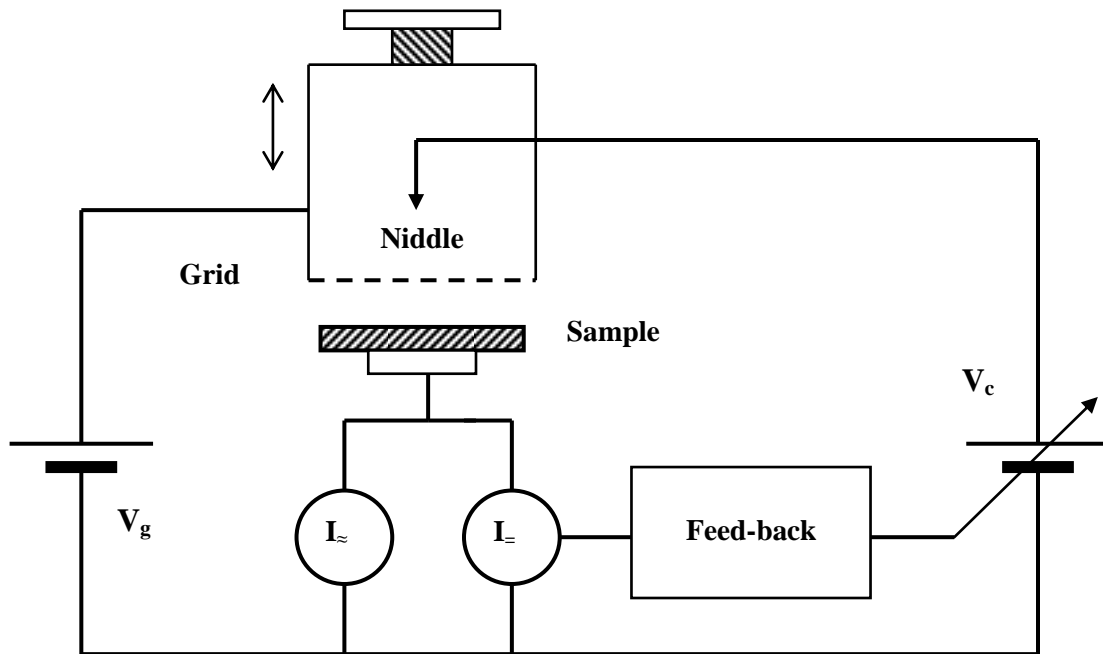


Fig. 1.5 Block - diagram of the corona triode set-up. Cylinder with a control grid was made vibrating in the vertical direction.

The heater's power was automatically adjusted by the electronic circuitry in such a way that either temperature constancy, or linear heating, or cooling with a given rate in the range of 0.5-5 K/min was provided. It was also provided for the possibility of rapid cooling of the samples at 35-40 K/min. The temperature was continuously recorded by a self-recording potentiometer.

The corona discharge of positive or negative polarity was initiated by a sharpened tungsten electrode (needle), which received a voltage from an automatically regulated rectifier, the feedback circuit of which produced a signal proportional to the DC component of the poling current. Thus, the set-up worked, if necessary, with the stabilization of the poling current, the value of which was set by the regulator in the feedback circuit. It was also possible to manually adjust the constant voltage on the corona electrode in the range from zero to $\pm 25 \text{ kV}$.

Between free surface of the sample and the corona electrode, a metal control grid was placed, whose potential from zero to ± 4 kV was set by a stabilized power supply.

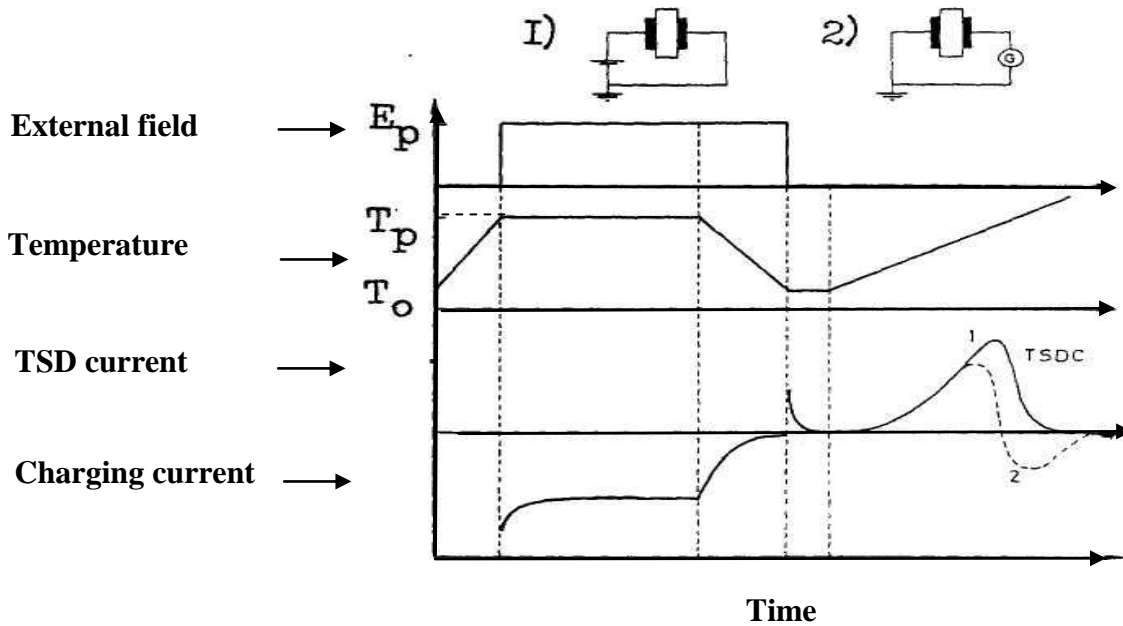


Fig. 1.6. Principles of the thermoelectret poling (1) and depolarization (2) methods

The principal difference of the applied scheme from the previously described [78] was the use of a vibrating grid, which allowed continuous measurement and recording both the charging current and the effective electret potential. To eliminate parasitic modes, the frequency of the grid oscillation was chosen close to the frequency of the main mechanical resonance of the system. With grid vibration, the current through the sample contained DC and AC components, which were distributed using two RC chains. The signal proportional to the charge stomp was fed directly to the electrometer amplifier and the recording potentiometer. The AC component proportional to the potential difference between the electret potential of the sample surface and the voltage applied to the grid was fed to the narrow-band amplifier, which was tuned to the frequency of grid oscillations [63]. The transmitted signal through the detector and the amplifier came to another recording potentiometer. Linearity was ensured between the readings of the measuring device and the electret potential value at both polarities in the entire range from 0 to 4 kV.

The scheme for obtaining a thermoelectret is shown in Fig. 1.6. The sample was heated to a polarization temperature T_p of about 80-120 °C in case of PVDF. Then, a constant electric field E_r was applied and maintained for the time of polarization t_p . Then

the sample was swiftly cooled to room temperature T_c in the field E_r and the polarizing voltage was disconnected. In the high field method, an electric field with a strength of about 60-150 MV/m was applied to the sample for a definite time at room temperature.

The method of fractional poling of samples was also applied, which consisted in analyzing the response (electret potential) to the effect of rectangular current pulses. Therefore, the whole process of poling was divided into a number of separate fractions. Periodic irradiation of the sample took place during the application of DC current of a pulse followed by the stages of relaxation (discharging) after each current pulse.

Unilaterally metallized samples of PVDF and P(VDF-TFE) films were placed in the set-up for poling in a corona discharge (Fig. 1.5). The samples were poled by rectangular pulses of $90 \mu\text{A}/\text{m}^2$ current. Spacing between the pulses was equal to their duration and was 300 seconds. The "charge-discharge" cycles were repeated until the electret potential continuously measured by the Kelvin method, did not become equal to the control grid potential. Thus, within each fraction there was a section of potential growth at a constant charging current and a potential decay in the gap between the current pulses.

1.6. Application of ferroelectric polymers

Prospects of using PVDF and its copolymers are due to a number of specific properties, namely:

- 1) High technological capacity;
- 2) The possibility of obtaining large areas of the active element, which allows the design of second generation sensors;
- 3) Wide bandwidth up to 500 MHz required in diagnostic systems;
- 4) The proximity of the acoustic impedance of PVDF to the impedance of human tissue and water used in creation of sensors for medical diagnostics and hydrophones;
- 5) High impact strength of polymer films (this quality of PVDF is used in shockwave sensors);
- 6) High chemical resistance of PVDF (this property is necessary when working in active media);
- 7) Low dielectric permittivity values and, respectively, higher (almost order and higher) values of the piezo constants g and sensitivity to the pyroelectric signal (p/ε);

than in ceramics;

8) Lower thermal conductivity of PVDF in comparison with piezoceramic and the possibility of obtaining thin films;

9) The possibility of providing the material of arbitrary shape (cone, dome, etc.), allowing to create elements with special radiation patterns.

One of the most important properties is the presence of longitudinal and cross-sectional piezoelectric effects in PVDF films and its copolymers. It is used in the creation of of high frequencies headphones and loudspeakers [5,76].

From the new applications of piezoelectric polymers, it should be noted that they are used in robot stereoscopic viewers [71], field sensors in which the optical fibers are coated with a piezoelectric polymer [37], and also in hybrid-type sound pressure sensors consisting of directly contacting the layers of the piezopolymer and the semiconductor [92]. In digital loudspeakers based on piezoelectric polymers, one can directly convert digital signals into sound [91]. Piezoelectric cells from PVDF can be used to create a gas sensor, and the possible application area is the control of binary gas mixtures with known components [80,143].

The advantages of using PVDF in medicine are related to the proximity of the acoustic impedance to the impedance of water and biological object ($Z = 1.4 \cdot 10^6$ kg/(m²s)), which allows the transfer of 50% of the energy produced in the film into water, whereas this value in case of piezoceramics is an order of magnitude lower [183]. This property of PVDF allows it to be used to measure electrocardiograms or to control breathing.

PVDF-based films are already used as pyroelectric materials in infrared radiation sensors. They are also used in fire detectors, as well as in the devices of the security. PVDF-based ferroelectric polymers are proved to be suitable for different kinds of sensor and actuator applications [3]. Actually the ferroelectric polymers are multifunctional electroactive materials [142].

As noted in [20], ferroelectric polymers are the most promising electroactive materials with outstanding properties that can be integrated into a variety of flexible electronic devices. A new field of the ferroelectric polymers and composites application is the energy harvesting [85,39,136]. Ferroelectric polymer-based nanocomposites have prospects for application in high energy density capacitors [172].

Their multifunctional capabilities, ability to bend and stretch, ease of processing,

chemical stability, and the high biocompatibility of polyvinylidene fluoride (PVDF)-based polymers make them attractive for applications in flexible memories, energy transducers, and electronic skins. Here, recent advance in the research of PVDF-based flexible electronic devices is reviewed, including nonvolatile memories, energy-harvesting devices, and multifunctional portable sensors.

Chapter 2. Formation of the polarized state in ferroelectric polymers

2.1. Transfer of charges and formation of polarization in FP_s

Most researchers believe that in electrets, including ferroelectric polymers, electron conductivity predominates in high fields at low temperatures, while at high temperatures and in weak fields, charge transfer is carried out by ions [138]. Due to the presence of an amorphous phase, the zone theory of solids, strictly speaking, can not be applied to ferroelectric polymers. However, it is sometimes believed that the bandgap width in high-strength polymers, which include PVDF, is 6-9 eV [97,151]. It is also believed that there are localized states in the forbidden zone, the energy distribution of which is monotonous and continuous. The presence of relaxation processes characteristic for polymers introduces elements of discreteness in this distribution [173].

The transfer of charge in a ferroelectric polymer is accompanied by the periodic transition of carriers from a free state to a localized state, that is, the mobility is modulated by the charge traooing. Mitsutani and Ieda [128] showed that the atoms of fluorine attract electrons, and hydrogen atoms attract holes. Since in PVDF the concentration of fluorine and hydrogen is the same, then both types of carriers should be mobile. This experimentally confirmed in the study of radiation-induced charge transfer in PVDF [151]. Gross and others [82], measuring the mobility of injected in PVDF electrons from a virtual electrode, found that in the field strength below the coercive field, the charge mobility has the order of $2 \cdot 10^{-12} \text{ m}^2/(\text{V} \cdot \text{s})$. At the same time, Faria et al., [40], investigating radiation-induced conductivity in PVDF under X-ray irradiation, have found that the mobility of carriers was four orders of magnitude smaller. Kaur et al [101] calculated the mobility in PVDF from the decay of the electret potential and obtained the value $(6-10) \cdot 10^{-14} \text{ m}^2/(\text{V} \cdot \text{s})$ for unoriented films and $(0.2-2.5) \cdot 10^{-14} \text{ m}^2/\text{V} \cdot \text{s}$ for oriented films. On reduction of conductivity at the stretched PVDF film it was

reported also in work [4]. Das Gupta and others [23] measured the mobility in PVDF by four methods and obtained values from $3 \cdot 10^{-14}$ to $4 \cdot 10^{-16} \text{ m}^2/(\text{V} \cdot \text{s})$. Giacometti [79] found that the mobility of charge carriers in PVDF is $9.3 \cdot 10^{-16} \text{ m}^2/(\text{V} \cdot \text{s})$, while the residual polarization had a value of 0.19 C/m^2 by analyzing curves of the electret potential kinetics at the films poled in a corona discharge.

The dispersal of the mobility values in several orders reported by various authors suggests that the method of the mobility finding is imperfect and requires further development. Kurtz and Hughes [107], measuring the photoconductivity of PVDF after X-ray irradiation, found that charge transfer occurs in a dispersion mode, and the dispersion parameter depends on the structure of the polymer, the polarization regime and irradiation. The dispersion mode of charge transport in PVDF was also considered in the model proposed by Arkhipov, Fedosov and others [2].

In the weak fields and at elevated temperatures, the ionic component of conductivity in the PVDF plays a role, although its presence has not been experimentally proved. It is believed that ions of impurities such as *Na*, *Ca*, *Al*, as well as *F* formed during the decomposition of a polymer may be mobile. The conductivity of PVDF in the weak fields is influenced by the presence of oxygen and water vapor in the atmosphere [40]. Legrand [121] found that the electrical and mechanical properties of ferroelectric polymers depend on the properties of the amorphous phase.

The reason for the fragmentation and contradiction in the above data is, in our opinion, caused by ignoring the specificity of PVDF as a ferroelectric polymer. In most works, it is considered as an ordinary polar dielectric. At the same time, the presence of a ferroelectric phase must have a significant impact on conductivity, the processes of transfer and trapping of the charges. Important is the question of the ratio of phases conductivity in ferroelectric polymers and composites. If the poling time exceeds the Maxwellian relaxation time, then the voltage is distributed between the polymer matrix and the ferroelectric phase in proportion to their conductivities. Since conductivity of the filler in composite materials is usually higher than that of the polymer, the efficiency of the polarization may be low [135]. At the same time, the artificial increase in the conductivity of the polymer by introducing additives can negatively affect the formation and stability of the bulk charge. This question, like many others, is still underdeveloped.

It is known that in order to maintain a stable polarization in ferroelectrics, local compensation of a depolarizing field due to presence of the polarization charge is

necessary [123].

Obviously, free charge carriers on the electrodes and the surface charge can only neutralize the total mean field, while in order to compensate the local depolarizing field in each crystal, space charges are required [150]. There is a lot of information about the presence of space charge in these materials, but they are fragmentary and contradictory. Lang [116], comparing polyethylene and PVDF, found that in both polymers, the ratio of polarization to bulk charge is almost the same, indicating the existence of their interrelation. In [35], space charge layers on both sides of the central polarized region in PVDF were detected.

The interrelation of the space charge and polarization in ferroelectric polymers is probably similar to the analogous processes in ferroelectric ceramics, where, as is known, a space charge has a stabilizing effect on residual polarization and screens it. It should, however, be noted that the particles are not rigidly clamped in ferroelectric polymers, but relatively free in the amorphous matrix, so that the conditions for charge trapping and screening are different. That is why the piezoelectric coefficient d_{33} in the composites is much larger than the d_{31} coefficient.

The space charge is formed by trapping the carriers in traps under conditions that the relaxation time of this charge is much longer than the experiment duration [105]. It is believed that the most probable places of charge carriers' localization in polymers are unsaturated double bonds, finite groups, while impurities play a small role.

More specific data, especially concerning ferroelectric polymers, are very limited. Kurtz and Hughes [107] found that the PVDF photoconductivity decreases during polarization growing. In the works [107,35,86], assumptions are expressed about irreversible changes and the formation of additional traps. Eliasson [36] predicted that new localized states are in the place where polymer chains bend on the crystalline lamellae surface.

A model for polarization formation in corona-charged ferroelectric polymers was developed in works of Fedosov and Sergeeva [57,61,63,150]. They suggested that large-scale potential fluctuations occur on the boundaries of polarized regions, which act like deep traps. Injected charge carriers are attracted by these traps compensating the depolarizing field and stabilizing residual polarization in crystallites. As a result, the thermal equilibrium between delocalized and trapped charge carriers is shifted toward increasing concentration of the latter that phenomenologically manifests itself in the

reduction of the effective conductivity.

The question of the interrelation of the ferroelectric polarization with the space charge in semiconductor ferroelectric polymers is still open and it requires additional research.

2.2. Method of quasi-stationary volt-ampere characteristics measuring

When measuring the volt-ampere characteristics (VAC) of PVDF and other ferroelectric polymers, a number of difficulties arise. When applying a constant voltage to PVDF, non-exponential processes with a high relaxation time are observed, and absorption current decreases over time, even in a few hours, does not reaching a constant value. Since the films under investigation have a specific resistance of the order of 10^{10} - 10^{14} $\Omega \cdot m$, the currents are small that makes it difficult to measure them under the background of noise.

In our work, for obtaining the volt-ampere characteristics, the sample was placed at the grounded metal plate, which served as an anode of the corona discharge triode. A definite potential was supplied to the control grid of this triode. This potential was equal to the required surface potential (electret potential) of the sample. The measurements showed that equality between potentials of the grid and the surface was installed in 5-7 seconds. The current was measured by an electrometer with a self-recording device.

Initial voltage at the grid and correspondingly the electret potential was zero. Then the voltage was set in steps at 200 V above the previous one and was applied for 5 min. Then the corona discharge was switched off and the kinetics of the decaying potential was measured for 5 minutes. In some experiments, current measurements were repeated at the same voltage three times alternating with the stages of the potential decay (at zero current). The VACs were measured again on the same samples in 24 and 48 hours. Measured VAC films of PVDF and P(VDF-TFE) covered a range of electric fields with a strength from 4 to 120 MV/m. Measurements were performed at room temperature of 20 °C.

2.3. Volt-ampere characteristics of PVDF films

The volt-ampere characteristics of ferroelectric polymers in the form of the

dependence of the current density (or effective conductivity) on the applied voltage (or field strength) were studied for the investigation of the processes of polarization formation, as well as charge accumulation and their relation to conductivity (Figs 2.1 and 2.2).

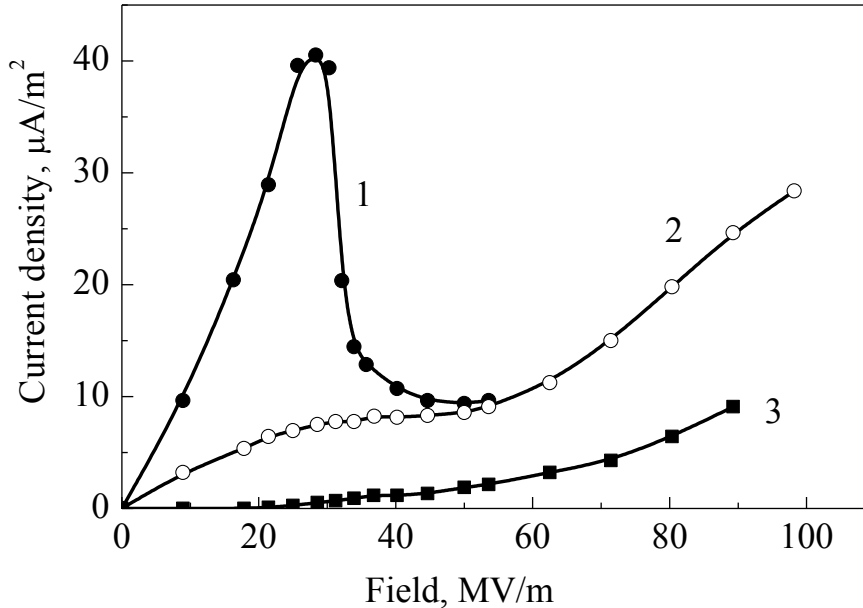


Fig. 2.1. Volt-ampere characteristics in the process of primary (1), repeated (2) and third poling of PVDF films in a negative corona discharge at 20 °C.

The following are the main features of the experimental curves [150]:

1) During initial poling, VAC contains three regions and has a *N*-like appearance with a clearly defined area of negative differential resistance in the range of 35-50 MV/m fields strength. The position of the current minimum is the same for positive and negative corona discharge polarity.

2) The initial portion of the VAC is nonlinear. Failure to comply with Ohm's law indicates the importance of injection processes.

3) Effective conductivity during initial poling highly depends on the field strength (Fig. 2.2) that indicates presence of both processes of charge carriers generation and deep trapping of the charges. A sharp decrease in conductivity is observed in the voltages range of 1.2-2.0 kV.

4) There is a significant decrease in current (Fig. 2.1) during repeated measurements in the range of field strengths corresponding to the negative differential resistance.

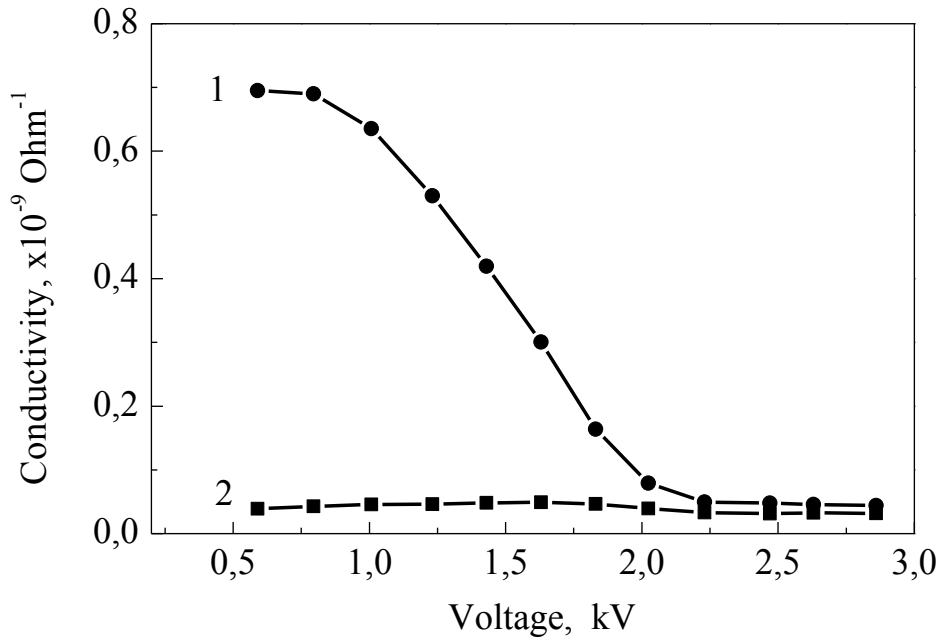


Fig. 2.2. Dependence of the PVDF effective conductivity on the applied voltage during primary (1) and repeated (2) poling in the corona discharge.

Therefore, the VAC in this area is not quasi-stationary, but reflects a certain stage of the transient process due to the intensive processes of the polarization formation and the trapping of charges .

5) N-shaped type of VAC is not observed during repeated poling. In initially polarized samples, there is a plateau or a weak current maximum. The current monotonically increases in completely polarized sample with increasing the field strength remaining 1-2 orders of magnitude lower than in case of initials poling (Fig. 2.1). It follows from Fig. 2.2, that a sharp decrease in the effective conductivity observed in the process of initial poling is irreversible.

The measurements also showed that during the growth of the polarizing voltage, an abnormal increase in the relative stability of the electret potential is observed. In case of ordinary electretes, a reverse phenomenon is characteristic typical for processes of the first order kinetic. The relaxation rate of the potential usually increases with increasing the potential's value.

In medium and high fields when the Ohm law is not fulfilled several conduction mechanisms are possible. Let us consider the processes controlling the conductivity and

determining the kind of the VACs. If we assume that the current is due to the Richardson-Schottky emission, the VAC equation should look like [112]

$$i = AT^2 \exp[-(Q - \beta_s \sqrt{V})/kT], \quad (2.1)$$

where $\beta_s = \sqrt{e^3 \alpha / 4\pi \epsilon_o \epsilon x_o}$ is the Schottky coefficient; A is the constant of Richardson-Deshman; Q is the height of the potential barrier at the "electrode-polymer" boundary in the zero field; α is a correction factor taking into account the field heterogeneity in the film near the electrode; x_o is the thickness of the sample. For $\alpha = 1$, $x_o = 26 \mu\text{m}$ and $\epsilon = 10$, the calculated value of β_s/kT is $0.088 \text{ V}^{-1/2}$.

If the current is limited by the space charge, then the quadratic Mott-Gurney law [112] is valid in presence of small traps:

$$i = (9/8)\Theta \mu \epsilon_o \epsilon V^2 / x_o^3 \quad (2.2)$$

where Θ is a dimensionless parameter for capturing carriers by small traps; μ is the charges mobility.

The field-stimulated Poole-Frenkel emission is described by the following equation

$$i = i_o \exp(\beta_{PF} \sqrt{E} / 2kT) \quad (2.3)$$

where β_{PF} is the Poole-Frenkel coefficient.

One or another conduction mechanism can be identified by the type of the VAC. The experimental curve for PVDF films is linear in coordinates $\ln i - \ln V$ in weak fields and in higher fields with $\beta_s/kT = 0.118 \text{ V}^{-1/2}$ and $\alpha = 1.34$. The height of the potential barrier is $Q = 0.72 \text{ eV}$, and the rate of the current dependence on the voltage is equal to 1.52 instead of 2.

Thus, we assume that the current at the initial stage of the VAC is controlled both by electrode processes and by the space charge. The Schottky's emission probably dominates in weak fields, while the current is limited by the space charge in the higher fields. Since $\alpha > 1$, the field is inhomogeneous in the thickness direction that is consistent

with the available literature [73] and our data. The case of $n < 2$ indicates a partial current limitation by the electrode injection not only in weak fields.

A sharp decrease in conductivity is observed at the second section of the VAC at voltages of 1.2-2.0 kV. This can be explained by the trapping of charge carriers in deep traps formed at the boundaries between crystallites with the amorphous phase and on the boundaries of macroscopic polarized zones. Reducing conductivity may also be due to purification in the field by removing ionic impurities [99]. However, because of low mobility of ions at room temperature, the most probable is the process of carriers trapping stimulated by high polarization. One can expect that the ion component makes the greatest contribution to the full current in high fields in the third section of the VAC.

It is believed that the motion of an ion represents a series of successive jumps between localized states according to the following equation [147]:

$$i = i_o \exp(-Q/kT) \text{sh}(\lambda \cdot e \cdot E/kT), \quad (2.4)$$

where $i_o = 2\nu \cdot e / \lambda^2$; Q is the activation energy of the impurity conductivity; λ is the average length of the jump; ν is the frequency of jumpings. In fields of 80-120 MV/m VACs of PVDF films straightened in coordinates $\ln i - E$. The calculation on the basis of our experimental data gives 8.7 Å as the average length of the ion jump. The obtained by us values of λ in PVDF are in the same order as those given in the literature: 25 Å at room temperature [124] and 9 Å at 50 °C [19].

When recording VACs in high fields and with repeated poling, there is a dependence characteristic both for the Schottky emission and for the Poole-Frenkel effect (activation energy is 1.1 eV). This technique does not allow separating these processes, but for general reasons, the effect of the Poole-Frenkel should be expected in higher fields.

Thus, it has been found that the effective conductivity of PVDF decreases during the polarization formation. This leads to increase of the relaxation time τ . The results of the τ calculation are shown in Fig. 2.3.

Practically, the constant relaxation time at a voltage lower than 1.2 kV during initial poling corresponds to a Maxwellian relaxation time, when high ferroelectric polarization is still absent. Further growth of τ can be related to the irreversible decrease in conductivity due to charge trapping, since high values of τ are retained during poling at high voltages. The obtained data are in good agreement with results of research on

kinetics of poling by rectangular current pulses.

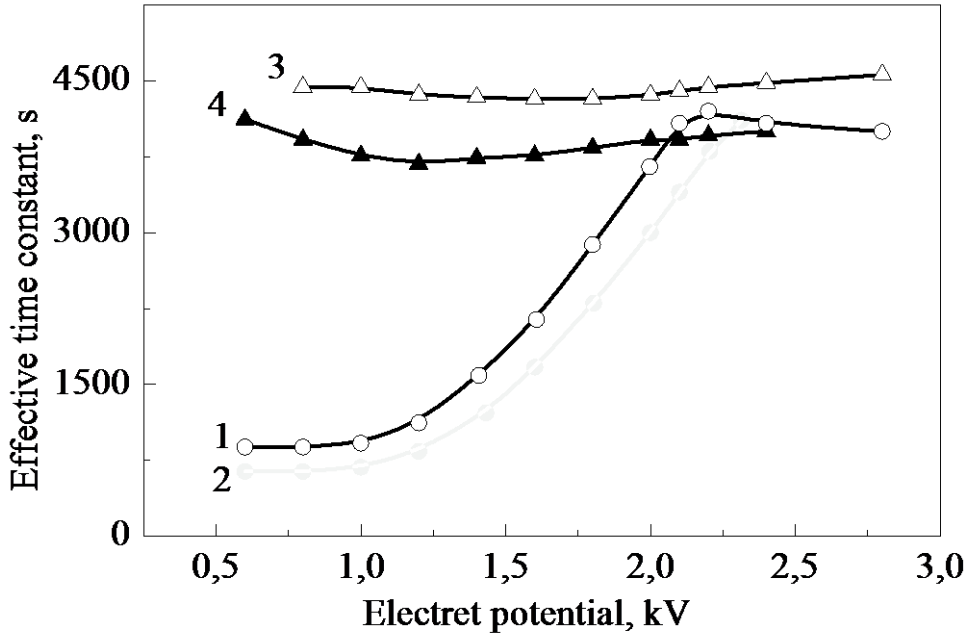


Fig. 2.3. The effective time constant of the electret potential decay in the process of primary (1,2) and repeated (3,4) poling in the positive (1,3) and negative (2,4) corona discharges.

2.4. Electric displacement during constant voltage poling

Let us analyze the components of the complete electric displacement measured during initial poling, as well as during the short circuit and repeated poling in the mode of the constant poling voltage. We also will show how to calculate the ferroelectric component of polarization, the reversible polarization and the conductivity contribution to the total electric displacement.

The equation for a full current density in the general case has the following form:

$$i(t) = \varepsilon_0 \varepsilon \frac{dE(x,t)}{dt} + \frac{dP(x,t)}{dt} + \mu\rho(x,t)E(x,t) \quad (2.5)$$

Given the presence of a stable P_{st} component of the polarization and the unstable (reversible) P_{unst} component of the total time-dependent polarization P , and assuming that the field and polarization inside the sample are homogeneous, one can obtain

expressions for displacement in the process of switching $D_s(t)$ and re-electrifying in the same direction $D_r(t)$

$$D_s(t) = \int_0^t i(t') dt' = \frac{1}{A} (C_s \Delta V)_s + \Delta P_{st}(t) + \Delta P_{unst}(t) + \frac{1}{A} \int_0^L dx \int_0^t \mu \rho(x, t') E(x, t') dt' \quad (2.6)$$

$$D_r(t) = \int_0^t i(t') dt' = \frac{1}{A} (C_s \Delta V_s) + \Delta P_{unst}(t) + \frac{1}{A} \int_0^L dx \int_0^t \mu \rho(x, t') E(x, t') dt' \quad (2.7)$$

Considering the constancy of full current at any point, the displacement $D(t)$ on the measuring capacitor C_o can be written as

$$D(t) = \int_0^t i(t') dt' = \frac{1}{A} [C_o V_o(t)]. \quad (2.8)$$

For very small times (high equivalent frequency), we can assume that $\rho(x, t) \approx 0$, $\Delta P \approx 0$. Then it follows from (2.6) and (2.8) that the measured value of $V_o(t)$ at any time is proportional to the total displacement $D(t)$. The applied voltage V is divided inversely proportional to the capacitance of the sample and the capacitance of the measuring capacitor $\frac{V_s}{V_o} = \frac{C_o}{C_s} \approx 10^3$. Since $V_s \gg V_o$, then $\Delta V_s \approx V$.

In longer time, it is necessary to take into account the conduction current and its contribution to the total measured displacement. The quadratic dependence of the conduction current on the applied field (Child's law) revealed by us indicates that in our case, most likely, there is a mode of the space charge limited current (SCLC) [112]. Therefore the measured conductivity is caused most probably by the injected charges, but not by the intrinsic ones. Using known expressions for the current density i , the time of flight t_{tr} and the average density of the space charge ρ in the mode of SCLC at $t > t_{tr}$, we have

$$i = \frac{9}{8} \varepsilon_o \varepsilon \mu \frac{V^2}{d^3}, \quad (2.9)$$

$$t_{tr} = \frac{4 d^2}{3 \mu V}, \quad (2.10)$$

$$\rho = \frac{3}{2} \varepsilon_o \varepsilon \frac{V}{d^2} \quad (2.11)$$

It is possible to estimate the values of mobility and charge density ($\mu = (3-8) \cdot 10^{-12} \text{ cm}^2 \cdot \text{V}^{-1} \cdot \text{s}^{-1}$, $\rho = 8 \text{ mC} \cdot \text{cm}^{-3}$ and $\tau = 350 \text{ s}$) to use them in the equation (2.6). However, analytical calculations of the effect of conductivity are very indistinct and ambiguous. Therefore, we applied a different, more direct and precise method in order to separate all components of the complete displacement, including conductivity [149].

Equations (2.6) and (2.7) are valid for $\tau \geq t \geq 0$ where τ is the poling time. If the sample is short circuited at $t \geq \tau$, then

$$D_s(t) = D_p(\tau) - \frac{1}{A} C_s V - \Delta P_{unst}(t - \tau), \quad (2.12)$$

$$D_r(t) = D_r(\tau) - \frac{1}{A} C_s V - \Delta P_{unst}(t - \tau)]. \quad (2.13)$$

If the superposition principle is valid for an unstable part of polarization (this has been proved by us), then $\Delta P_{unst}(t) = \Delta P_{unst}(t - \tau)$. With this in mind, replacing $\Delta P_{unst}(t) = \Delta P_{unst}(t - \tau)$ in (2.12) and (2.13) by the corresponding expressions $D_s(\tau)$ and $D_r(\tau)$ with (2.6) and (2.7), we can write the following expression for a certain moment $t_o \geq 2\tau$

$$D_s(t_o) = \Delta P_{st}(\tau) + \frac{1}{A} \int_0^L dx \int_0^\tau \mu \rho(x, t') E(x, t') dt'; \quad (2.14)$$

$$D_r(t_o) = \frac{1}{A} \int_0^L dx \int_0^\tau \mu \rho(x, t') E(x, t') dt' . \quad (2.15)$$

We define four components of the complete displacement $D(t)$ as

$$D_{cap}=(C_s V/A)=(\varepsilon_o \varepsilon V/L), \quad D_{st}(t)=\Delta P_{st}(t), \quad D_{unst}(t)=\Delta P_{unst}(t)$$

$$D_{cond}(t) = \frac{1}{A} \int_0^L dx \int_0^t \mu \rho(x, t') E(x, t') dt' \quad (2.16)$$

where D_{cap} is an almost instantaneous capacitive component, D_{st} is a stable (ferroelectric) component of the remaining polarization after the completion of initial poling or switching, D_{unst} is an unstable component of polarization that slowly relaxes to zero after a short circuiting, D_{cond} is a component of conductivity due to motion of the charge carriers.

With the experimental graphs $D_s(t)$ and $D_r(t)$ for $0 \leq t \leq 2\tau$ (Fig. 2.4), we can not only calculate the final values of each component, but also obtain information about their dynamics, for example

$$\Delta P_{st}(t) = D_s(t) - D_r(t) - D_{cap} \quad \text{at } t \geq \tau \quad (2.17)$$

shows how stable polarization grows ($\Delta P_{st}(t) = \Delta P_{st}(\tau) = \text{const}$ at $t \geq \tau$).

$$\Delta P_{unst}(t - \tau) = D_r(t - \tau) - D_{cap} \quad \text{at } t \geq \tau \quad (2.18)$$

shows the relaxation of unstable polarization, and

$$D_{cond}(t - \tau) = D_r(t_o) \quad \text{при } t_o \geq t \geq \tau \quad (2.19)$$

shows the contribution of conductivity accumulated over the whole time of poling τ .

Experimentally measured curves of complete displacement kinetics are shown in Fig. 2.4 in case of polarization switching for 50 s and with repeated poling of a polarized film in the same mode (forward poling). From the position of four characteristic points A, B, C, and D, it is possible to calculate the contributions of the ferroelectric polarization D_{st} , D_{cap} , D_{unst} , D_{cond} . The method of calculations is as follows.

The total displacement at point A is equal to the sum of all the indicated components

$$D_A = D_{st} + D_{unst} + D_{cap} + D_{cond} \quad (2.20)$$

, The residual polarization at point *B* is maintained after the relaxation of the capacitive component and the unstable part of the polarization, that is,

$$D_B = D_{st} + D_{cond} \quad (2.21)$$

At the point *C*, there are all components of the point *A*, except for the ferroelectric component, i.e.

$$D_C = D_{unst} + D_{cap} + D_{cond} \quad (2.22)$$

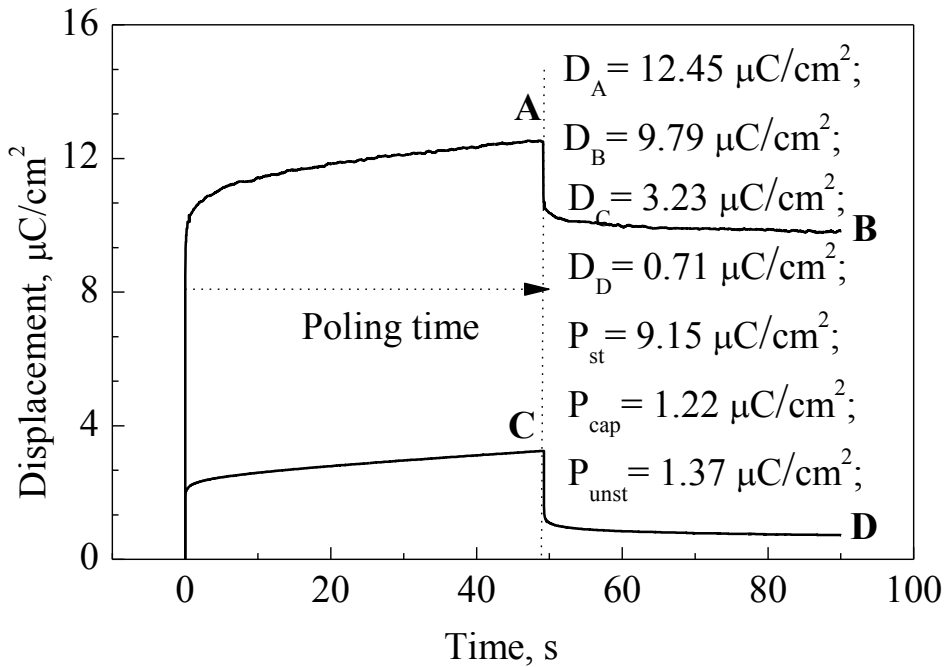


Fig. 2.4. Switching of polarization (A-B) by a pulse of voltage at the field strength of 120 MV/m applied for 50 sec and by repeated application of the same pulse (C-D). The displacement values are shown, as well as the values of a stable, an unstable and a capacitive component of polarization in characteristic points.

Only the conductivity component remains at point *D*

$$D_D = D_{cond} \quad (2.23)$$

Denoting for simplicity $D_A = A$, $D_V = B$, $D_C = C$ and $D_D = D$, we solve the system of equations (2.20) - (2.23) and obtain

$$D_{st} = A - C = B - D; D_{cond} = D; D_{unst} + D_{cap} = A - B = C - D \quad (2.24)$$

D_{cap} is caused by the voltage jump ΔV on the measuring capacitor C_o when the voltage is switched on and off

$$D_{cap} = \frac{C_o \Delta V}{A} \quad (2.25)$$

It is interesting to note that $A - C > B - D$ means that a part of the ferroelectric polarization is switched back during the short circuiting due to insufficient compensation of the depolarizing field [175].

2.5. Isothermal kinetics of the electret potential in PVDF films

The process of formation of a polarized state in ferroelectric polymers was investigated by the method of poling in a corona-discharge triode with a vibrating grid and a continuous measurement of the electret potential by the Kelvin method [78].

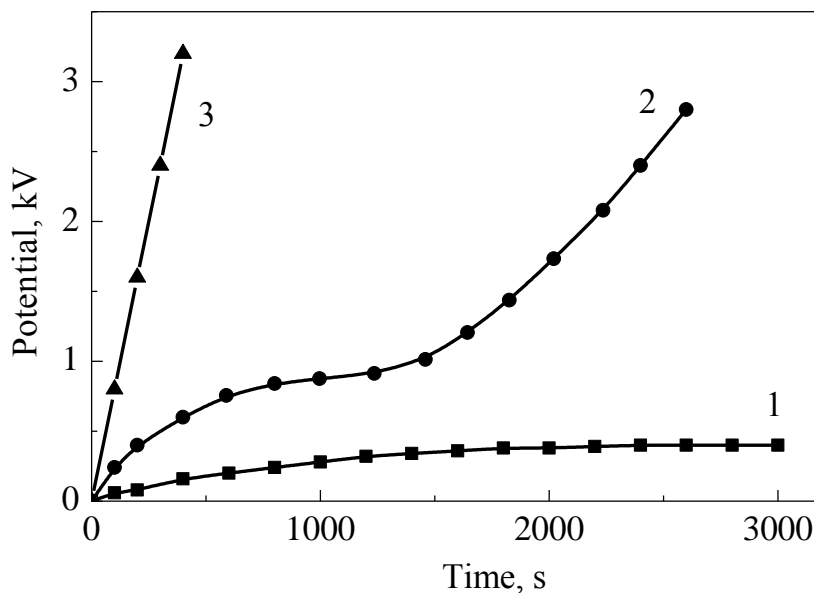


Fig.2.5 Kinetics of electret potential during poling of PVDF samples in a corona discharge at different values of the charging current ($\mu\text{A}/\text{m}^2$): 1 – 15, 2 – 80, 3 – 300.

Dependence of the electret potential on time in the process of PVDF films poling with a thickness of 26 μm at three values of the constant charging current is shown in Fig. 2.5. At small currents up to 10-20 $\mu\text{A}/\text{m}^2$ (curve 1 in Fig. 2.5), saturation of the electret potential is observed at values corresponding to the field strength below the coercive value, while the entire current at large times is a purely conduction current. At average values of the charging current (curve 2 in Fig. 2.5), there is a characteristic dependence of the electret potential on time consisting of three sections corresponding to three stages of the polarized state formation: the initial area of fast growth of the potential, the plateau and the second section of fast potential growing. At high values of the charging current (curve 3 in Fig. 2.5), the potential is swiftly increasing. If the current is maintained constant, an electrical breakdown of the film occurs. The same is observed at the end of the third stage when poling is performed by moderate currents [148].

Analysis of the curves in Fig. 2.5 was conducted taking into account the full-current equation, which can be written in the following form

$$i_o = \varepsilon_o \varepsilon \frac{\partial E(x,t)}{\partial t} + \frac{\partial P(x,t)}{\partial t} + gE(x,t), \quad (2.26)$$

where ε_o is the permittivity of a vacuum; ε is the dielectric constant, taking into account all processes of polarization, except the ferroelectric polarization; E is the field strength; P is the ferroelectric polarization; g is the effective conductivity considered as a constant value in the first approximation; i_o is the charging current density.

Neglecting the injection and integrating (2.26) in the thickness direction of the film x_o , we have

$$I_o = \frac{\varepsilon_o \varepsilon}{x_o} \frac{dV}{dt} + \frac{1}{x_o} \frac{dP}{dt} + g \frac{V}{x_o}, \quad (2.27)$$

where V is the electret potential for which the following expression corresponds

$$V(t) = \int_0^{x_o} E(x,t) dt. \quad (2.28)$$

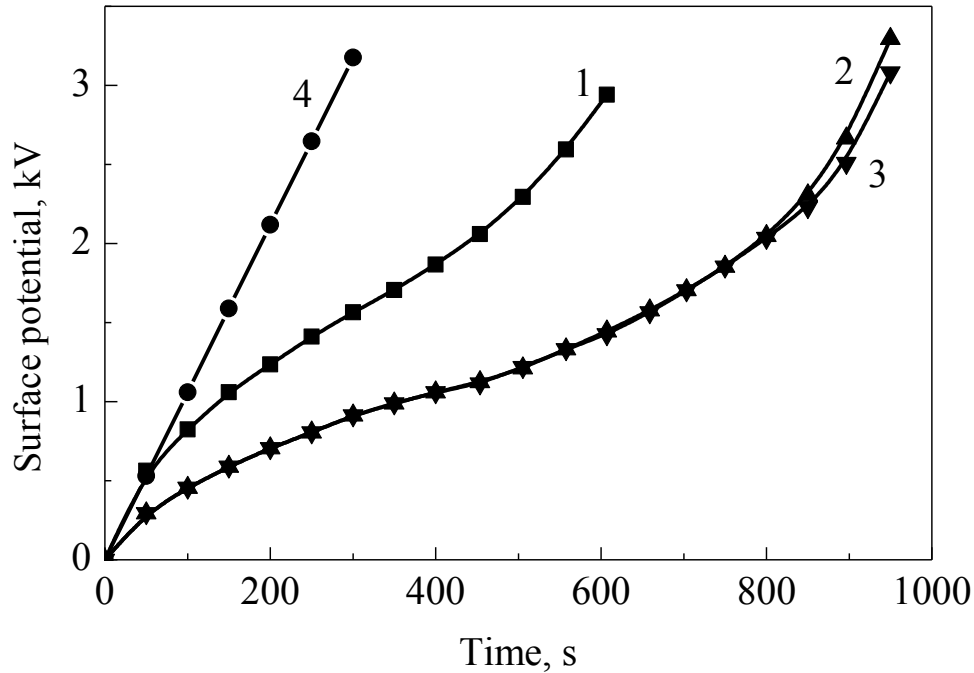


Fig. 2.6. Kinetics of PVDF film potential during primary poling (1), recharging (4), switching to negative (2) and positive (3) corona discharge.

The three components in the right side of (2.27) correspond to the capacitive, polarization and ohmic components of the full charging current.

The ferroelectric polarization is formed if the applied field is higher than the coercive field, that is, at high voltages. Therefore, at low current I_0 at the initial stage, the capacitive component dominates, and at full saturation, the full current is the conduction current (curve 1 in Fig. 2.5). The transition from rapid initial growth of voltage to a flat region on the curve 2 of Fig. 2.5 is naturally associated with the appearance of the polarization component of the current and the deceleration of the voltage increase as a result of this. After completing the polarization, the capacitive current component and the voltage on the sample are increased again. The correctness of the presented qualitative picture of poling is confirmed by a detailed analysis and is consistent with the results obtained in works [25,37,40].

It is interesting to compare graphs 1-3 in Fig. 2.6. In case of repeated poling (curve 4), the second part is absent corresponding to the formation of polarization, since it is already formed during initial poling (curve 1). As a result, the polarization component of the current is not present, and the electret potential is increasing rapidly with time. If polarity of the corona discharge changes, the direction of polarization is switched to the

opposite. The sloping area of the potential kinetics (curve 3) is elongated in comparison with initial poling (curve 1), because it is necessary for switching to provide the film twice as much charge as during initial poling. The type of the potential kinetics graphs in Fig. 2.5 and 2.6 clearly shows the ferroelectric nature of the investigated films. The shape of the curves is the same in case of PVDF and in case of the P(VDF-TFE) copolymer

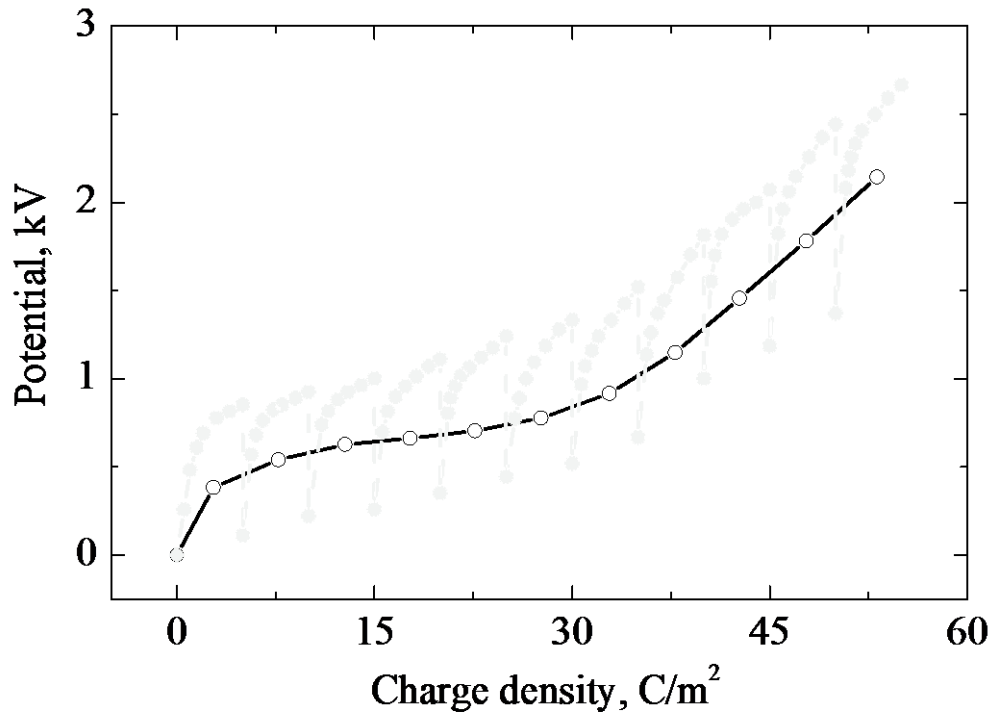


Fig. 2.7. Kinetics of the PVDF electret potential on the poling regions by rectangular current pulses and average voltage (solid line). Specific charge of one pulse is 24 mC/m².

The method of finding of relaxation processes parameters by using fractional poling in a corona discharge combines advantages of the DC corona charging method and the method of electret potential isothermal decay. As can be seen from Fig. 2.7, the general outlook of the poling curve when charged by rectangular current impulses has the same features as the curve of poling by the direct current (Fig. 2.5 and Fig. 2.6). The dynamics of the the surface potential increment during poling when the film obtains the same charge shows that the incremented potential in the region of the flat section of the curve is minimal. This is probably due to the fact that the main component of the charging current in this area is the polarization component. After completing the polarization at the third section, the potential increment increases almost twice, because the capacitance

component of the charging current increases. The potential relaxation between the current pulses is always smaller than its increasing during the charging stage. Namely this leads to increasing of the average electret potential of the film.

As poling increases, the difference between the increment of potential and its recession increases indicating the increase in the electret potential stability. This is also confirmed by the relaxation kinetics of the electret potential in the intervals between the charging current pulses.

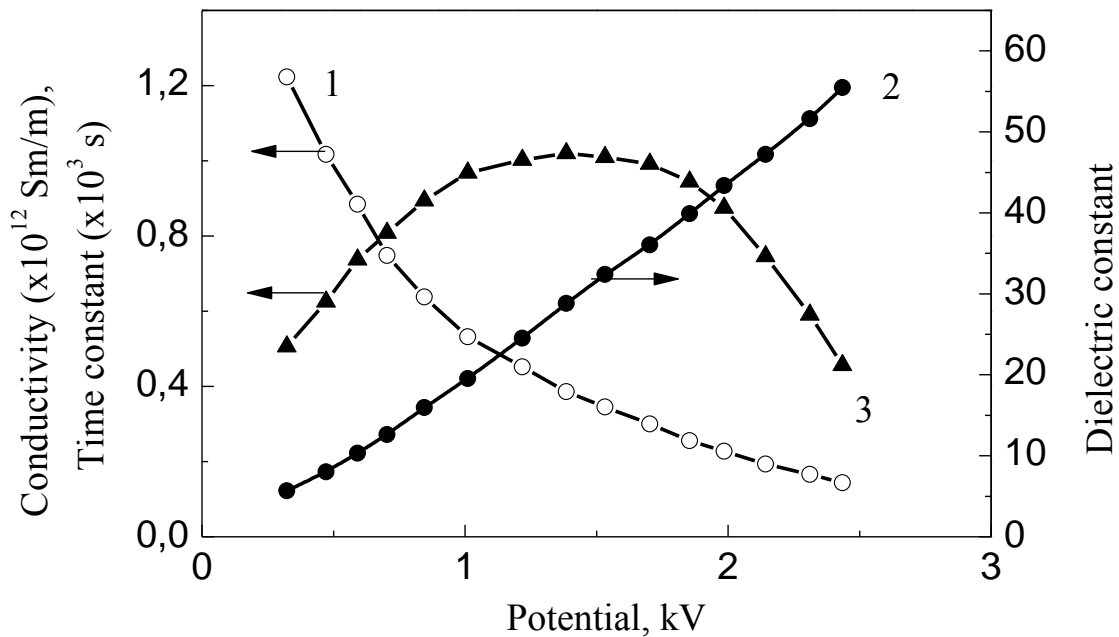


Fig. 2.8. Dependence of the effective conductivity (1), the time constant (2) and the dielectric constant (3) on the electret potential.

Such anomaly has never been observed in ordinary polar electrets, and this is probably due to decreasing of the apparent conductivity in the process of the polarization development.

Dependences of the relaxation time τ , dielectric constant ϵ and conductivity g on the average electret potential calculated according to our method are shown in Fig. 2.8.

It is known that the dielectric permittivity of PVDF and P(VDF-TFE) measured by standard methods at a frequency of 1 kHz in a low signal mode is 8-12 [73,151]. During poling, as follows from Fig. 2.8, ϵ increases reaching values of 40-50. The reason is that ϵ in the adopted model takes into account all types of polarization. Therefore, dielectric

constant ϵ increases during the ferroelectric polarization development, while transition from polarization to saturation is accompanied by decrease of ϵ to its usual values, as shown in Fig. 2.8.

Irreversible reduction of the effective conductivity during the polarization development, as shown in Fig. 2.8, may be related either to restriction of the charge carriers injection, or to the changing in the ratio between delocalized and trapped charges in the direction of increasing the concentration of the latter. Probable places of the charges localization are interphase boundaries where large-scale potential fluctuations similar to deep traps emerge with appearance of the high polarization in crystallites. It is also possible that the charges are trapped at the boundaries of macroscopic polarized regions, in which, according to Poisson's equation, the polarization gradient coincides with the space charge equal to the gradient (at zero field). It should be noted that the concept of the traps appearance during poling of PVDF was advanced earlier [35], but no assumptions were expressed about the mechanism of this phenomenon.

Thus, on the basis of the obtained experimental data, we can conclude that 1) the process of the polarized state development in a ferroelectric polymer poled at a constant charging current has a three-stage nature; 2) there is an irreversible decrease of the effective conductivity in the process of the ferroelectric polarization growth; 3) the dielectric constant increases during the formation of polarization, and then returns to the usual values that is consistent with the characteristic non-linear dependence of polarization on the field strength in ferroelectrics.

2.6. Phenomenological model of constant charge poling of FPs

High piezoelectric and pyroelectric activity of PVDF and its copolymers electrets is due to the presence of high residual polarization [151]. In contrast to the polar thermoelectrets, in which the polarization is "frozen" when the films are cooled in a polarizing field, the residual polarization in the PVDF has a ferroelectric nature [68]. This feature was not sufficiently taken into account in the study of such films poling. In a series of papers [62,134,178], the nonlinear dependence of polarization on the electric field strength typical for ferroelectrics was considered in the phenomenological model of PVDF film poling. At the same time, a number of assumptions were made in [134] for

the sake of simplification contradicting to experimental facts. This concerns the field and polarization homogeneity in the film volume, presence and constancy of the PVDF conductivity, the ohmic regime in the gap between the control grid and the sample in case of a corona discharge.

In fact, it is known that the field and polarization are essentially heterogeneous [35], the effective conductivity decreases with increasing of the ferroelectric polarization [154], and the implementation of the Ohm law in dielectrics, especially at high fields, is not confirmed in the experiment.

In the model of the ferroelectric polymer films poling developed by us [150], an important role is given to the injected charge carriers. Being trapped in deep traps, these carriers create a heterogeneous distribution of the space charge and the electric field in the thickness direction of the film. In contrast to the traditional approach that involves analyzing the current response to a stepwise change of the applied voltage, we consider the case of stabilizing the charging current. This approach has several advantages in the study and analysis of transient processes.

Consider the one-dimensional charging mode (thin film) with the x axis directed in depth of the specimen. The $x = 0$ point is on the injecting electrode, which can be either a real metal electrode, or a virtual one, such as the bare surface subjected to action of the discharge ions in case of corona discharge poling.

The second (reverse) electrode is grounded. Since the charging current is stabilized, the electret potential is an experimentally measured parameter, kinetics of which reflects the poling features.

We believe that injection is monopolar and its level is high enough to ignore the intrinsic conductivity of the polymer. It follows from the comparison of microscopic and effective mobility that the concentration of the free carriers is considerably fewer than the concentration of the trapped charges. At the same time, given the disordered structure of the polymer and presence of the amorphous phase, we believe that the degree of the traps filling is far from saturation.

The electric displacement is represented in the following form

$$D = \varepsilon_o \varepsilon E' + P', \quad (2.29)$$

where ε is the dielectric permittivity taking into account all reversible polarization processes; ε_0 is the permittivity of a vacuum; E' is the field strength; P' is the high polarization of the ferroelectric type.

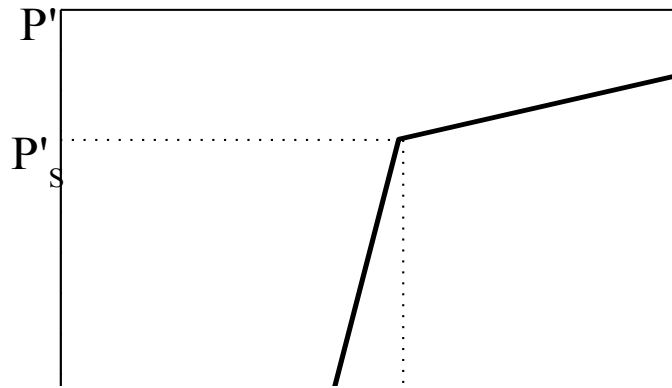


Fig. 2.9. Dependence of polarization on the field strength, which was used in calculating the model of the polarized state development in PVDF.

The nonlinear dependence of polarization P' on the field strength E' for ferroelectrics has a form of a hysteresis loop [62,68,178] in case of the periodic change in magnitude and direction of the field. In case of initial poling, the dependence $P'(E')$ consists of three sections. As long as the field is smaller than the coercive value E_k , the polarization is zero.

Then it sharply grows in the second section passing to the state of almost full saturation in the third section. The dependence $P'(E')$ assumed by us is schematically shown in Fig. 2.9 and analytically it looks like:

$$P' = \begin{cases} 0; & E' \leq E_k'; \\ \varepsilon_0 \varepsilon' (E' - E_k'); & E_k' \leq E' \leq E_s'; \\ \varepsilon_0 \varepsilon'' (E' - E_s'); & E_s' \leq E', \end{cases} \quad (2.30)$$

where ε' and ε'' are dynamic dielectric permeabilities.

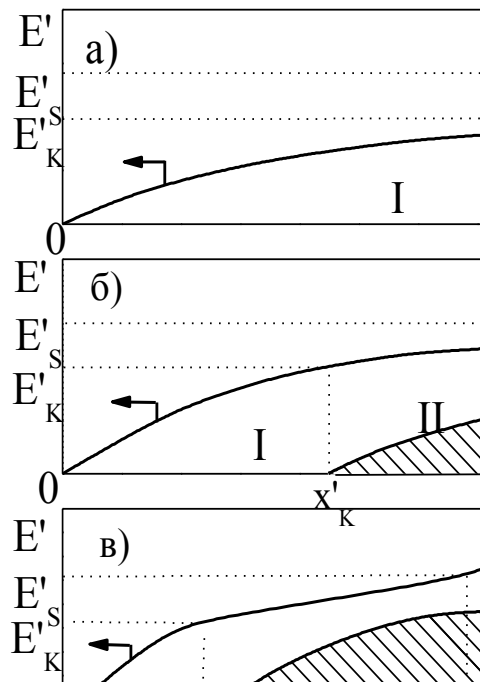


Fig. 2.10. Schematic distribution of field strength (E') and polarization (P') along the thickness of the film at different moments of time during the first (a), second (b) and third (c) stages of poling by direct current.

Since the switching time of polarization in polymer ferroelectric films is in the order of microseconds [68], and the time constant of increasing the voltage with stabilized charging current is hundreds of seconds, one can not take into account the delay of P' in relation to E' , that is, to consider the quasi-stationary polarization mode.

Taking into account the above assumptions, the charging process is divided into three stages (phases) (Fig. 2.10). In the first phase, the field is everywhere in the film ($0 \leq x' \leq h$) is smaller than the critical E'_q , so $P'(x', t') = 0$. In the second phase, the field near the rear electrode is higher than the coercitive value. Polarization is generated there and the zone II is formed, which expands with time of poling. In the third phase, in the part of the film where the field is higher than the critical value E'_s , the zone III is formed. The second phase begins at the moment t_o determined from the condition $E'(x_o, t_o) = E'_k$, while the third stage commences at the moment t'_s corresponding to the equation $E'(x_o, t'_s) = E'_s$.

In the beginning of the coordinate, the injection condition [112] is fulfilled, that is, $E'(0, t') = 0$. The equations $E'(x'_k, t') = E'$ and $E'(x'_s, t') = E'_s$ are valid at the boundaries x'_k and x'_s between the zones.

Let us consider the features of each charging phase and get an expression for the kinetics of the electret potential at a constant charging current by solving the transport equation of charges in all zones of the film. The adequacy of the model is analyzed by comparing the calculated and experimental kinetics when charging PVDF films in the corona discharge. From this comparison, we will estimate the influence of mobility on the trapping time, the coercive field, the saturation polarization, the dynamic dielectric permittivity of the films, and some other parameters.

The first phase. Given the slow changing of the field near the injecting electrode, we will assume that the conduction current is much larger than the displacement current. We will write the equations characterizing the transfer and trapping of charges, as well as the kinetics of the electret potential. We assume that Ohm's law is valid in the initial phase at low voltages, that is, the charging current density i_o is proportional to the concentration of free carriers n_c , their mobility μ , and the magnitude of the field strength E_1'

$$en_c\mu E_1' = i_o; \quad n_t \gg n_c; \quad (2.31)$$

In presence of excess (injected) charges n_t , the electric field gradient appears, and the relation between these quantities is determined by the Poisson equation

$$\varepsilon_o\varepsilon \frac{\partial E_1'}{\partial x'} = en_t; \quad 0 \leq x' \leq x_o \quad (2.32)$$

We assume that the trapping of charges on deep traps corresponds to the first order kinetics

$$\frac{\partial n_t}{\partial t'} = \frac{n_c}{\tau_o}; \quad 0 \leq t' \leq t_o; \quad (2.33)$$

The expression for the electret potential has the following form

$$U'(t') = \int_0^{x_o} E_1' dx'. \quad (2.34)$$

In the equations (2.30) - (2.34) the following notations are adopted: x_o is the thickness of the film; e is the elementary charge; i_o is the constant charging current density; μ is the microscopic mobility; n_c and n_t are concentrations of free and trapped charge carriers; τ_o is the carrier trapping time; $U'(t')$ is the voltage on the film (electret potential).

As can be seen from equation (2.33), the model assumes existence of only deep traps. The validity of such assumption will be discussed when comparing estimated and experimental data.

From equations (2.30) - (2.34) we obtain

$$\varepsilon_o \varepsilon \mu \tau_o E_1' \frac{\partial^2 E_1'}{\partial x' \partial t'} = i_o. \quad (2.35)$$

The solution of equation (4.7) has the form

$$E_1' = 2 \sqrt{\frac{i_o x' t'}{\varepsilon_o \varepsilon \mu \tau_o}}. \quad (2.36)$$

From (2.34) and (2.36) we obtain the final expression for the calculated kinetics of the potential in the first phase

$$U'(t') = \frac{4}{3} \sqrt{\frac{i_o x_o^3 t'}{\varepsilon_o \varepsilon \mu \tau_o}}. \quad (2.37)$$

The second phase. In the second phase of charging the film consists of two zones (Fig. 2.10). In zone I ($0 \leq x' \leq x_k'$), the equation (2.37) is still valid. In zone II ($x_k' \leq x' \leq x_s'$), due to the rapid growth of polarization, it is not possible to neglect the displacement current, as we did in the first phase. In addition, it is advisable to take into

account the effect of the high field on the mobility. It was shown in [179] that the charge carriers range before their trapping in polytetrafluoroethylene films (PTFEs) does not depend on the field, which is a consequence of the inverse dependence of μ on E' and the constancy of the carriers velocity. Polymers PTFE and PVDF have much in common. They are linear-chain polymers and both belong to the ethyl series of fluoroplastics having a semi-crystalline structure with an amorphous matrix in which crystallites are scattered. The chemical formula of PVDF ($-\text{CH}_2-\text{CF}_2-$) differs from the PTFE formula ($-\text{CH}_2-\text{CH}_2-$) only by two atoms of fluorine in repeating units instead of two hydrogen atoms. Given the structural and chemical community of PTFE and PVDF, we can assume that in PVDF the mode of constant velocity of carriers and constancy of the range before their trapping is realized.

When writing the transport of carrier equation in the zone II, it is necessary to take into account the presence of polarization. In addition to the current of conductivity, there is still a displacement current, which has two components: capacitive and polarization ones. Then one can write

$$\varepsilon_o \varepsilon \frac{\partial E_2'}{\partial t'} + \frac{\partial P'}{\partial t'} + en_c V_o = i_o, \quad (2.38)$$

where V_o is the constant velocity of the carriers. In the Poisson equation, a term corresponding to the gradient of polarization should be added

$$\varepsilon_o \varepsilon \frac{\partial E_2'}{\partial x'} - \frac{\partial P'}{\partial x'} = en_t, \quad (2.39)$$

and the initial and boundary conditions will have the form

$$\frac{\partial n_t}{\partial t'} = \frac{n_c}{\tau_o}; \quad t_o \leq t' \leq t_s'; \quad x_k' \leq x' \leq x_o; \quad (2.40)$$

$$E_2'(x_o, t_o') = E_k'; \quad E_2'(x_k', t') = E_k'; \quad E_2'(x_o, t_s') = E_s', \quad (2.41)$$

From expressions (2.38) - (2.40) we obtain

$$\varepsilon_o(\varepsilon + \varepsilon') \frac{\partial E_2'}{\partial t'} + V_o \tau_o \varepsilon_o(\varepsilon + \varepsilon') \frac{\partial^2 E_2'}{\partial x' \partial t'} = i_o. \quad (2.42)$$

We will solve the equation (2.42) by pre-introducing the following dimensionless quantities

$$t = \frac{t'}{t_o}; \quad x = \frac{x'}{x_o}; \quad \alpha = \frac{V_o \tau_o}{x_o}; \quad E = \frac{\varepsilon_o(\varepsilon + \varepsilon')}{i_o t_o} E'; \quad U = \frac{\varepsilon_o(\varepsilon + \varepsilon')}{i_o x_o t_o} U'. \quad (2.43)$$

Then the equation (2.42) with the initial and boundary conditions takes the form

$$\frac{\partial E_2}{\partial t} + \alpha \frac{\partial^2 E_2}{\partial x \cdot \partial t} = 1 \quad x_k \leq x \leq 1; \quad 1 \leq t \leq t_s; \quad (2.44)$$

$$E_2(1,1) = E_k; \quad E_2(x_k, t) = E_k; \quad E_2(1, t_s) = E_s.$$

Solution of the equation (2.44) are sought in the following form

$$E_2 = t - F(t) \exp\left(-\frac{x - x_k}{\alpha}\right) + A, \quad (2.45)$$

where the function $F(t)$ and constant A are found from the condition $E(x_k, t) = E_k$ and the continuity of the charge on the rear electrode during the transition from the first phase of charging to the second phase:

$$F(t) = t + \alpha\beta - 1; \quad (2.46)$$

where β is the dimensionless coefficient calculated by the following formula

$$\beta = \left(1 + \frac{\varepsilon'}{\varepsilon}\right) \sqrt{\frac{\varepsilon_o \varepsilon x_o}{i_o t_o \mu \tau_o}}. \quad (2.47)$$

Equation for the boundary x_k between zone I and zone II is found from equation (2.42) taking into account the expressions (2.45) and (2.47):

$$x_k(t) = \frac{1}{t}. \quad (2.48)$$

The final expression for kinetics of the potential in the second phase of charging has the following form

$$U(t) = \int_0^{x_k} E_1 dx + \int_{x_k}^1 E_2 dx = \frac{4\beta}{3t} + \left(1 - \frac{1}{t}\right)(t + E_k + \alpha\beta - 1) - \alpha(t + \alpha\beta - 1) \left[1 - \exp\left(-\frac{t-1}{\alpha \cdot t}\right)\right] \quad (2.49)$$

where E_I is the field strength in zone I obtained by normalization of the expression (2.37) in accordance with the formulas (2.44) and (2.48).

The third phase. The third phase commences at a time t_s , which can be found by solving the following equation

$$(t_s + \alpha\beta - 1) \left[1 - \exp\left(-\frac{t_s - 1}{\alpha \cdot t_s}\right)\right] = E_s - E_k. \quad (2.50)$$

The equation for the boundary x_s is found from the expression (2.50) after the substitution of the condition $E(x_s, t) = E_s$;

$$x_s(t) = \frac{1}{t} - \alpha \ln \left[1 - \frac{E_s - E_k}{t + \alpha\beta - 1}\right]. \quad (2.51)$$

Expression for the full current in the zone III differs from the equation (2.42) in zone II only by the value of the dynamic dielectric constant

$$\varepsilon_o (\varepsilon + \varepsilon'') \frac{\partial E_3'}{\partial t'} + V_o \tau_o \varepsilon_o (\varepsilon + \varepsilon'') \frac{\partial^2 E_3'}{\partial x' \partial t'} = i_o. \quad (2.52)$$

Supplementing the formula (2.45) with the coefficient $\gamma = \frac{\varepsilon + \varepsilon'}{\varepsilon + \varepsilon''}$ and carrying out normalization, we obtain

$$\frac{\partial E_3}{\partial t} + \alpha \frac{\partial^2 E_3}{\partial x \partial t} = \gamma; \quad (2.53)$$

$$E_3(x_k, t) = E_k; \quad E_3(1, t_s) = E_s; \quad E_3(x_s, t) = E_s$$

We solve the equation (2.51) in the following form

$$E_3 = \gamma \cdot t - \varphi(t) \exp\left(-\frac{x - x_s}{\alpha}\right) + B, \quad (2.54)$$

where the function $\varphi(t)$ and constant B are found from the condition of the field constancy at the boundary x_s and the continuity of the charge at the rear electrode

$$\varphi(t) = \gamma(t - t_s) - E_s + E_k + t_s + \alpha\beta - 1; \quad (2.55)$$

$$B = E_k - t_s(\gamma - 1) + \alpha\beta - 1. \quad (2.56)$$

The final expression for kinetics of the potential in the third phase of the charging consists of three parts according to the number of zones in the film [150]:

$$\begin{aligned}
U(t) = & \int_0^{x_k} E_1 dx + \int_{x_k}^{x_s} E_2 dx + \int_{x_s}^1 E_3 dx = \frac{4\beta}{3t} + \left(x_s - \frac{1}{t}\right)(t + E_k + \alpha\beta - 1) - \\
& - \alpha(t + \alpha\beta - 1) \left[1 - \exp\left(-\frac{x_s t - 1}{\alpha \cdot t}\right)\right] + (1 - x_s)[\gamma(t - t_s) + t_s + E_k + \alpha\beta - 1] - \\
& - \alpha[\gamma(t - t_s) - E_s + E_k + t_s + \alpha\beta - 1] \left[1 - \exp\left(-\frac{1 - x_s}{\alpha}\right)\right]
\end{aligned} \tag{2.57}$$

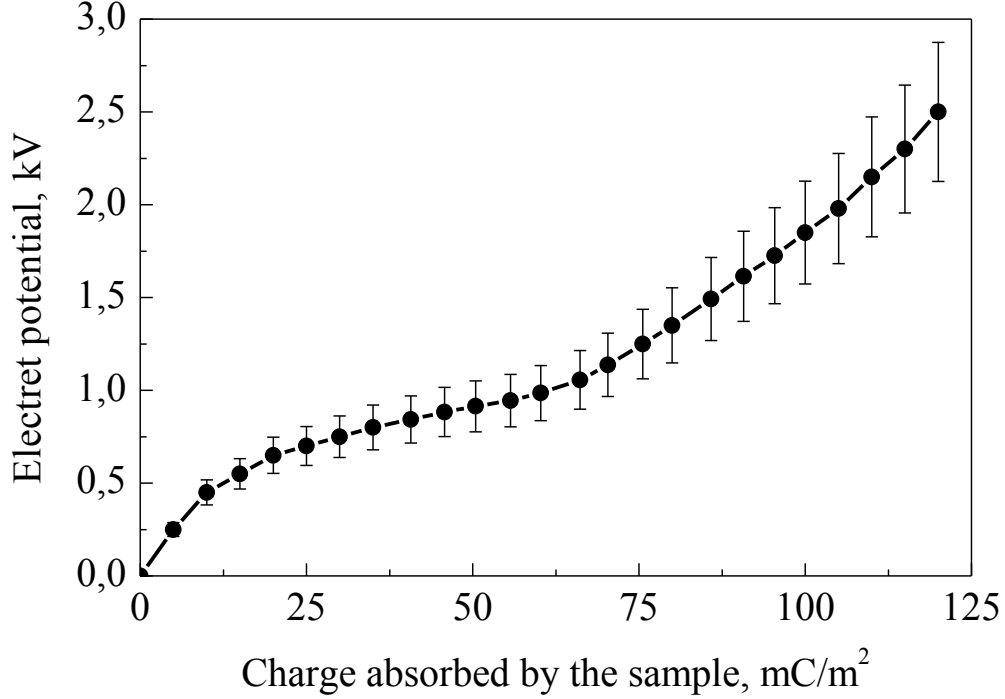


Fig. 2.11. Experimental dependence of the PVDF electret potential on the obtained charge and the calculated curve at $i_o = 100 \mu\text{A}/\text{m}^2$.

Fig. 2.11 shows the generalized experimental kinetics of the potential when PVDF is poled in the negative glow discharge. It is based on the data from more than one hundred experiments.

The calculated curve is also shown. All points fall within the range of experimental values confirming the fundamental correctness of the proposed model.

Numerical values of the parameters used in the calculation of the electret potential kinetics are presented in Tabl. 2.1.

Table 2.1

Numerical values of parameters during the calculating of the electret potential

Parameter	Value	Parameter	Value	Parameter	Value
$i_o, \mu\text{A}/\text{m}^2$	100	t_o, s	250	$\mu\tau_o, \text{m}^2/\text{V}$	$1.3 \cdot 10^{-11}$
$x_o, \mu\text{m}$	25	t_s, s	600	$v_o \tau_o, \text{m}$	$6 \cdot 10^{-6}$
ε	10	α	0,23	$E_c', \text{MV}/\text{m}$	42
ε'	725	β	5,47	$E_s', \text{MV}/\text{m}$	51.5
ε''	45	γ	13,3	$P_s', \text{C}/\text{m}^2$	0.061

Chapter 3. Switching of polarization in ferroelectric polymers

3.1. Method of studying the ferroelectric polarization switching

The switching experiments were performed using the set-up shown in Fig. 3.1. The constant voltage $U_o = 2 \text{ kV}$ was applied from the high-voltage power supply connected through a high-voltage capacitor of sufficiently large capacity ($0.5 \mu\text{F}$) to withstand the necessary switching currents. The actual switching was carried out with the help of the electronic high-power push-pull switch. There was an opportunity to stop the switching process within a very short time of about 50 ns.

To perform the switching (polarization reversal), the voltage U_o was applied in the direction opposite to the direction of initial poling for a definite time from 10^{-6} to 200 s set by a low-voltage pulse generator. The voltage of 2 kV was applied again to the sample for 200 seconds after each polarization switching to convert the sample to the original polarized state (conditioning).

The measuring circuit consisted of a sample, a resistor of 1 k Ω for limiting the current, and a measuring capacitor with a capacity of 0.2 μF . The voltage drop across the capacitor was recorded using the digital oscilloscope connected through a high impedance amplifier with an internal resistance $R_{in} = 10^{13} \Omega$. The introduction of this amplifier was necessary to prevent the loss of charge and voltage during the measurement. The charge leakage from the measuring capacitor was measured and was found to be neglected even at the maximum measurement time.

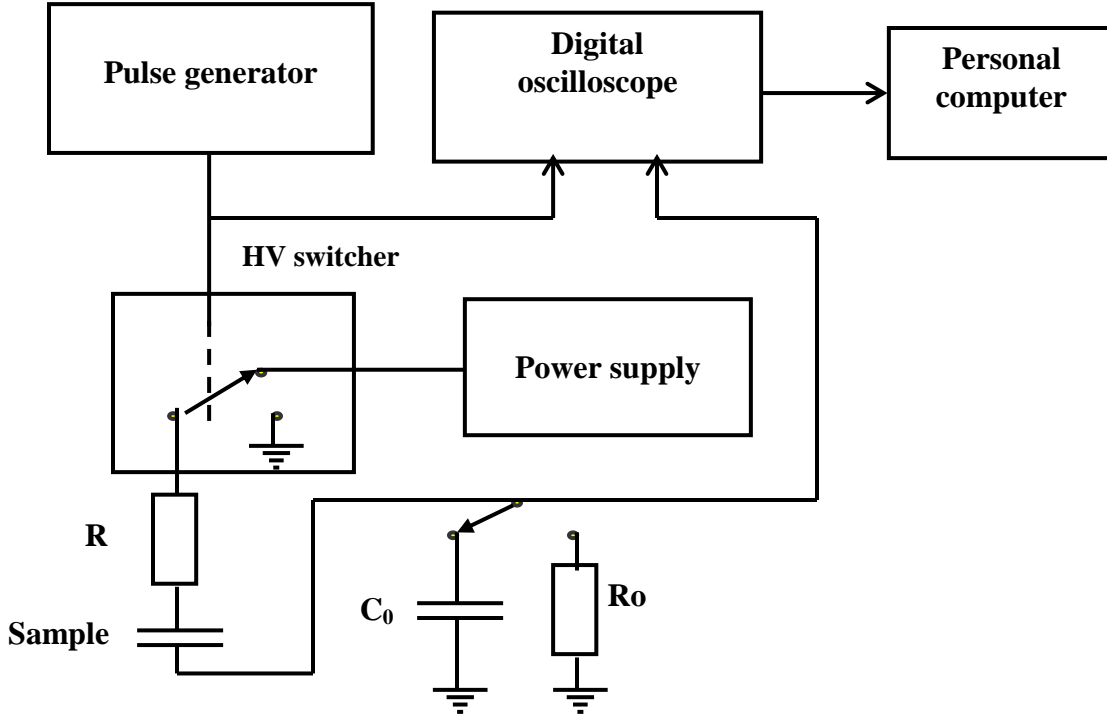


Fig. 3.1. Block diagram of the set-up for measuring ferroelectric polarization switching.

The voltage on a serial capacitor was used to determine the total displacement D_1 , which included the reversible components and a ferroelectric component of polarization, as well as that caused by the current flowing through the sample due to its non-zero conductivity. After each switching and shutdown in the short-circuited state, re-poling was performed in the direction of switching. The corresponding displacement curves D_2 contained all components of D_1 except for the switched ferroelectric polarization. Therefore, the average ferroelectric polarization P_m was calculated as the difference between D_1 and D_2 .

In the mode of measuring the charging current, instead of the measuring capacitor, the calibrated measuring resistance R_0 (Fig. 3.1) was connected in series with the sample. Then, the voltage drop at R_0 was proportional to the charging current.

3.2 Switching of the ferroelectric polarization in PVDF

It was shown In the works of von Seggern and Fedosov [175,178] that the development of polarization in PVDF takes place in two stages, and the second (slow)

stage is controlled by the conductivity. Thus, the discrepancies between the expected and actually measured switching times were explained. However, in case of the polarization switching, there is still no clear understanding of what physical processes are involved. Therefore, it seemed timely to reconsider some commonly accepted points of view on the processes of the polarization switching in ferroelectric polymers and, in particular, on the role of conductivity and space charge in these processes.

Experiments were carried out on a biaxially stretched PVDF films having thickness of 12.5 μm with aluminum electrodes of 0.2 cm^2 area deposited by evaporation and condensation in vacuum. The samples were poled at $U_o = 2$ kV during $\tau = 200$ s and short-circuited for 15 minutes.

In order to compare the measured P_m and the calculated values of the ferroelectric polarization, it should be taken into account that only 70% of crystallites contain a ferroelectric β -phase, while the crystallinity of PVDF is about 50%. Since P_m is the mean value throughout the sample thickness, the relationship between the measured polarization P_m and calculated polarization P has the form $P_m = 0.35 \cdot P$. Accordingly, for estimation of the ferroelectric polarization on the basis of the measured value P_m it is necessary to use the following ratio $P = 2.86 \cdot P_m$.

In the literature on polarization switching in PVDF and other ferroelectric polymers, the concept of the field-dependent switching time τ is widely used. Dependence of the switching time from the field strength is calculated using the following phenomenological formula [67]:

$$\tau = \tau_o \exp\left(\frac{E_a}{E}\right) \quad (3.1)$$

where $\tau_o \approx 20$ ns and $E_a \approx 1.2$ GV/m. It follows from (3.1) that the switching time in the field of 160-200 MV/m should be about 10 μs . The actual dependence of the polarization switching time (Fig. 3.2) measured by us shows that for only, only 17% of the polarization is switched for 10 μs . A half of the polarization switches in 200 μs , and no full switching is observed even after 20 seconds of the switching voltage application. Thus, the difference between the expected and actual switching time is 10^6 times. Apparently, as in case of initial poling, the slow-moving processes associated with the conduction and the charge accumulation play an important role.

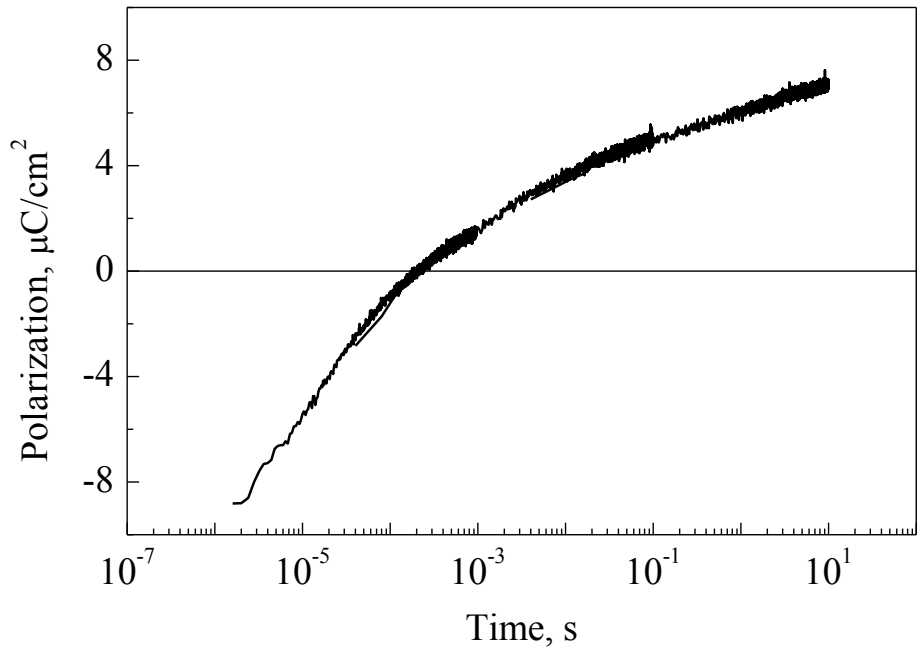


Fig. 3.2. Experimental curve of the PVDF polarization switching time dependence under influence of the constant voltage of 2 kV ($E = 160$ MV/m).

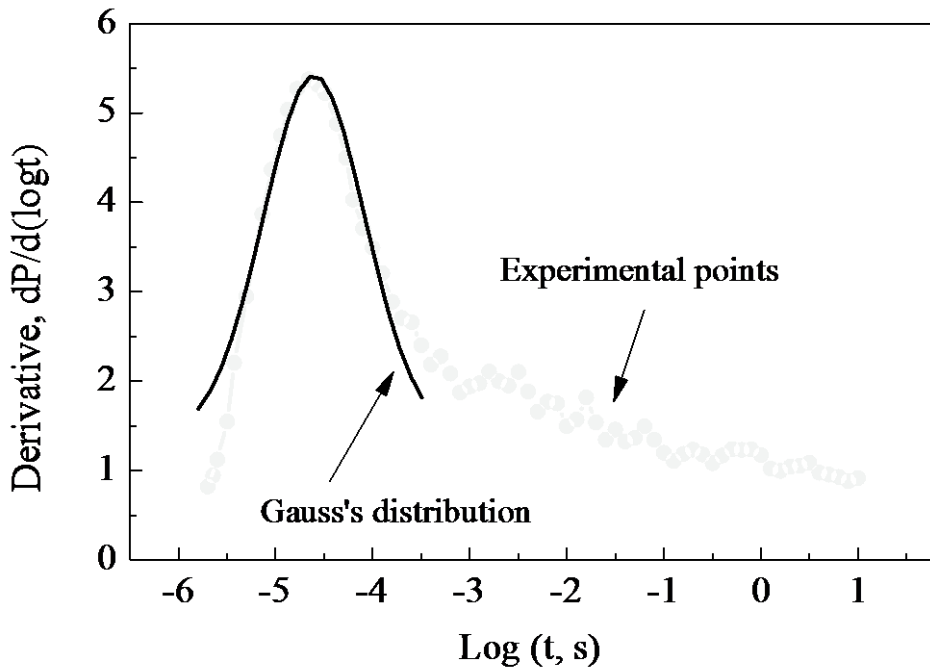


Fig. 3.3. Function $P(\log t)$ derived from the experimental curve of the polarization switching at a constant voltage of 2 kV, which illustrates presence of a fast and a slow phases of the polarization switching.

Fig. 3.3 shows a derivative of the $P(\ln t)$ function that can be considered as a kind of

the switching current. From the graph, it is evident that the switching current consists of two parts corresponding to two phases of the switching process. The first fast phase is completed at a time of about 100 μs for which less than 50% of polarization is switched. The second slow phase is clearly visible in the form of a long tail captivating five orders of magnitude from 100 μs to 10 sec. If we compare the curve of the polarization switching with the kinetics of its formation (initial poling), then there is no sharp transition from the first phase to the second phase during the switching. Besides, the switching rate is higher compared with the initial development of the polarization [148].

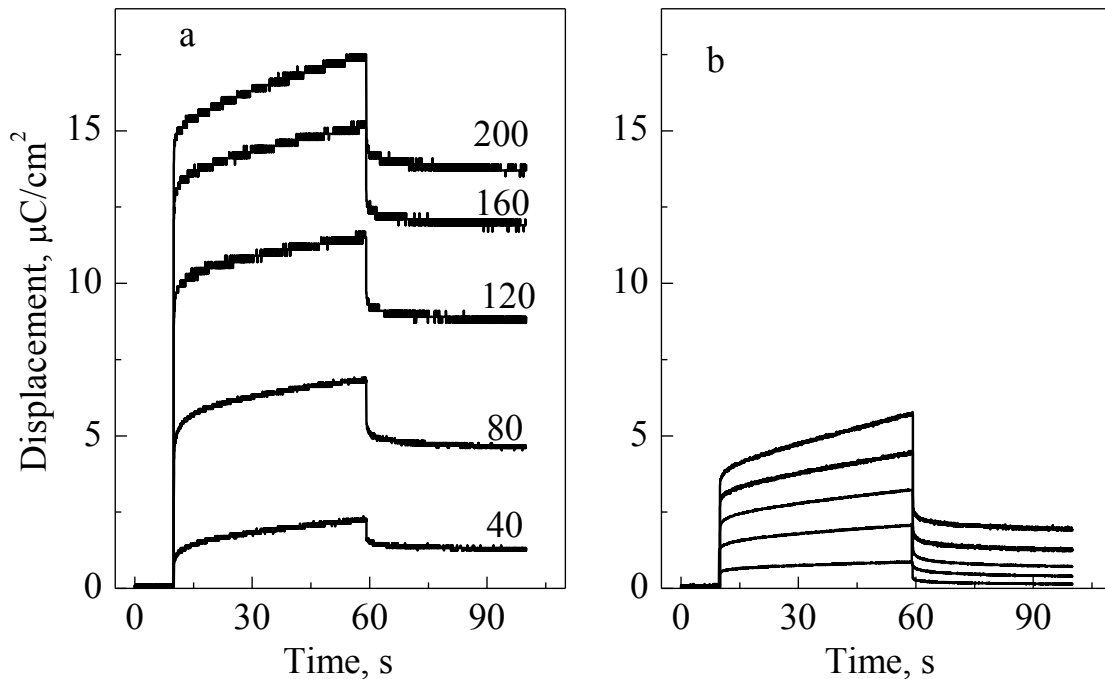


Fig. 3.4. Dependence of the total electric displacement during the polarization switching by voltage pulses of 50 s duration at different field strength (a) and during repeated influence of the same voltage pulses (forward poling) (b).

In the study of switching processes, it is important to find the dependence of the switched polarization on the value of the switching field strength and on the time of the switching voltage application. Several series of experiments were conducted in which these dependencies were found experimentally. As an example, in Fig. 3.4 shows the graphs of the electrical displacement during switching in different electric fields for 50 s and with the repeated application of the same fields within the same time on a fully polarized sample, but with a voltage polarity that is opposite to that at what the polarization was switched. Such series of experiments were conducted for different

switching times, starting with $0.5 \mu\text{s}$, and according to these data, the values of the switched polarization were calculated (Fig. 3.5). It is seen from the graph that the magnitude of the switched polarization is a complex function of the field and time. The obtained data are practical, since they allow one to select the mode of the polarization switching depending on the conditions. For example, one and the same magnitude of the polarization can be switched by using different combinations of the field strength and the switching time.

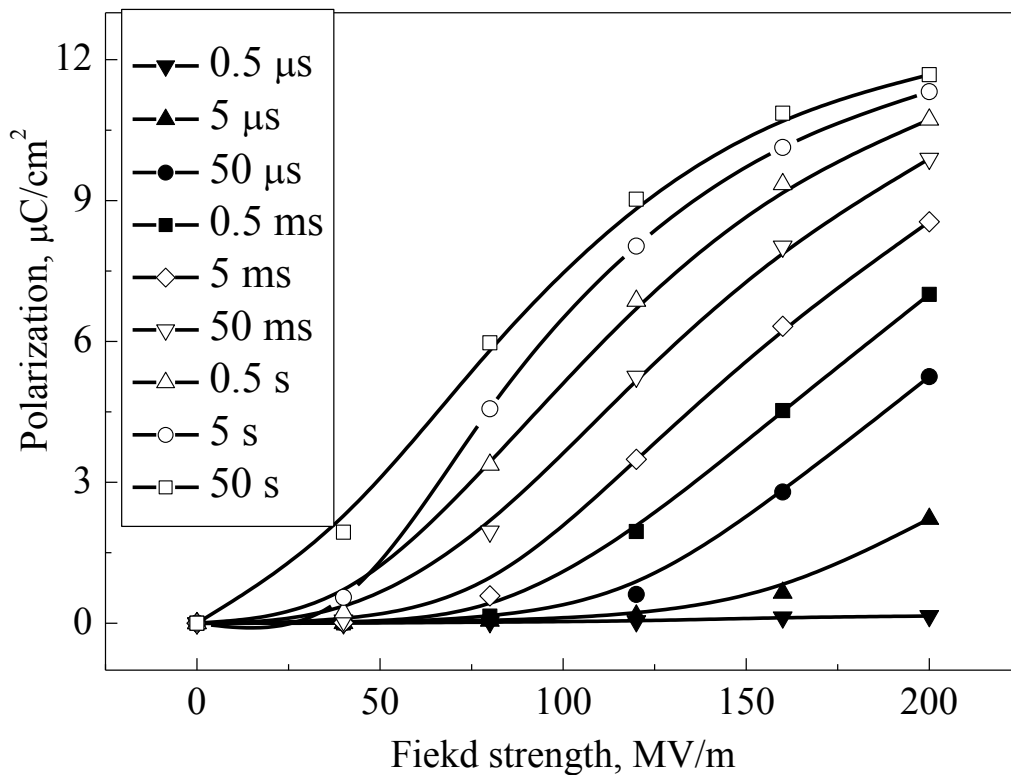


Fig. 3.5. Dependence of the polarization switching in PVDF on the field strength at a different duration of switching voltage pulses from $0.5 \mu\text{s}$ to 50 s .

3.3. Features of polarization switching in copolymers

Vinylidene fluoride copolymers with tetra-fluorethylene P(VDF-TFE) and trifluoroethylene P(VDF-TrFE) have several advantages over PVDF. PVDF crystallizes from the melt in a nonpolar α -phase. In order to obtain the ferroelectric β -phase in PVDF crystallites, uniaxial or biaxial stretching is performed, as a result of which a significant part of the α -phase (but not all) is converted into β -phase. In the process of

such a stretching, there are mechanical stresses in the film, which can cause deformation of the film or even its shrinkage.

Copolymers P(VDF-TFE) and P(VDF-TrFE) during crystallization from the melt immediately form the β -phase, therefore the need for orientational stretching disappears. In addition, the crystallinity of PVDF is about 50%, and it cannot be increased with further processing. Therefore, the average polarization is at least two times smaller than the polarization in crystallites. At the same time, the crystallinity of the copolymers can be 90% or more that firstly increases the average value of the polarization and, secondly, reduces the negative effect of the amorphous phase on the development of polarization in the crystallites. That is why the switching rate of polarization in copolymers is much higher than in pure PVDF polymer.

The disadvantages of copolymers are the complex technology of their preparation and the dependence of the Curie temperature on the composition. In PVDF, this temperature is not experimentally determined, because it is above the melting point ($> 180\text{ }^{\circ}\text{C}$). In the copolymer, the Curie point corresponds to lower temperatures, which limits utilization of the copolymers at high temperatures. The most studied is a copolymer P(VDF-TrFE), while only a few studies are devoted to the properties of P(VDF-TFE). That is why our task was to study the peculiarities of the formation and relaxation of the polarized state in P(VDF-TFE).

According to the technology developed for the study of PVDF, a series of experiments on switching polarization in P(VDF-TFE) was performed. The experiments consisted in initial poling of the films in a high field for a long time (about 200 second) to obtain a nominally fully polarized state. Subsequently, pulses of the switching voltage of different duration from $10\text{ }\mu\text{s}$ to 100 s were applied. After each switching, the fully polarized state was restored (conditioning) and, without changing the polarity of the voltage, the corresponding pulse of the same duration was again applied. The difference in displacements in the first and the second cases gives the kinetics of the ferroelectric polarization switching.

Comparison of data obtained on copolymer and PVDF allowed drawing the following conclusions:

- 1) The value of the switched polarization in copolymer P(VDF-TFE) is much higher than in PVDF.
- 2) Full polarization switching in the copolymer takes place for about 10^{-4} s, while

switching in PVDF occurs smoothly and the saturation is not observed even after 100 s of the field application.

3) The displacement graphs in case of the copolymer have almost rectangular shape indicating the absence of an unstable part of the dipole polarization, the presence of which is characteristic for PVDF.

4) The hop-like displacement changes when the applied voltage is switched on and off in P(VDF-TFE) is much smaller than in PVDF indicating a lower effective copolymer dielectric constant compared to PVDF.

These features are probably due to the lack of the amorphous phase influence and the lower conductivity. Since the processes of the polarization switching proceed very quickly, the method of measuring current on the reference resistor connected in series with the sample [149].

In the first microseconds of the switching voltage application, a characteristic shape of a full current curve was observed with the presence of a flat part or even a weak maximum. If we subtract the exponentially decreasing capacitive component of the current from the full current, then we obtain the current responsible for the polarization switching. This current has a maximum at about 3 μ s. It is precisely this value that can be considered as the switching time of polarization in P(VDF-TFE).

For more complete picture of the polarization switching in the copolymer and its dependence on the switching field strength and on the time of the voltage application, several series of experiments were carried out. The electrical displacement was investigated under the action of pulses of 140 MV/m switching field with duration from 5 μ s to 50 s applied to a completely polarized sample P(VDF-TFE) and the same pulse of re-poling, as well as the kinetics of the ferroelectric polarization development. These measurements allowed constructing the kinetics of the ferroelectric polarization switching. The dependence of the switched polarization on the field strength in P(VDF-TFE) was calculated for different duration of switching voltage pulses.

A comparison with the corresponding dependences for PVDF showed that the coercive field in the copolymer has the same order of magnitude as in PVDF (about 50 MV/m). The results obtained are practical because they allow one to select switching options. For example, the application of fields below 60 MV/m is inappropriate, because the switched polarization is very small. At the same time, when electric fields exceeding 120 MV/m are used, the switching occurs very quickly and there is no significant

difference in application of 5 ms, 50 ms or even 5 seconds pulses.

3.4. Model of the polarization switching in PVDF at a constant voltage

In the studies of Fedosov and von Seggern on the dynamics of polarization in PVDF in the process of poling by pulses of constant voltage and short circuiting [62,174,178], importance of conductivity and formation of the space charge were proved. In the above mentioned paper, the authors have successfully applied an approach that considers PVDF as a material consisting in two phases, namely, the ferroelectric phase and the amorphous phase.

The sample has been modeled by using a layered structure with alternating ferroelectric crystalline and paraelectric amorphous layers (Fig. 3.6). We also apply this approach to simulate the polarization switching process in PVDF.

We are going to show the important role of charges on a concrete example. The equations for the applied voltage U_o and the electric displacement D continuity at the boundary between the paraelectric amorphous phase (index 1) and the ferroelectric crystalline phase (index 2) without taking into account the conductivity have the following form

$$D = \varepsilon_o \varepsilon_1 E_1 = \varepsilon_o \varepsilon_2 E_2 + P, \quad (3.2)$$

$$U_o = x_1 E_1 + x_2 E_2, \quad (3.3)$$

At the constant applied voltage U_o in the process of initial poling and with the total thickness of amorphous (x_1) and crystalline (x_2) layers, it follows that increase of the ferroelectric polarization P in crystallites is accompanied by decrease in the field strength E_2 in the ferroelectric part, so that the increase of polarization P is eventually stopped as soon as the field E_2 becomes equal to the coercive field E_c .

In the process of the following short circuiting of the sample, the field strength E_2 changes its direction, so it is possible that some back switching of the already developed polarization is possible [62]. It follows from equations (3.2) and (3.3) that there is a maximum polarization P_{max} that corresponds to the equation $E_2 = E_c$ under the condition

of a short circuit ($U_o = 0$)

$$P_{\max} = \varepsilon_o \left(\varepsilon_1 \frac{x_2}{x_1} + \varepsilon_2 \right) E_c \quad (3.4)$$

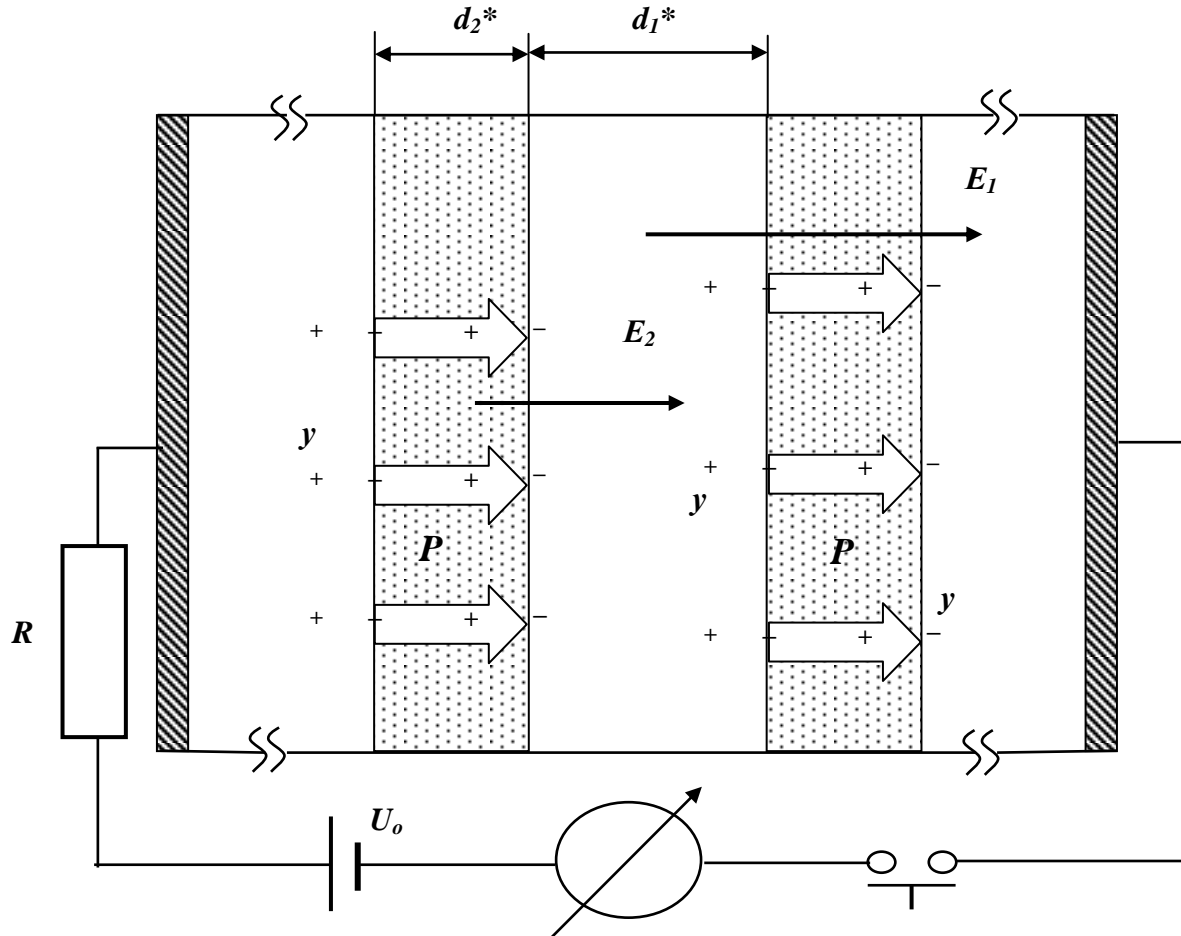


Fig. 3.6. Schematic model of a two-phase ferroelectric polymer with alternating layers of ferroelectric and paraelectric phases.

Taking into account that $E_c = 50$ MV/m, $\varepsilon_1 = 19,6$, $\varepsilon_2 = 12,9$ and $x_1 = x_2$ [37-40] in case of PVDF we have $P_{\max} = 1,44 \mu\text{C}/\text{cm}^2$, which is only 11% of the maximum polarization $P_s = 13.1 \mu\text{C}/\text{cm}^2$ that can be obtained in case of a finite conductivity and accumulation of charges at the boundaries of crystallites.

Thus, the role of the charges is not only in compensating (screening) the depolarizing field, as is usually believed. The charges interfere with the relationship between the field in the crystallites E_2 and the polarization of P in the poling process in such a way that it helps to maintain the field strength E_2 at a high level regardless of the continuously

increasing polarization. A similar phenomenon is observed not only in case of initial poling, but also when the polarization switching in an already electrically charged polymer takes place.

Let us consider phenomenologically the process of the polarization switching in PVDF. To do this we use the model proposed by von Seggern and Fedosov [174,177] assuming that the PVDF film consists of $2n$ alternating paraelectric and ferroelectric layers shown in Fig. 3.6. The layers d_1^* correspond to the amorphous phase plus non-ferroelectric crystalline α -phase, while the layers d_2^* represent the ferroelectric crystalline β -phase. Total thickness of the layers is $d_1 = nd_1^*$ and $d_2 = nd_2^*$. Since the linear dimensions of the sample are much smaller than the thickness of the sample, one can consider the one-dimensional case, replacing the vectors of the field strength and the polarization with the corresponding scalars.

For a qualitative description of the switching process, consider two adjacent ferroelectric crystallites, as shown schematically in Fig. 3.7. In the initial unpolarized state (Fig. 3.7a) dipoles in crystallites are oriented randomly providing zero mean polarization. For simplicity, the 180-degree switching model is assumed, although there is some evidence that 60° switchings are also take place [176]. At the beginning of initial poling, the state of the random distribution of ferroelectric dipoles $P = 0$ means that the polarization of $+(1/2) \cdot P_o$ is generated by a half of the total number of dipoles, while the other half creates the polarization equal to $-(1/2) \cdot P_o$. This state is thermodynamically stable without compensating charges, because the pairs of neighboring dipoles are mutually compensate each other, as shown schematically in Fig. 3.7a. Thus it is assumed that there is a certain domain structure in separate crystallites with completely compensated polarization. Mutual compensation of dipoles will not work if all dipoles within one crystallite are oriented in one direction.

Assume that the sample is electrified by applying a constant voltage $-U_o$ for time sufficient to achieve a polarized state with the preferred orientation of the dipoles along the external field E , as shown in Fig. 3.7b. The equilibrium state collapses in the process of initial poling, since a half of the dipoles changes their orientation resulting in the polarization switching of $\Delta P_1 = -(1/2)P_o - (1/2)P_o = -P_o$. The other half of the dipoles does not change their orientation, i.e. they will not be switched ($\Delta P_2 = 0$). Therefore, the total average polarization changes in the process of initial poling from 0 to $-P_o$. Finally, the obtained polarization $-P_o$ is conventionally called negative ($P = -P_o$).

The orientation of the dipoles results in the associated appearance of the polarization charges on the crystallite surfaces, which create the so-called depolarizing field seeking to turn the switched dipoles into their initial state. As was shown earlier [174,177], the process of the polarization forming is always accompanied by the gradual accumulation of the compensating charges σ on the boundaries, which appear either as a result of injection from electrodes, or by the redistribution of the intrinsic free charges (peculiar thermoemission). As can be seen from Fig. 3.7b, the field E_c created by the compensating charges coincides in the direction with the external polarizing field E and is opposite to the depolarizing field.

It is important to note that the shielding (screening) charge ensures the stability of the ferroelectric polarization after disconnecting the external field and short circuiting ($U = 0$) by compensating the depolarizing field E_d and preventing the return of the dipoles in the initial state (back-switching), as shown in Fig. 3.7a. In one-component and monocrystalline ferroelectrics, the screening is usually performed by free excess charges on the electrodes appeared due to redistribution of charges through an external circuitry. It can be proved that in a two-component system similar to PVDF, full compensation is not possible only by the electrode charges, and therefore, the role of the boundary charges is greatly increased. If the field E_c that occurs due to accumulated charges is equal to the depolarizing field E_d , as shown in Fig. 3.7b, the polarization $-P_o$ is stable after a short circuiting, since the electric field becomes zero at all points of the sample.

The switching process begins at the moment of the constant voltage U_o application to the sample, which creates an external field E oppositely directed in relation to the initial polarization, as shown in Fig. 3.7c. The polarization switching involves reorientation of the dipoles under the action of the field E . As soon as a part of the polarization ΔP is switched, an appropriate compensating charge is immediately released $\Delta\sigma = \Delta P$. It should be emphasized that, as in case shown in Fig. 3.7a, thus switched polarization does not need to be screened by real charges, since adjacent oppositely directed dipoles compensate each other, as shown schematically in Fig. 3.7c. The residual polarization continues to be fully compensated by charges ($\sigma_o - \Delta\sigma = P_o - \Delta P$) and the equality of the fields is maintained until ΔP becomes equal to P_o , indicating that the average polarization P becomes zero ($P = 0$).

As can be seen from the comparison of Fig. 3.7b and 3.7d, charges brought in the process of the primary polarization and localized at the boundaries of crystallites are

released when the polarization is switched contributing to increase of the apparent conductivity, which substantially exceeds the initial dark conductivity due to a huge number of additional released free charge carriers.

We have found experimentally that the polarization switching in PVDF occurs much faster than its initial formation. In particular, there are no two time ranges (stages), as if the second (slow) stage was shortened and shifted towards the shorter times. This may indicate that the time constant of the second stage is inversely proportional to the conductivity and becomes small in comparison with the "normal" Maxwell relaxation time. This hypothesis can be explained by assuming that charges at the boundaries of crystallites trapped in the process of poling are released and contribute to the increased conductivity

$$g = g_o + \Delta g \quad (3.5)$$

The Δg corresponds to the contribution of the previously trapped charges. It reaches a maximum at a time when the residual polarization $-P_o$ is switched to zero, as shown in Fig. 3.7d. During the ongoing switching from 0 to $+P_o$, the released charges will be gradually trapped again. Thus, the conductivity in the switching process increases at the beginning to a maximum and then decreases so that its value g_o at the end of the switching at $P = +P_o$ becomes the same as in the initial polarized state at $P = -P_o$.

The conductivity in the process of switching polarization can change not only due to releasing and trapping of the charge at the crystallites boundaries, but also as a result of recombination. At the beginning of the switching, the ferroelectric polarization in the crystals $-P_o$ is completely compensated by equal to this polarization screening charge σ_o trapped at the boundaries of the crystallites. As soon as polarization switching from $-P_o$ to 0 occurs, the trapped compensating charges are gradually released becoming free charges. Since the polarization at any moment is completely compensated by the charge, the volume density of the released charge is equal to

$$\rho_{rel} = \frac{|P_o| - |P|}{x}, \quad (3.6)$$

where x is the mean distance between two adjacent crystallites including amorphous and

crystalline components assuming that the released charge is evenly distributed in this volume. Since the density of the released charges is much greater than the equilibrium value, it is reasonable to assume that recombination processes take place. Therefore, a part of the released charges is recombined, so that the free charges density ρ responsible for the additional conductivity

$$\Delta g = \mu \cdot \rho, \quad (3.7)$$

is less than the volume density of released charges ρ_{rel} . Then, the dynamics of free charges can be described by the following expression

$$\frac{d\rho}{dt} = \frac{1}{x} \frac{dP}{dt} - \frac{\rho^2}{k}, \quad (3.8)$$

where the first term on the right side of the equation is positive and corresponds to the rate of free charge carriers increase due to releasing of the trapped charges. The second term corresponds to the rate of decrease in the density of charges through recombination with the coefficient of recombination k .

In the second phase of the polarization switching from 0 to $+P_o$, the conductivity gradually decreases, firstly due to the trapping of compensating charges at the boundaries of the crystallites and, secondly, due to recombination. The dynamics of free charges in the second phase is described by the following expression

$$\frac{d\rho}{dt} = -\frac{1}{x} \frac{d\sigma}{dt} - \frac{\rho^2}{k}, \quad (3.9)$$

Equations (3.8) and (3.9) should be included in the set of differential equations that describe the switching process.

The initial orientation of the dipoles changes its direction at a time when the polarization P passes through zero, after which the newly formed polarization begins to increase. As in case of primary poling when the polarization is formed, it creates its depolarizing field E_d , while the screening charge σ_o is again accumulated at the

crystallite boundaries, as shown in Fig.3.7d. The conductivity decreases due to the decrease in the density of free charges reaching at the end the initial value g_o . When the switching polarization is completed the situation shown in Fig. 3.7d is similar to that corresponding to initial poling (Fig. 3.7b). However, there is a significant difference between initial poling and the polarization switching. Due to the increased conductivity, the rate of accumulation of the boundary charge increases sharply, and the equivalent Maxwell relaxation time decreases. In the process of initial poling, charges are supplied by injection from electrodes or or internal thermoelectric emission, while in case of the polarization switching, previously released free charges already exist, so that they are easily trapped at the boundaries of crystallites. Therefore, polarization switching occurs faster than its initial formation.

Let us now conduct an analytical description of the polarization switching model in PVDF under the action of constant voltage pulses. The initial conditions before the polarization switching are as follows

$$P(0) = -P_o, \quad \sigma(0) = -P_o, \quad E_1(0) = E_2(0) = 0. \quad (3.10)$$

The switching voltage U_o is applied to the sample through the limiting current resistor R at the time $t = 0$. Since the total current $I(t)$ at any moment of time is the same in different parts of the electric circuit, we obtain

$$I(t) = \frac{U_o - (E_1 d_1 + E_2 d_2)}{R} = A \left[\varepsilon_o \varepsilon_1 \frac{dE_1}{dt} + gE_1 \right] = A \left[\varepsilon_o \varepsilon_2 \frac{dE_2}{dt} + \frac{dP}{dt} + gE_2 \right] \quad (3.11)$$

where A is the surface area of the sample, ε_1 and ε_2 are the dielectric permittivities of the non-ferroelectric and ferroelectric phases, taking into account all the linear components of the polarization, ε_o is the permittivity of a vacuum.

The equation (3.11) shows that the current in the outer part of the circuit is a pure conductivity current, whereas in the paraelectric layers it consists of a capacitive component and a conduction component, while a polarization component of the current is added to the ferroelectric regions.

We assume that the dynamics of polarization is described by the modified Debye equation with the relaxation time τ depended on the field strength [27,64]

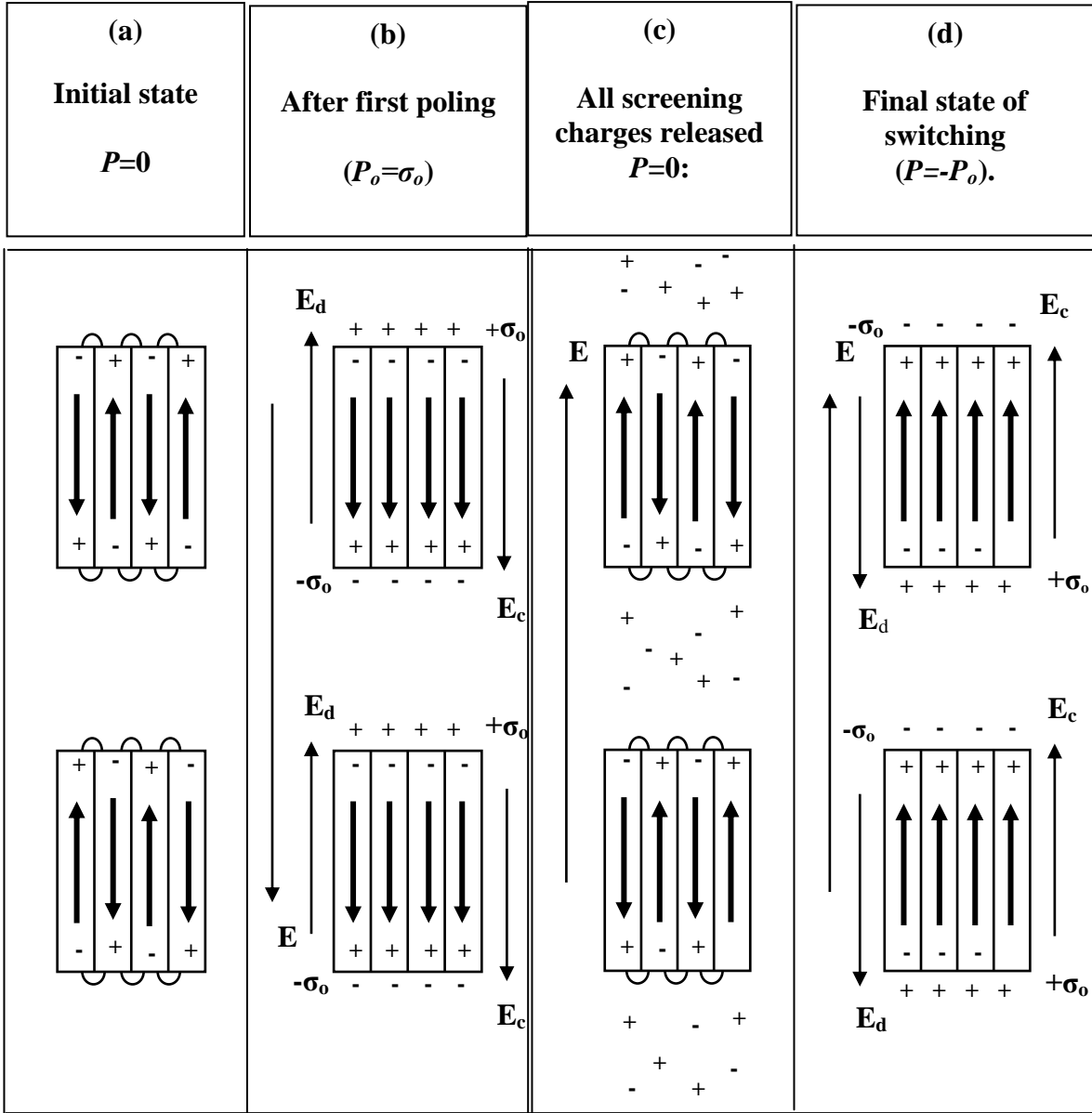


Fig. 3.7. Schematic description of processes taking place during the polarization switching in PVDF.

$$\frac{dP(E_2, t)}{dt} = \frac{P_{st}(E_2) - P(E_2, t)}{\tau(E_2)}, \quad (3.12)$$

where $P_{st}(E_2)$ is the quasi-stationary dependence of ferroelectric polarization on the field strength, represented by the hysteresis loop in Fig. 3.8 and is expressed analytically as

$$P_{cm} = -P_o + \frac{2P_s}{E_s - E_c}(E_2 - E_c), \quad (3.13)$$

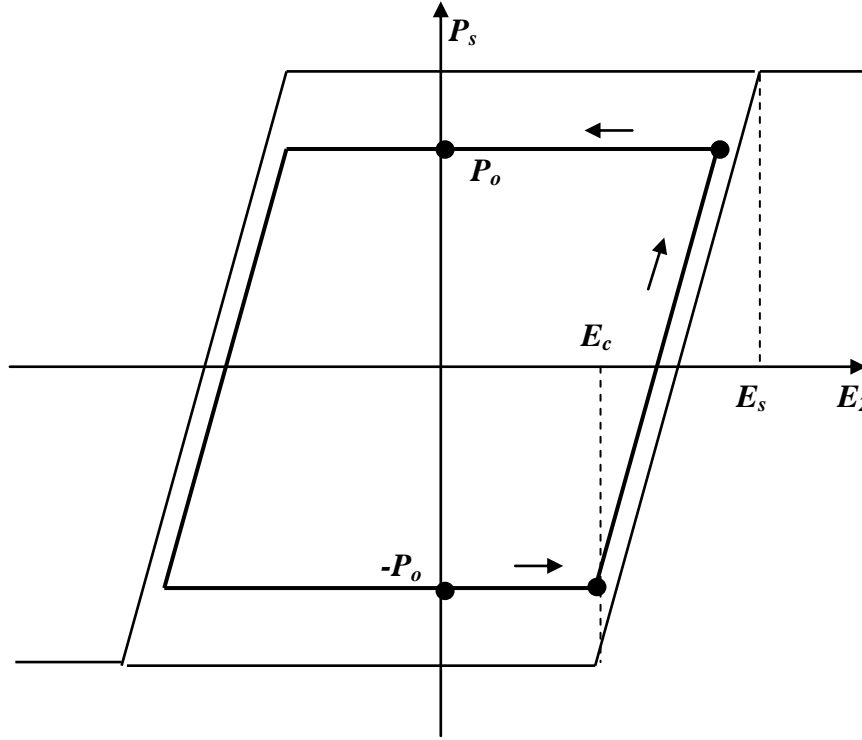


Fig. 3.8. Schematic dependence of polarization in PVDF crystallites on the electric field strength during the polarization switching from $-P_o$ to $+P_o$ if $P_o < P_s$.

where E_c is a coercive field, P_s is the residual saturation polarization, E_s is the minimum field at which the value of P_s is obtained. Equation (3.13) implies that $P_{st}(E_2)$ is not installed instantaneously, but with a certain field-dependent time constant $\tau(E_2)$. This dependence initially introduced for inorganic ferroelectrics can also be applied to ferroelectric polymers [25,67]

$$\tau(E_2) = \tau_o \exp\left(\frac{E_A}{E_2}\right), \quad (3.14)$$

where E_A is the activation energy, τ_o is the characteristic time.

From the condition of the electric displacement vector continuity at the boundaries between adjacent layers we obtain

$$\varepsilon_o \varepsilon_1 E_1(t) = \varepsilon_o \varepsilon_2 E_2(t) + P(E_2, t) - \sigma(t). \quad (3.15)$$

The charge $\sigma(t)$ is accumulated at the boundaries due to the difference between the fields E_1 and E_2

$$\frac{d\sigma}{dt} = g(E_1 - E_2). \quad (3.16)$$

It should be noted that the accumulation of charges $\sigma(t)$ is due not only to the well-known Maxwell-Wagner effect, which takes into account the difference in the conductivity and dielectric permittivity of the adjacent layers. To a large extent, it is also due to the presence of the ferroelectric polarization in crystallites, which is absent in the amorphous phase.

Equations (3.11) - (3.16) form a complete set of differential equations that have been solved to obtain the dependence of the fields $E_1(t)$ and $E_2(t)$, the ferroelectric polarization $P(t)$, the screening charge $\sigma(t)$, and the conductivity g during the polarization switching process.

Table 3.1

Parameters used in model calculations

U_o	n	d_1	d_2	ε_1	ε_2	d	μ
2 kV	42	200 nm	100 nm	19.6	12.9	12.5 μm	10^{-13} $\text{m}^2/\text{V}\cdot\text{s}$
P_o	g_o	P_r	E_s	E_c	τ_o	E_A	
-9.6 $\mu\text{C}/\text{cm}^2$	$3 \cdot 10^{-11}$ Sm/m	13.1 $\mu\text{C}/\text{cm}^2$	200 MV/m	50 MV/m	20 ns	1.2 GV/m	

The parameters that were used in model calculations are given in Table 3.1. Evidence of the choice of the values of the dielectric constants ε_1 and ε_2 , the conductivity g_o , the saturation polarization P_s , the coercive field E_c , and the characteristic field E_s are given in [104]. The applied voltage corresponds to the field strength, which substantially exceeds the coercive field in order to observe the ferroelectric polarization both during

initial poling and and the polarization switching.

The assumed thicknesses of the individual ferroelectric and paraelectric layers correspond to the data on the bulk-shaped PVDF structure with a thickness of crystallites of about 100 nm [5]. Thus, $x_2 = 100$ nm was used in model calculations, x_1 is the thickness of the amorphous phase plus non-ferroelectric α crystallites. Considering the crystallinity of PVDF as 50%, and the ratio $\alpha : \beta = 30 : 70$, we have $x_1 = 200$ nm. The total number of layers $2n = 84$ corresponds to the film thickness of 12.5 μm .

A thorough analysis of the published data showed that there are no reliable values of many parameters required for model calculations of the polarization switching in PVDF.

Despite intensive research, the exact values of dielectric constant are not known either in PVDF, or in crystalline and amorphous components. The reported values vary from 2 to 30, depending on the methods of measurement, calculations, pre-processing, structure and composition of samples [87,104,144,184].

Karasawa and Goddard [100] calculated dielectric constants of amorphous ε_a and crystalline ε_c phases of PVDF and obtained values of $\varepsilon_a = 8-13$, $\varepsilon_c = 2.2-3.5$. Furukawa [67] measured the dielectric constant ε of PVDF, which is not related to ferroelectric polarization under the action of a constant high displacement voltage. He also discovered that ε is a function of the field strength having a value of $\varepsilon = 19$ in a zero field and $\varepsilon = 9$ when the ferroelectric polarization reaches saturation and $\varepsilon = 30$ when the polarization is switched near the coercive field.

Due to the large variety of published values of the dielectric constant ε , the corresponding values for the non-ferroelectric ε_1 and ferroelectric ε_2 phases of PVDF were calculated in the assumption that all the electronic and dipole polarization components are linear in the non-ferroelectric phase of the PVDF, and another nonlinear component of the polarization is added in the ferroelectric phase.

Taking into account the known value of the dipole moment $7.6 \cdot 10^{-30}$ C·m for the cell $-\text{CF}_2-\text{CH}_2-$ in PVDF [88] and the different density of amorphous $\rho_a = 1.68$ g/cm³ and crystalline $\rho_c = 1.93$ g/cm³ phases [124], we obtained the dielectric constant for the amorphous phase $\varepsilon_1 = 11.3$ and for the crystalline phase $\varepsilon_2 = 12.9$ at room temperature which are in good agreement with the values of the PVDF dielectric constant given in [181].

In addition, we took into account a new aspect that some orientation of the unit dipoles $-\text{CF}_2-\text{CF}_2-$ is possible under the action of the external field also in the amorphous

phase. This will create an additional reversible polarization P' proportional to the field that completely disappears at the zero field like electron and dipole polarizations.

Assuming that P' is responsible for an experimentally observed unstable polarization component in PVDF [124] of about $1.6 \mu\text{C}/\text{cm}^2$ at $E = 160 \text{ MV}/\text{m}$, the effect of this polarization can be taken into account as an additional part of the dielectric constant for the amorphous phase, which is 8.3. Therefore, the effective dielectric constant of the amorphous phase becomes 19,6. This value was applied to non-ferroelectric layers in the simulation of the processes switching.

Initial conductivity g_o was determined by two methods experimentally from the experiment of repeated poling of a fully polarized sample using the linear inclination of the curve $D(t)$ and the residual charge on the measuring capacitor after a short circuiting of the sample. The obtained value $g_o \approx 10^{-12} \text{ Sm}/\text{m}$ is in good agreement with the published data for semi-crystalline PVDF [131].

Both methods give practically the same values of g_o , however, the Ohm law is not valid because of the nonlinearity of the current-voltage characteristic, which can be approximated by an exponential function with index of 1.6 indicating that the conductivity has a mixed nature with a quadratic dependence characteristic for injection currents bounded by space charge [112], which are superimposed with a linear dependence due to the internal conductivity of the sample.

It is interesting to note that the density of free carriers of order of $n_{\text{cryst}} = 2,1 \cdot 10^{28} \text{ m}^{-3}$ is much lower than the concentration of dipoles $-\text{CF}_2-\text{CH}_2-$ indicating that one free charge carrier corresponds to $2 \cdot 10^6$ dipoles. This result shows that it is impossible to quickly screen the depolarizing field with free charges, so it takes a long time to accumulate compensating charges. It is necessary to emphasize again that presented in Table 3.1 values of conductivity and mobility correspond to the fully polarized state of the sample.

A very important parameter of any ferroelectrics is the coercive field of E_c . In general, the dependence of the polarization on the applied field in ferroelectrics has the form of a hysteresis loop with the coercive field E_c and the residual polarization P_r , being the main characteristics of the ferroelectric. Data on the coercive field of PVDF are numerous and at the same time very controversial not only through different measurement methods and composition of the samples, but also because what is understood as the term "coercive field". In our opinion, the coercive field is the

maximum field strength applied during initial poling at which the development of the ferroelectric polarization is not yet observed.

If we accept this definition, then the coercive field can be regarded as some property of the material itself, as some limit value. Otherwise, if the coercive field is defined as the field E'_c , at which $P_r(E'_c) = 0$, as often believed, then it becomes dependent on the initial magnitude of the polarization and the maximum voltage applied in the process of the switching experiment. The published data on the value of E_c in PVDF for the films used by us vary from 30 [26] to 120 MV/m [182]. Although there is not one single value of the coercive field E_c in the literature, however, $E_c \approx 50$ MV/m was chosen by us as adequate to describe the results, but no attempts have been made to optimize this value.

The exact value of the saturation polarization P_s in PVDF crystallites is unknown. For 100% orientation of the $-\text{CF}_2-\text{CH}_2-$ dipoles considered as hard rods, Lines and Glass [123] obtained the saturation polarization $P_s = 13.1 \mu\text{C}/\text{cm}^2$, while Broadhurst and Davis [15] using the Clausius-Mossotti equation and using the Onsager approach received the value of $P_s = 22 \mu\text{C}/\text{cm}^2$, which does not correspond to the experimentally measured value at all. Al Jishi and Taylor [1] took into account the effect of the internal field and obtained the value of $P_s = 12.7 \mu\text{C}/\text{cm}^2$. In our calculations we used $P_s = 13.1 \mu\text{C}/\text{cm}^2$ proposed by Lines and Glas [123] being in good agreement with experimental data.

Measured values of the residual polarization differ significantly from one author to another. Bur [16] on the basis of X-ray experiments obtained $P_r = 4.3 \mu\text{C}/\text{cm}^2$ for non-oriented samples and made the fitting of experimental results to the model. Kepler and Anderson [102] for a biaxially oriented PVDF containing 50% α -phase in crystallites yielded $P_r = 6.3 \pm 0.2 \mu\text{C}/\text{cm}^2$ with a hysteresis loop and $P_r = 5.7 \pm 0.1 \mu\text{C}/\text{cm}^2$ by integration the depolarization current. A similar value $P_r = 6 \mu\text{C}/\text{cm}^2$ was reported by Vishnevsky and others [184] for biaxially oriented PVDF of 12.5 μm thickness. Bauer [5] reported that by using his proprietary poling procedure he obtained $P_r = 9.2 \pm 0.2 \mu\text{C}/\text{cm}^2$ in a biaxially oriented PVDF.

The residual polarization P_r reported in the literature does not correspond to the polarization of saturation P_s in the ferroelectric phase of PVDF, since the measured value is averaged over the entire sample volume, while the ferroelectric phase occupies only a certain portion of the volume.

We compared the experimental and calculated dependences of the ferroelectric polarization E_2 on the switching time and found that there is a good correspondence

between the theoretical and experimental dependences. With these calculations, the switching process was divided into several stages.

At the first stage of switching the field strength in the paraelectric phase E_1 and in the ferroelectric phase E_2 increase exponentially with time until the calculated polarization P_o and charge σ_o remain constant. Then, in the second phase, there is a gradual switching of the polarization, and the magnitude of the polarization changes from $-P_o$ to 0. The charges trapped during initial poling become free contributing to the increased effective conductivity in accordance with the equations (3.5-3.7). The field E_2 is not affected by polarization at this stage, as in case of initial poling, because equality continues to be maintained. As a result, the polarization switches from $-P_o$ to zero.

After passing zero, the polarization of P again begins to increase in the direction opposite to initial poling. With the development of polarization, as follows from (3.15), the field E_2 would decrease, if the charge σ was not taken into account. At the first and second stages, one can neglect the influence of conductivity and charges on the switching since the completion time of the second phase is about 0.5 ms being much fewer than the Maxwell relaxation time.

If we continue to neglect the conductivity, then the maximum of polarization $P_{max} = 0.7 \mu\text{C}/\text{cm}^2$ is achieved very fast that corresponds to the polarization switching of $\Delta P = P_{max} - P_o = 10.3 \mu\text{C}/\text{cm}^2$. The obtained value is only 54% of the theoretically possible $\Delta P_{max} = 2P_r = 19.2 \mu\text{C}/\text{cm}^2$.

Thus, the fast switching phase ends in less than 1 ms and a slow phase begins, which is practically completely controlled by the conductivity. In the calculation of the slow phase, we considered dependence of the polarization on the quasi-stationary field, since the switching time calculated by the formula (3.14) was significantly less than the Maxwell relaxation time.

Calculations of the field strengths dependence on the time in the paraelectric and ferroelectric phases and the kinetics of the effective conductivity showed that the polarization switching in the second phase and the screening of the depolarization field are highly influenced by the magnitudes of the fields strength E_1 and E_2 and by their dynamics. Due to growth of the polarization, the field E_2 becomes smaller than E_1 , as predicted by the equation (3.15). The conductivity initially increases reaching its maximum and then decreases. Since the conductivity increase Δg is much greater than the initial value g_o , the switching is faster than the initial development of the polarized

state.

Thus, the model of the polarization switching in PVDF in the mode of the constant voltage, takes into account the following features:

- two-phase structure of the polymer ferroelectric,
- presence of the intrinsic conductivity and injection of charges from the electrode,
- trapping of the charges at the boundaries of polarized crystallites and their release,
- partial recombination of the released charges and their secondary trapping,
- dependence of the polarization switching time on the field strength,
- nonlinear dependence of the quasi-stationary polarization on the field strength .

The field strengths in both phases were used as variables in the system of equations describing the process of the polarization switching. The polarization in crystallites, the effective conductivity and the surface charge density at the interphase boundaries were studied. From the comparison of the experimental polarization switching curve with the theoretical model, important parameters, such as the effective mobility, the polarization switching time and the activation field were found. Based on the model, the difference between the initial polarization formation and its switching was explained.

The model and the method of calculating the polarization switching process developed by us can be applied to any system consisted of paraelectric and ferroelectric parts, for example, to ceramic-polymer composites.

At the same time, in case of copolymers, the crystalline phase may occupy more than 90%. Then charges and conductivity do not significantly affect the processes of polarization development and switching, and as a result, the time range of these processes is sharply reduced compared to PVDF, in which the paraelectric amorphous phase occupies about 50% of the volume.

Chapter 4. Polarization profiles in ferroelectric polymers

4.1. Distribution of polarization along the thickness of FPs films

Information on the spatial distribution of polarization in PVDF films is extremely important both from the scientific and the practical points of view. Even in earlier works [28,162] it was noted that the piezoelectricity and pyroactivity in PVDF films near the positive electrode are higher than near the negative one that was erroneously associated

with injection of holes and the formation of a nonuniformly distributed positive space charge. Further studies [13,34,46] showed that in some cases not only the space charge, but also the polarization are distributed non-uniformly in the thickness direction.

For the first time, heterogeneity of polarization in PVDF was detected by Day et al. [28] by different values of the pyroelectric activity near two sides of polarized films. Sassner [162] found that from tightly pressed to each other three films only the film adjacent to the positive electrode was highly polarized. It was found [35] that in the high field ($E > 150$ MV/m), the polarization is almost homogeneous, while in the middle fields the maximum of polarization is either in the center of oriented films, or near the anode in the unoriented ones.

Gerhard–Mulhaupt et al. [74] investigating the distribution of piezoactivity by the method of a pressure pulse generated by a powerful laser confirmed that during thermoelectret poling in the middle fields, the maximum polarization is near the anode, as in case of poling in a corona discharge. Authors of [56] believe that because of the high conductivity of PVDF, areas of excess charge cannot exist, and charge-compensated polarization zones are formed. At the same time, we have calculated Debye's length of screening L_D for the following PVDF characteristics: temperature $T = 300$ K, the dielectric permittivity $\varepsilon = 10$, the mobility of charge carriers $\mu = 10^{-12}$ m²/(V·s), the specific conductivity $g = 10^{-12}$ Sm/m. We obtained $L_D = 170$ μm that is much larger than the typical thickness of the films (10-50 μm). Therefore, the effect of screening by the space charge should be weakly expressed in PVDF.

Mopsik and de Reggi [129] found an increased value of the coercive field strength near the surface of the PVDF, and de Reggi and Brodhard [29] found that, in spite of the displacement of polarization to the anode, it is zero near the electrode. Sessler and Berraissoul [153] found that the piezoactivity near the electrodes and, consequently the polarization is very small. The weakening of the field, in our opinion, is an indication of the injection of charge carriers and, on the contrary, the field and polarization near the blocking electrode are increased.

In [34], the maximum polarization near the anode is reported after poling of PVDF in a positive corona discharge, although in the other work of the same authors it is indicated that the polarization in this case is concentrated in the central zone [35]. Bichler et al [13] found that the position of the maximum polarization depends on the mode of thermal and mechanical processing of PVDF. The authors of the paper [13]

concluded that the polarization in the PVDF containing the α -phase was shifted to the anode, while the polarization was uniform in the presence of the β -phase although the heat-treatment and stretching changed both the crystalline structure of the films and their other properties. In [151], the polarization attenuation near the anode is reported in corona poled PVDF films. Such contradictory data are explained by the fact that the selection of films for the study was random (various thicknesses, regimes of poling, annealing, and mechanical pre-treatment). In addition, the research methodology was imperfect in some cases, so that there was a subjective factor in interpreting the measurement results. Direct measurements of the polarization profile are possible only by the method of the pressure step, while all other methods should be considered as non-direct ones.

The dynamics of the polarization profile in PVDF was studied only in a few works. Thus, it was established [119] that polarization develops in the central zone in biaxially oriented PVDF films containing 70% β -phase in case of middle field (60 MV/m). However, when changing the polarity of the voltage, the complete switching near the anode does not occur and a bimorph structure is formed.

Fedosov and Sergeeva, investigating the distribution of polarization in films electrically charged in a corona discharge [46,49,175,178], found that the maximum polarization is near a positive electrode with a negative polarity of the corona discharge. This indicates that injection of negative carriers takes place, while the positive electrode is blocking. When charged in a positive corona there is a double injection: positive charges from the corona and negative charges from the electrode. It was found that the free surface of the film exposed to the corona discharge can be regarded as a virtual injection electrode.

In a number of studies, the thermal stability of polarization and its distribution in the thickness direction in PVDF and P(VDF-TrFE) [29], as well as in P(VDF-TFE) [178] were investigated. The charge and polarization distribution in PVDF films poled by the electron-beam method [154] was studied by the laser induced pressure pulse (LIPP) method. Fedosov and Sergeeva found that the trapped electrons in the volume are not concentrated in a thin layer at a certain depth, but are distributed with uneven density in a zone of the finite thickness [54]. These electrons form a virtual negative electrode, from which injection of charges in a non-irradiated region takes place leading to increase in the imaginary penetration depth of the electrons and to inhomogeneity of

polarization in the non-irradiated region.

The importance of the injection processes, but not the distribution of intrinsic charges in volume was evidenced by Mitsutani and Ieda [128]. They found that the poling current increases in 200 times, if a corona discharge is used instead of a metal electrode. The experimental results in papers [128,57] have been explained by the injection of charge carriers. At the same time, some authors believe that the corona discharge forms an ideal blocking contact with any dielectric [151]. Thus, the question of the injection of charge carriers and their role in the formation of polarization remains open and controversial.

The reasons of the fragmentary and contradictory nature of the literature data on the polarization profiles in PVDF are the complexity of experimental methods and ambiguity in interpretation of the results.

To study the profile of polarization and space charge in thin polymer films, one of the following three methods is used:

- 1) The method of the piezoelectrically generated pressure step (PPS);
- 2) The method of the thermal wave induced by a modulated laser (LIMM);
- 3) The method of the laser induced pulse pressure (LIPP).

The analysis of the efficiency, sensitivity and resolution of these methods showed that the measured current in the PPS method is proportional to the polarization or gradient of the space charge, whereas in the LIPP method the measured signal is proportional to the charge (if any) and the gradient of polarization. Given the features of the LIPP method, only zones where polarization changes in thickness direction is detected. Therefore, a high homogeneous polarization and complete absence of the polarization give the same signal. Despite the resolution of the LIPP method is practically the same as the resolution of the PPS method, it should be recognized that the method of the pressure step (PPS) is more reliable and informative.

In the LIMM method, the depth of the thermal wave penetration decreases with the increase of the modulating frequency, so at very high modulation frequencies above 10 MHz it is possible to investigate very thin near-to-electrode layers of less than 1 μm in thickness. However, the resolution of the LIMM method drastically decreases with increasing the distance from the surface to the depth of the sample, and this is a significant disadvantage of the LIMM.

Taking into account the results of the analysis, we have chosen the PPS method,

which provides a fairly high resolution of about 2-4 μm and the possibility of observing the real-time polarization profile on oscilloscope's screen. It does not require complex calculations, assumptions, and solutions of incorrect inverse tasks as in case of the LMM method. The colossal advantage of the PPS method is the ability to study the dynamics of the polarization profile "*in situ*" directly in the process of poling, polarization switching, and short-circuiting of the samples.

4.2. Methodology for studying polarization profiles in FPs

Most methods for measuring polarization and space charge profiles in dielectrics are applied to already polarized samples providing the information about the final state, while the process of the polarization development and its profile remained inaccessible for a direct experimental study. In this sense, a unique possibility is provided by the piezoelectrically generated pressure step (PPS) method, in one of the modifications of which there is the ability to measure the profile "*in situ*" directly when the polarizing voltage is applied or the specimen is short-circuited. Such measurements of the dynamics of the polarization profile are extremely important for understanding the physical processes occurring in ferroelectric polymers during their poling and switching of polarization.

The PPS method developed by Eisenmenger et al. [35] was applied by us, and all measurements were performed in the laboratory of Prof. W. Eisenmenger at the Department of Physics of the Stuttgart University. The method is based on the generation of an electric signal (a current pulse) when a pressure step generated by a piezoelectric crystal passes through the sample. The piezoelectric pressure step results from a voltage step with a very steep front. The front of the pressure wave extends with a sound speed of (2250 m/s), creating a current pulse in the short-circuited sample. The shape of the current pulse repeats the profile of the polarization distribution in the thickness of the film.

The block diagram of the installation of the PPS method is shown in Fig. 4.1. The voltage step is formed by means of a constant voltage source (500 V) loaded with connected in series a resistance and a capacitor. This chain with a frequency of about 100 Hz is locked to a resistance of 50 Ω , in parallel with which a quartz crystal is connected. A sample is pressed to the back side of the piezoelectric crystal, to which a

grounded copper electrode is connected.

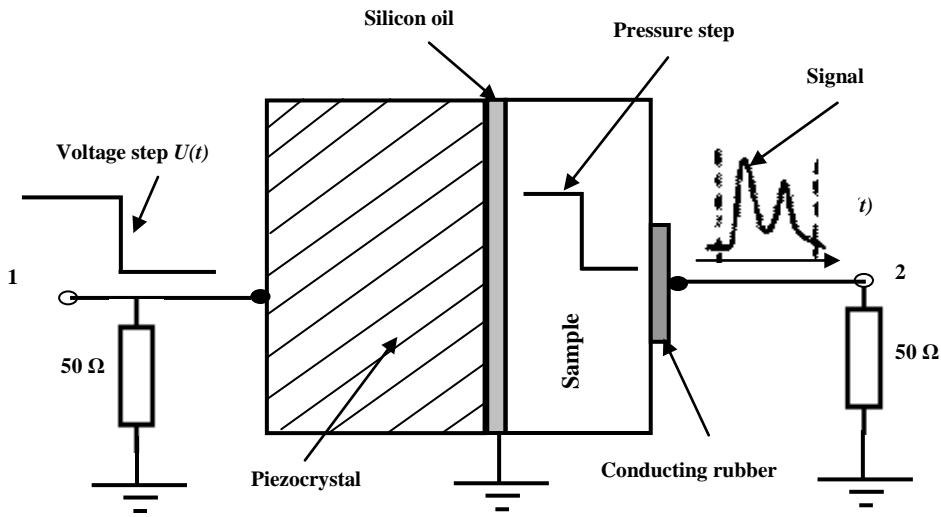


Fig.4.1. Schematic diagram of the polarization profile measurement by the piezoelectrically induced pressure step (PPS) method.

For better transferring of the pressure wave from quartz to the specimen, a thin layer of silicone oil is applied between them. The electric signal is taken from the rear side of the sample with the help of a clamping conductive rubber electrode. The load is the resistance of 50Ω , the signal from which is fed to the broadband amplifier and then either to the spectrum analyzer, or to the oscilloscope. In case of thin specimens, a $23\text{-}\mu\text{m}$ thick polypropylene gasket was used to reduce the capacity.

Measurements have shown that the steepness of the pressure step front is of the order of 0.4 ns , the sound speed in PVDF at room temperature is about 2250 m/s . Thus, the time of the pressure wave passage through the sample at its thickness of $20 \mu\text{m}$ is of the order of 10 ns . The duration of one voltage pulse was 100 ns , that is, a step-by-step mode was implemented.

All used devices (amplifier, spectrum analyzer, and oscilloscope) had a bandwidth of more than 1 GHz . The sensitivity of the PPS method was about $2 \mu\text{m}$ and was limited by the steepness of the pressure step. An electrical signal in the spectrum analyzer was converted into a numerical code to allow the the computer processing of the data.

To investigate the polarization profile, several series of experiments were performed on PVDF films. Aluminum electrodes of 4.5 mm in diameter on both sides were pre-deposited at the samples by vacuum evaporation. Initial poling and the polarization

switching were carried out at room temperature by applying a constant voltage of a certain magnitude and polarity. The magnitude of the voltage was chosen so that average field was 60 MV/m in a series of polarizing and switching, which is slightly higher than the coercive field for PVDF according to the literature data [151]. Such a mode was named as "middle fields". In another series, the polarizing field strength was 160 MV/m that is much higher than the coercive value. Such regimes were classified as "high fields". In the middle and in the high fields, full polarization cycles on each sample were investigated. After each phase of polarization or switching, the specimen was short-circuited for a time sufficient to establish a quasi-stationary state (from 200 to 2000 s).

The polarization profiles were measured about 100 times per second and recorded from the oscilloscope's screen. Then the analog information of selected frames was converted into numeric and entered into the computer for further processing. All results are presented in the form of graphs of dependence of polarization on the distance from the sample from its surface.

4.3. Spatial distribution of polarization in PVDF films

Measuring the polarization profiles and the space charge gives important information about their interrelation in the process of the polarized state formation and in ensuring of its stability. This allows us to move from hypotheses and assumptions to concrete experimental facts, the analysis of which contributes to the deeper understanding of the ferroelectric polymers characteristics.

That is why special attention was paid to the dynamics of polarization profiles in PVDF films not only during the process of poling but also during the polarization switching and short-circuiting both in the middle fields close to the coercive (50-60 MV/m) and in high fields with a strength of about 160 MV/m. The obtained results allowed to construct models, which take into account the relation between injection and separation of charges, presence of deep charge trapping zones and its interrelation with the residual polarization. The impossibility of a complete switching of an inhomogeneously polarized ferroelectric polymer [59] discovered by us is of great practical importance for the choice of poling modes and shows how strong is relation between the ferroelectric polarization with the surface charge.

4.3.1. Polarization profile dynamics: poling and switching in middle fields

From Fig. 4.2 it can be seen that, with the average field strength close to the coercive value $E_c = 50$ MV/m [68], the dynamics of the polarization profile is characterized by

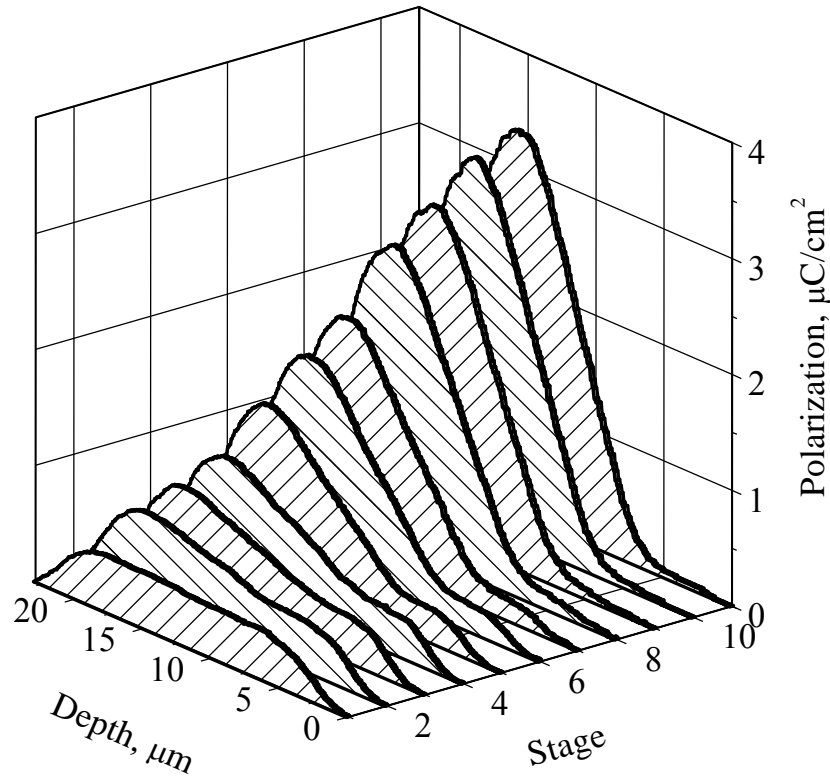


Fig. 4.2. Distribution of polarization in P(VDF-TFE) film during its poling in the field of 60 MV/m. The stage number corresponds to different times after the starting of poling: 1 – 8 s, 2 – 70 s, 3 – 100 s, 4 – 150 s, 5 – 250 s, 6 – 350 s, 7 – 450 s, 8 – 750 s, 9 – 1000 s, 10 – 1510 s, 11 – 2000 s.

1. At the initial stage of poling, after 8 seconds after the voltage application, the polarization distribution is uniform, but its value is very low ($0.5 \mu\text{C}/\text{cm}^2$).
2. Over time, the distribution of polarization in the thickness direction becomes non-uniform with the maximum near a positive electrode.
4. After poling of PVDF in the average field for 2000 s, a sharply heterogeneous asymmetric distribution of the residual ferroelectric polarization appears with a layer of about $5 \mu\text{m}$ thickness near the negative electrode, in which the residual polarization is zero.
5. When the voltage is disconnected and the sample is short-circuited, the character of the polarization distribution does not change and the polarization remains

heterogeneous, but its magnitude decreases from 3.31 to 1.71 $\mu\text{C}/\text{cm}^2$ in the region of the maximum.

The resolution of the method for measuring the polarization profile is of the order of 2-3 μm , which leads to appearance of smooth polarization profiles in near-to-electrode regions and other places of the virtually sharp polarization change. For example, it was shown [46] by measuring the polarization profile electrode by the LIMM method having the resolution near the electrodes of the order of 0.1 μm that the polarization changes sharply from the maximum value to zero within the limits of 1 μm close to the positive electrode. In the vicinity of a negative electrode where polarization is absent, distortion of the profile due to the finite resolution does not occur. The effect of resolution, probably, also affects the boundary between the first and the second zones where the polarization changes more sharply than it follows from the curves in Fig. 4.2.

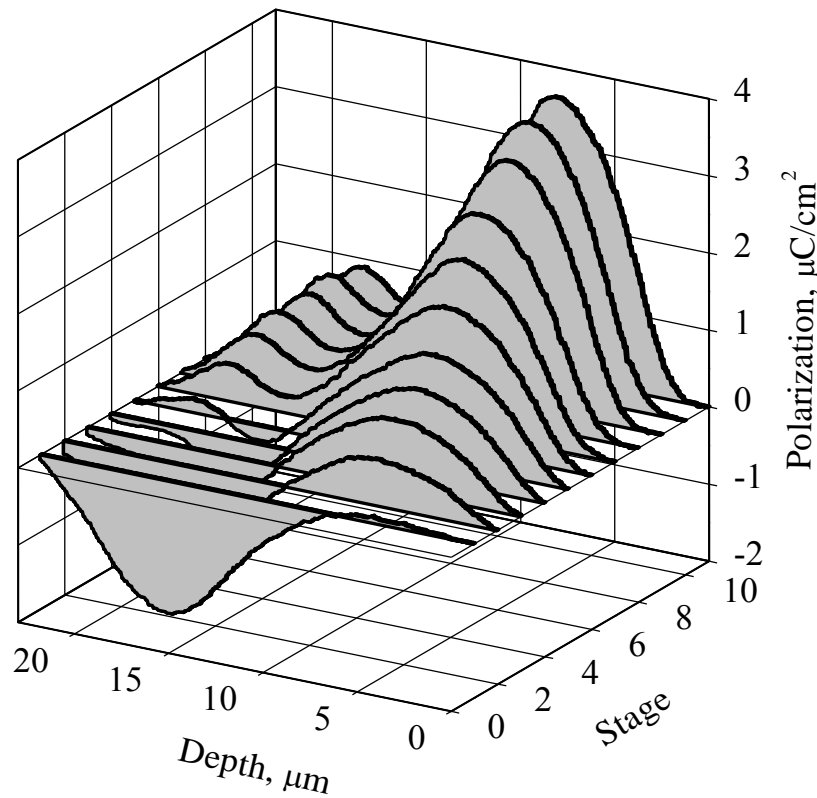


Fig. 4.3. Polarization profiles in the P(VDF-TFE) film during the polarization switching in the field 60 MV/m after initial poling and the short-circuiting. The stage corresponds to different times from the starting of the switching: 1 – 0 s, 2 – 0.2 s, 3 – 0.5 s, 4 – 1 s, 5 – 5 s, 6 – 50 s, 7 – 200 s, 8 – 500 s, 9 – 1000 s, 10 – 1500 s, 11 – 2000 s.

After changing the voltage polarity (Fig. 4.3) a minimum is formed in the place of the former maximum at a depth of about 16 μm , because the polarization in this place is not completely switched, but even does not reach zero. At the same time, the oppositely directed polarization is formed to the right and to the left of this intersection. High polarization is formed again only near the positive electrode now connected to the opposite side of the film. It should be noted that the polarization switching is faster than initial poling, and the residual polarization in the peak area is almost 1.5 times greater than after initial poling.

Comparison of polarization profiles after several switchings showed that with even number of switchings, practically identical profiles are appeared. In case of odd number of switchings, the profiles are also the same, except for the profile after the first charging when there is no reverse polarization near the negative electrode.

Thus, the profile is determined by whether the number of switchings is either even, or odd. In both cases, the distribution of polarization is sharply heterogeneous and asymmetrical with respect to the center of the sample. The main polarization maximum, regardless of the parity of the phases, is always near the electrode, which was positive in the last previous experiment, and the magnitude of this maximum is almost 1.5 times greater than in case of an odd number of switchings than with the even number. The time for quasi-stationary state formation decreases with increase in the number of voltage switchings from 2000 s during initial poling to 250-500 s during the subsequent transitions.

In some studies, for example [29,31], the information that the coercive field near the surface is greater than that in the volume are incorrect, in our opinion, because the incomplete switching is, most likely due to heterogeneity of the field. Due to the injection of charge carriers, the field strength the near the surface is always smaller than in the volume, and therefore the polarization is poorly switched there.

4.3.2. Impossibility to completely switch non-uniformly polarized FPs

It is seen from Fig. 4.2 and Fig. 4.3 that in the middle fields (60 MV/m) polarization is heterogeneous at any polarity of the voltage, and the complete switching does not occur in any section of the sample. The formed bimorph structure is stored regardless of

the direction of the external switching field. At the same time, as will be shown below, homogeneous polarization is formed in high fields (160 MV/m), which then remains homogeneous with any changes in the magnitude and sign of the applied voltage up to complete depolarization. In this regard, it was interesting to investigate behavior of the polymer ferroelectric films in high fields, originally poled in middle fields. If the initial polarization inhomogeneity is due to the fact that the field is not high enough, homogeneity should increase after applying a high field, due to expansion of the polarized region. However, we have found that the polarization does not become homogeneous, and the polarized region does not expand under the action of a high field

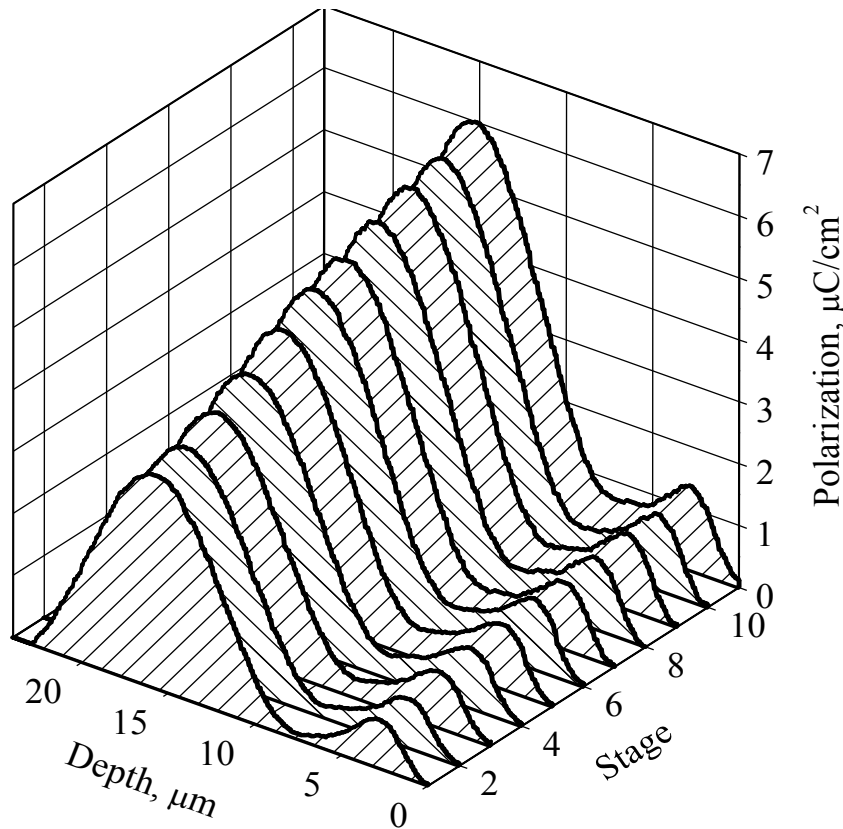


Fig. 4.4. Polarization profiles in the P(VDF-TFE) film during the the stepped voltage increase from 1.2 kV (primary poling) to 3.2 kV. The value of the voltage step is 0.2 kV, the exposure time at each voltage is 50 s.

Experiments were carried out as follows. PVDF films were placed in a field of 60 MV/m and polarization profiles were measured. As can be seen from Fig. 4.2 and 4.3, the spatial distribution of polarization was sharply heterogeneous. Further, without interrupting the measurements of the polarization profile we increased the voltage to 3.2

kV by steps of 200 V. The fields strength at 3.2 kV is several times greater than the coercive value.

However, as it follows from the graphs in Fig. 4.4, the increase in the field strength did not lead to the expected improvement of the polarization uniformity. Only the magnitude of the maximum increased, while the non-uniform character of the polarization distribution remained unchanged.

Thus, in order to obtain the high and homogeneous residual polarization, it is not enough to apply a high field. It is necessary to take into account the conditions in which the sample was poled for the first time. If initial poling was carried out in the high field, then the residual polarization will be homogeneous at any applied forward poling or switching voltage. If initial poling was carried out in medium or weak fields, then the heterogeneity of the residual polarization can not be corrected or eliminated by applying the high field. In this case, for obtaining the uniform profile of the residual polarization, we recommend a complete thermal depolarization of the sample and its annealing in the short-circuited condition at about 160 °C for several hours, so that the trapped charges in the volume will be completely dissipated. After cooling the sample, it is necessary to re-pole it, but necessarily in the high field.

4.3.3. Polarization profile dynamics: poling and switching in high fields

In case of high fields (160 MV/m), as seen from Fig. 4.5, polarization is much more uniform than in case of middle fields, and the polarization uniformity appears even after initial poling.

When polarity of the polarizing voltage changes, the symmetric switching of polarization occurs. By applying the voltage of the opposite polarity, and by increasing it in small steps, it is possible to almost completely depolarize the sample. The field strength at which this occurs corresponds to a value of 60 MV/m. Namely this value can be considered as a real coercive field.

It is interesting to note that the subsequent application of an external field of 60 MV/m of any polarity provides homogeneous residual polarization, which cannot be obtained after initial poling in such a field. The complete depolarization of a highly polarized sample irrespective of the polarity of the external field occurs at field strength of 60 MV/m, which indicates the symmetry of the hysteresis loop if initial poling was carried

out in high fields [59].

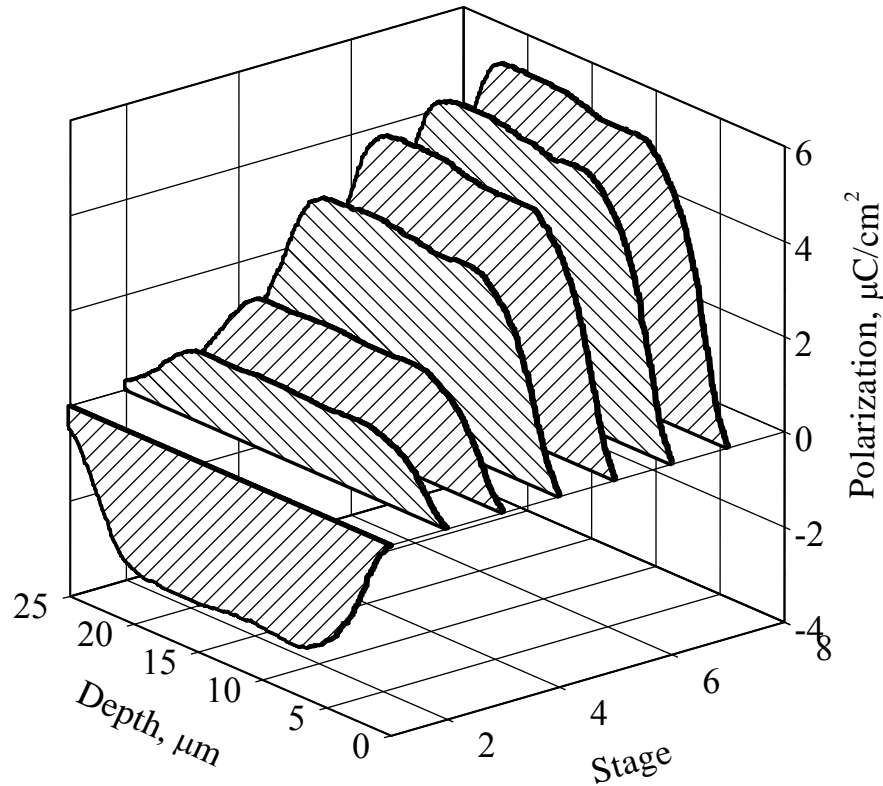


Fig. 4.5. Polarization profiles in the P(VDF-TFE) film initially poled at 3 kV after applying the opposite polarity voltage of different values. Stages: 1 – initial state, 2 – 1.2 kV, 3 – 1.6 kV, 4 – 2.0 kV, 5 – 2.4 kV, 6 – 2.8 kV, 7 – 3.2 kV.

Thus, the main features of poling and switching in high fields are as follows:

1. Polarization in the sample volume is homogeneous and symmetric with respect to the central section;
2. There is no difference in the shape of the profile and the magnitude of polarization at different polarizing voltages;
3. Polarization is easily switched over the entire volume, and full depolarization is possible;
4. Homogeneity of polarization is stored not only in high but also in middle fields.

Of great importance to practice, we have the effect of "formatting" or "conditioning" in a high field, after which homogeneous polarization is provided at any field strength, including the coercive field. This enables, if necessary, to change the magnitude and sign of the residual polarization in a wide range from zero to saturation that cannot be

achieved without this formatting.

4.4. Model of the polarization profile formation at constant voltage poling

From Fig. 4.2 it follows that in the initial stage of poling at 8 seconds after the application of a constant voltage creating an average field strength of 60 MV/m the polarization is uniform and corresponds to about $0.5 \mu\text{C}/\text{cm}^2$. This indicates a uniform distribution of the field strength and absence of injected charges [112]. At the same time, the stationary value of polarization, can be calculated by the formula corresponding to initial poling [67] taking into account its non-linear dependence on the field strength, the presence of the coercive value E_c and at 50% crystallinity

$$P_{st} = \frac{P_r}{2 \cdot (E_s - E_c)} (E - E_c) \quad (4.1)$$

Substituting in (4.1) the value of $P_r = 13 \mu\text{C}/\text{cm}^2$ [123], $E_s = 200 \text{ MV}/\text{m}$ [68], $E_c = 50 \text{ MV}/\text{m}$, $E = 60 \text{ MV}/\text{m}$, we obtain $P_{st} = 0.43 \mu\text{C}/\text{cm}^2$. The reversible polarization component P_{cap} is proportional to the field strength and the dielectric permittivity

$$P_{cap} = \varepsilon_0(\varepsilon - 1)E \quad (4.2)$$

Assuming $\varepsilon = 10$ [151] and taking into account that $\varepsilon_0 = 8.85 \cdot 10^{-12} \text{ F}/\text{m}$ and $E = 60 \text{ MV}/\text{m}$, we obtain $P_{cap} = 0.3 \mu\text{C}/\text{cm}^2$. From the graph of the polarization profile dynamics, it is seen that the value of polarization after 8 s of the voltage action is about $0.5 \mu\text{C}/\text{cm}^2$. Thus, all polarization is reversible, that is, the ferroelectric component during this time is not yet formed.

With further application of the field, the polarization becomes non-uniform (Fig. 4.2) indicating appearance of inhomogeneous distribution of the field strength with its weakening near the negative electrode and the increasing near the positive electrode. According to the Poisson equation, inhomogeneous polarization of this kind is possible only in the presence of excessive negative charge in the place of the field heterogeneity

$$\varepsilon_o \varepsilon \frac{\partial E(x,t)}{\partial x} = \rho(x,t) \quad (4.3)$$

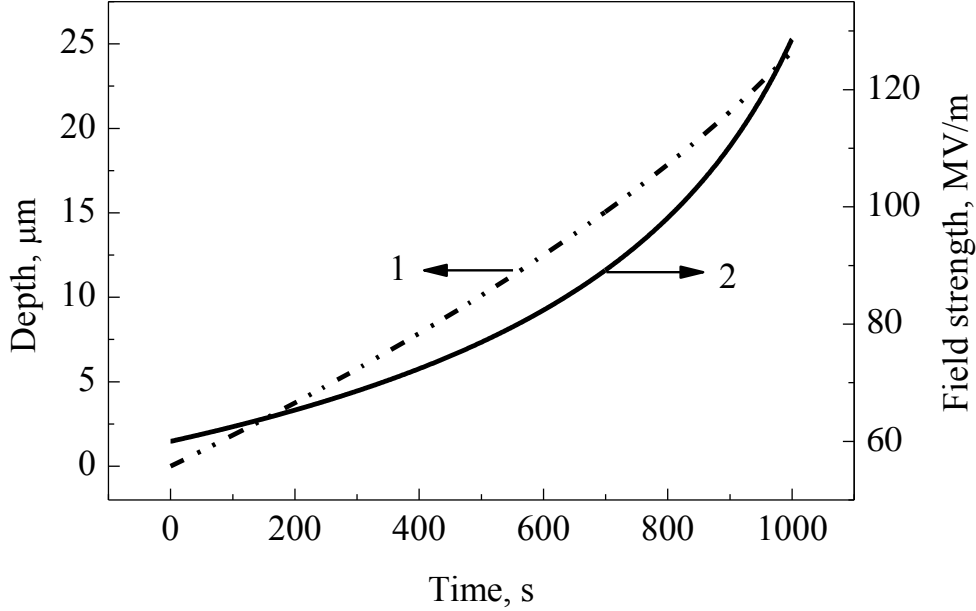


Fig. 4.6. Estimated graph of the front of injected charges motion after application of a constant voltage to the PVDF film under the charge mobility of $3 \cdot 10^{-16} \text{ m}^2/\text{V} \cdot \text{s}$ (1) and the time dependence of the field strength at the boundary, to which the front of the injected negative charges reached (2).

This charge is likely to be injected from a negative electrode and is present near this electrode extending with time to the sample depth. Without taking into account the formation of the ferroelectric polarization, it can be assumed that the charge distribution is close to the rectangular [119], and the speed of the charge front motion is determined by mobility μ and the field strength E_1 at the boundary x_l between the zone with the space charge and the zone free of excess volume charge

$$v(t) = \mu E_1 [x_1(t), t] \quad (4.4)$$

Since the applied voltage remains constant ($U_o = \text{const}$), the normalization condition is fulfilled

$$\int_0^{x_o} E(x,t)dx = U_o \quad (4.5)$$

The expression (4.5) is simplified when the rectangular distribution of the injected charge is assumed, since in the region from 0 to x_I , the field according to the Poisson equation (4.3) depends linearly on the coordinate, while in the other part of the sample it is constant and equal to E_I . Thus, for finding the $x_I(t)$ function and the field strength $E_I(t)$ we have the following system of equations

$$\frac{dx_1(t)}{dt} = \mu E_1(t) \quad (4.6)$$

$$E_1(t) \left[x_o - \frac{1}{2} x_1(t) \right] = U_o \quad (4.7)$$

The equations (4.6) and (4.7) were solved by numerical methods, and the graphs $x_I(t)$ and $E_I(t)$ are shown in Fig. 4.6 at $x_o = 23 \mu\text{m}$, $\mu = 3 \cdot 10^{-16} \text{ m}^2/\text{V} \cdot \text{s}$ [62], $U_o = 1380 \text{ V}$.

From the above graphs it follows that there is some acceleration of the motion of the injected charges front in time. At the same time, the field strength in the part of the sample which the injected charges has not yet reached increases with time exceeding the initial strength more than 2 times after 1000 s of poling.

The polarization switching time greatly depends on the field strength. Let us explain this provision in more detail. If we consider [68] that the switching time of the ferroelectric polarization in PVDF is about $5 \mu\text{s}$ at $E = 200 \text{ MV/m}$, and the dependence of the switching rate on the field strength is of the following form [67]

$$\tau = \tau_o \exp\left(\frac{E_A}{E}\right) \quad (4.8)$$

where τ_o has an order of 20 ns, then for the activation field E_A we will get the following

value:

$$E_A = E \ln \frac{\tau}{\tau_o} = 1.1 \text{ GV/m} \quad (4.9)$$

The polarization switching time in the field of 60 and 120 MV/m should be $\tau_{60} \approx 2 \text{ s}$, $\tau_{120} \approx 2 \cdot 10^{-4} \text{ s}$ in accordance with the formula (4.8).

Thus, the increase of the field strength by 2 times leads to decrease of the switching time by 4 orders of magnitude, but both values are small comparing to the time scale of the experiments. This allows to assume that the process of the ferroelectric polarization formation is quasi-stationary. In this case, we can disregard the dependence of the switching time on the field strength, but use the field dependence of the ferroelectric polarization (4.1) assuming that at any given time $P_{fe} = P_{st}$.

It was shown [178] that in the PVDF, in addition to the capacitive P_{cap} and the ferroelectric P_{fe} component of polarization, there is also a reversible component P_{rev} of the definitely not established nature, the presence of which is associated with dipole polarization in the amorphous phase of the polymer. The correlation between the components of polarization can be established by analyzing the evolution of the polarization profile after the voltage is switched off and the sample is short-circuited. In the process of poling, when the voltage is applied, there are all three components of polarization

$$P_I = P_{cap} + P_{fe} + P_{rev} \quad (4.10)$$

where $P_I = 3.31 \text{ } \mu\text{C}/\text{cm}^2$ at the point of maximum polarization. In case of the shortening, the components of P_{cap} and P_{rev} disappear and only the ferroelectric component remains, that is, $P_2 = P_{fe}$ with $P_2 = 1.71 \text{ } \mu\text{C}/\text{cm}^2$. Since the polarization formation process is rather slow, the experiment time is much greater than the Maxwell relaxation time

$$\tau_M = \frac{\epsilon_o \epsilon}{g} \approx 3 \text{ s} \quad (4.11)$$

At own conductivity of PVDF $g = 3 \cdot 10^{-11} \text{ Sm/m}$ [178], there is no reason to assume

that there is a partial back switching of the ferroelectric polarization due to insufficient compensation of the depolarizing field. Therefore, P_{fe} does not change with the short-circuiting. By the formula (4.1) we can find the corresponding polarization maximum of ($P_{st} = 1.71 \mu\text{C}/\text{cm}^2$) and the field strength $E = 89.5 \text{ MV}/\text{m}$. The capacitive component of the polarization $P_{cap} = 0.79 \mu\text{C}/\text{cm}^2$ according to the formula (4.2). Then the reversible component of the polarization will be equal to $P_{rev} = P_l - P_{cap} - P_{fe} = 0.81 \mu\text{C}/\text{cm}^2$.

Since the reversible polarization most likely, is due to the dipole structure of the amorphous phase, it can be taken into account by introducing the effective dielectric permittivity of the amorphous phase, which includes all the reversible processes

$$\varepsilon_a = (P_{cap} + P_{rev}) / \varepsilon_o E = 20.2 \quad (4.12)$$

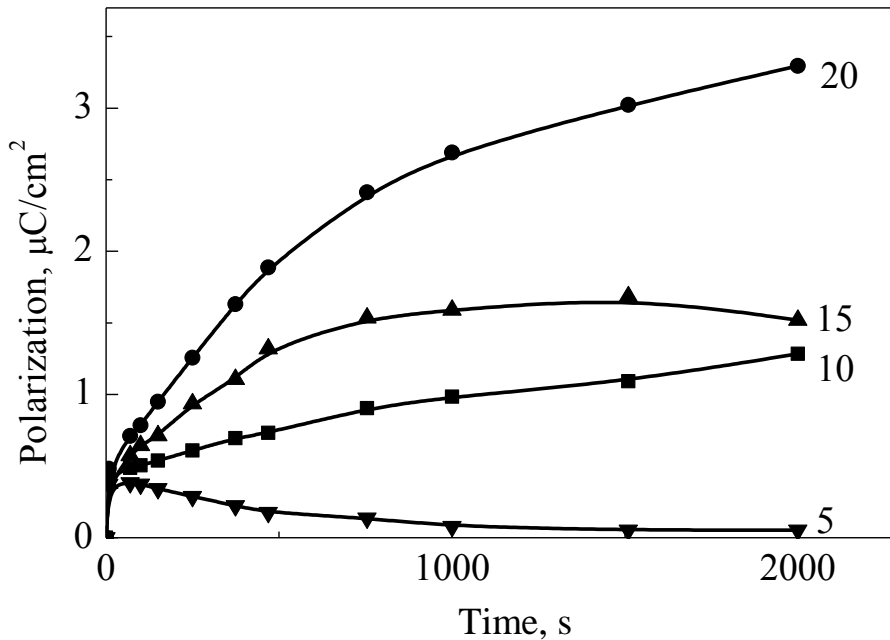


Fig. 4.7. Dynamics of polarization in the P(VDF-TFE) during initial poling in the field of 60 MV/m at different distances from the film surface (depth): 5, 10, 15 and 20 μm .

The obtained value of the same order (19,6) was used in the works of von Seggern and Fedosov [175,177] in calculations of the two-stage formation of the ferroelectric polarization in PVDF.

The dynamics of polarization in four cross sections (Fig. 4.7) shows that the degree

of heterogeneity increases, because the polarization of about $0.5 \mu\text{C}/\text{cm}^2$ near the negative electrode at the depth of about $5\text{-}6 \mu\text{m}$ does not increase in time, as it does in the second part of the sample, but it gradually decreases to zero (Fig. 4.7). At the same time, the maximum near the positive electrode located initially at a depth of $17.5 \mu\text{m}$, and then shifted to a coordinate of $15.4 \mu\text{m}$ increases with time.

This suggests that the ferroelectric polarization is not formed near the negative electrode, but there is a decrease of the field strength and polarization to zero. It is known from the theory of injection currents [112] that the field strength at the injecting electrode is very small or equal to zero, but near the electrode where excessive charge is located, the field is non-zero increasing linearly in case of the homogeneous charge distribution, as follows from the formula (4.6). If the charge density decreases in the direction of depth, the graph of the $E(x)$ dependence will be convex. That is, only injection of charges cannot explain the presence of a zone in the thickness of about $5\text{-}6 \mu\text{m}$, in which the field and polarization are almost zero. Obviously, there is another phenomenon that leads to decrease of the field strength and polarization near the negative electrode.

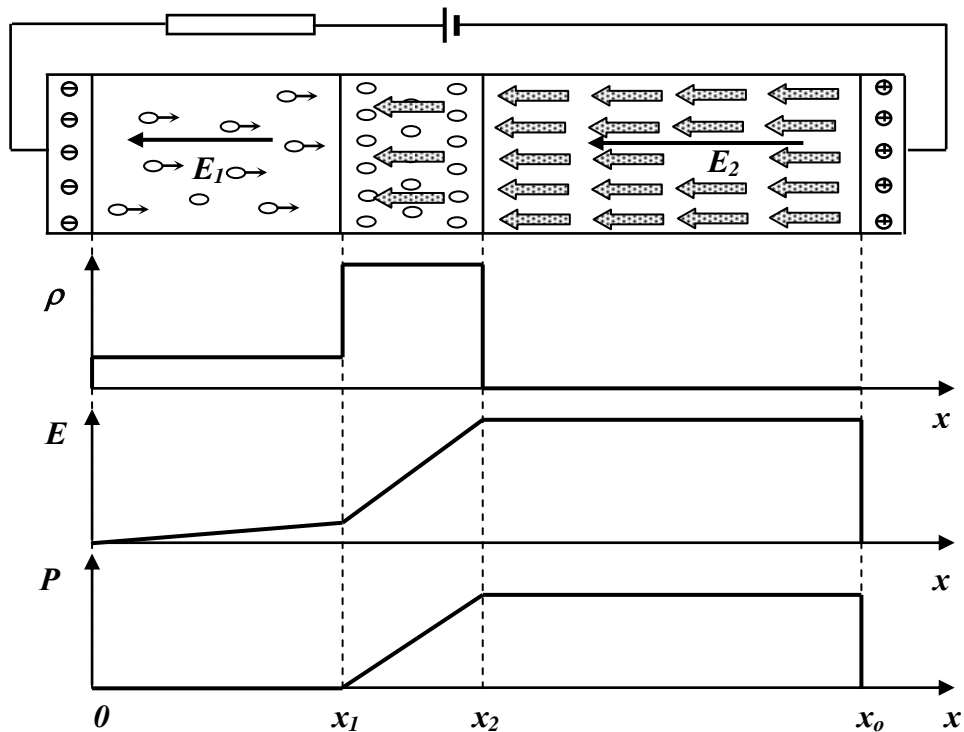


Fig. 4.8. Scheme of processes occurring during poling of PVDF films in middle fields and leading to formation of a heterogeneous three-layer structure. Also the distribution of the injected charge along the thickness, the field strength and polarization are shown.

It is known that the effective conductivity decreases sharply during formation of the ferroelectric polarization in PVDF [154], that is, it can be assumed that the conductivity of the polarized part of the sample is much smaller than that of the unpolarized part. In this case, the distribution of the total applied voltage U_o between the unpolarized and polarized parts occurs as between two connected in series resistors of different values. The voltage, and hence the field strength, is small in the unpolarized part, it is higher in the polarized part. This distribution of voltages contributes to the formation of even greater heterogeneity of the residuals polarization.

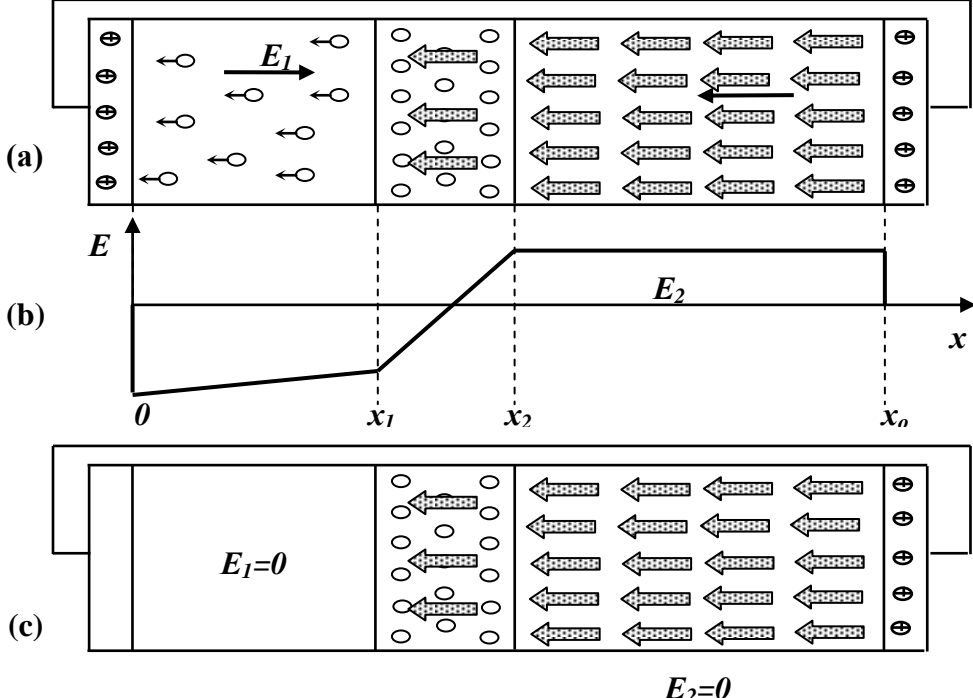


Fig. 4.9. Scheme of processes occurring in PVDF poled in middle fields at the moment of the short-circuiting (a), distribution of the field strength at the moment of cut-off (b), and state of the sample after aging in the short-circuited condition.

Thus, equations (4.6) and (4.7), which do not take into account the dependence of the effective conductivity on the ferroelectric polarization P_{fe} , only valid until the beginning of the P_{fe} formation. After this, the uniform motion of the injected charge is stopped, because its localization on the boundary of the polarized and unpolarized regions occurs in accordance with the Poisson equation (4.3). Chargers only partially penetrate into the polarized region or do not penetrate at all, that is, the effective conductivity of the polarized region decreases. There is a redistribution of the applied voltage, so that it

decreases at the unpolarized part, and increases at the polarized part. As a result, the field strength and reversible polarization decrease in the adjacent to the injection electrode region, while they increase in the polarized region. Exactly this is observed on the experimental curves of the polarization profile evolution (Fig. 4.2).

This phenomenon leads to the formation of a three-layer structure, schematically shown in Fig. 4.9.

In the area adjacent to the negative electrode, there is a high concentration of injected charges, high conductivity, low field strength and very low reversible polarization. At the boundary of the unpolarized and polarized regions, a layer of localized negative charges is formed. Within this layer, the field is heterogeneous and polarization sharply increases from zero to the maximum value. In the third zone, there is the homogeneous field and the homogeneous polarization.

When the sample is short-circuited after the completion of poling, the average field strength becomes zero. At the same time, the direction of the field strength vector in the unpolarized part of the sample E_1 (Fig. 4.9) becomes such that excess free injected charges from the first zone are "blown" through an electrode that was negative during poling. The reversible components of polarization in all zones are reduced to zero, the excess non-localized charges are dispersed due to their own conductivity, and the field strength at all points of the sample becomes zero with a time constant equal to the Maxwell's relaxation time (4.11), as shown in Fig. 4.9.

According to the experimental data of Fig. 4.2, the first zone occupies an area from $x=0$ to $x_1 = 6 \mu\text{m}$, the second zone is from $x_1 = 6 \mu\text{m}$ to $x_2 = 14 \mu\text{m}$, and the third zone is from $x_2 = 14 \mu\text{m}$ to $x_o = 23 \mu\text{m}$. As it follows from the experimental polarization profiles, the boundaries of the zones do not change with time. In the second zone, the excess negative charge is distributed almost uniformly. This is confirmed by the presence of practically linear sections of the polarization profile in this zone.

It is essential that the polarization profile changes with time at a constant voltage. This indicates that slow processes of transfer and redistribution of the space charge are involved in formation of the polarization and in its switching. In the general case, as follows from our data, the polarization is a complex function of the field, coordinates in the volume of the dielectric and time.

The obtained results correspond to the model, which provides an important role of the volume charge in the formation of the polarized zones in PVDF and the injection of

charge carriers from electrodes. Experimental data indicate that the level of injection of negative charges from the metal electrode is higher than from the positive electrode. It is also possible that the mobility of injected negative charges is much higher than positive charges. Intrinsic free carriers play a minor role in this case.

Thus, in case of initial poling, the homogeneity of the field is disturbed by injection of negative charges. In a large part of the sample near the injectable electrode, the field is attenuated and smaller than the coercive field, so the ferroelectric polarization is not formed there and the residual polarization is zero. At the same time, the field exceeds the coercive value near the positive electrode, and the high residual polarization is formed there. The polarization heterogeneity is fixed by negative charges trapped in the region where the gradient of polarization exists. The depolarizing field on the opposite side is compensated by positive charges located either at the electrode or in the near-to-surface layer.

After poling and short circuiting, the field in the peak area supports polarization. There is also a redistribution of moving charges: in the vicinity of the negative electrode, they move in the opposite direction to the injection until the field at all points of the volume becomes zero (Fig. 4.9). Uncompensated trapped charges remain only at the slopes of the polarization peak.

The massive trapping of injected charges at the boundary of the polarized region begins immediately as soon as a zone of the high polarization appears. This charged layer divides the volume into two parts. In the first part, adjacent to the negative electrode, there is no high polarization, and the concentration of free injected carriers is rather high. This results in a high apparent conductivity and, accordingly, in a weakened field in this zone in the process of poling. At the same time, the polarized region appears separated from the injection electrode by a layer of the trapped charge carriers, and its apparent conductivity becomes considerably smaller than in the first zone. This phenomenon can be considered as the Maxwell-Wagner effect induced by the non-homogeneous polarization, which leads to increasing field in the polarized region. That is why, with the passage of time, the polarized region does not expand, and the value of polarization increases. Phenomenologically trapping of charges and division into two zones is manifested in reducing the charging current at constant voltage, that is, in reducing the effective conductivity.

When polarity of the applied voltage is changed, the preferred injection of negative

charge carriers is again takes place, but they are injected from the opposite electrode. As a result, the region of the high field appears where the residual polarization was zero. This leads to the high polarization formation in new direction in this zone. In the area where residual polarization was strong, the field is weakened due to the injection of negative charges and presence of the negative bulk charge. Therefore, switching of polarization does not occur here, but a part of the residual polarization of the former direction remains.

In the zone of the negative space charge localization (8-15 μm), the direction and value of the polarization gradient do not change. This indicates that the negative charges trapped during initial poling are still in place, despite the fact that the polarization direction in the zone where they are located changes to the opposite direction. This unusual phenomenon is completely consistent with the Poisson equation for the case of a zero field. It is also possible that there is a delocalization of previously trapped carriers and their re-trapping without a significant change in the spatial position of localization.

Thus, after the switching, an asymmetric bimorph structure is formed, which is stored at subsequent transitions. The negative charge layer, judging by the polarization gradient in the region of 8-15 μm , is preserved as if it is fixed in the sample volume during all its transitions. The presence of this layer explains the faster formation of the polarization profile during switching compared to initial poling when this layer is not yet present. This same layer prevents formation of the homogeneous polarization even in case of high applied fields.

The effect of impossibility to improve the profile of polarization by increasing the applied voltage to the films initially poled in the middle fields can be explained by the influence of the injected and trapped charges [59]. From Fig. 4.7 it is seen that the polarization gradient at the boundary of the polarized region in the sample volume does not change the sign when the polarity of the switching external voltage changes. This indicates that in the volume there is a layer of deeply trapped negative charges, which plays the role of a barrier preventing the expansion of the polarized region. This layer is stable because it compensates for the depolarizing field in the regions lying at one and the other side of it (at different polarities of the external field). Since this layer obstructs the free motion of injected negative charges, their concentration in the region between this layer and the cathode is much greater than between the charged layer and the anode. Accordingly, the effective conductivities of these regions are different, and the applied

voltage is distributed unevenly, so that a significant part of the voltage is applied to the already polarized region.

Thus, increase in voltage can not increase the polarized region because of the presence of a blocking layer, that is, it does not improve polarization homogeneity. So, the initial inhomogeneous polarization remains inhomogeneous in high fields of any magnitude and polarity.

The phenomenon discovered by us is of fundamental importance from scientific, methodological and practical points of view. First, it further clarifies the mechanism of interrelation of the polarization with the trapped space charge. It would seem that a high field 3 times higher than the coercive field, should provide uniform polarization regardless of the initial conditions. However, this is not the case. The influence of the trapped charge is so significant that even high fields can not suppress it. Secondly, in the study of switching and hysteresis phenomena in ferroelectric polymers, it seemed self-evident to start electrifying from a weak field gradually increasing the applied field. That is how the hysteresis measurements are performed "at the infra-low frequencies". Taking into account our data it turns out that such measurements are incorrect, because the magnitude and, most importantly, the profile of polarization, depends not only on the field strength, but also on the pre-history of the sample.

It was established by studying poling and switching in high fields that polarization is homogeneous in this case and it is easily switchable over the entire volume. In case of high field initial poling, a complete depolarization is possible, and the polarization homogeneity persists not only in high but also in middle fields. These features can be explained by the fact that, given the presence of a high field, the polarized region quickly occupies almost the entire volume, which leads to blocking the movement of charges and a sharp weakening of the injection of charges role. The processes of compensation and neutralization of the depolarizing field occur in this case, either on the electrodes, or near the surface, so that the entire main volume remains free of injected and trapped charges, which could disrupt the field's uniformity and polarization. The change of the polarization gradient near the electrodes during the polarization switching indicates that the sign of the trapped compensating charges also changes. This is only possible if these charges are not trapped too deep, so they can be "shaken" from their traps under action of a high field with the subsequent localization in the same region.

4.5 Polarization profiles in P(VDF-TFE) films poled in corona discharge

Polarization profiles in P(VDF-TFE) have not been studied before, and the data obtained on other corona-charged ferroelectric polymers are rather fragmentary. For example, it was found that polarization occupies the central zone of a positively charged PVDF [33]. In another sample of PVDF, which was in similar conditions, the peak of polarization was found near the positive surface, while the biaxially stretched PVDF showed more or less uniform polarization [75]. The polarization profiles in polarized PVDF films that were poled in a negative corona turned out to be bell-shaped [72], while a significant decrease in polarization was observed near the positive side of a biaxially stretched PVDF poled in a positive corona [77]. Distortion of polarization homogeneity is usually considered as a consequence of the injected charge presence [33,44, 72,75,77], but the details of this mechanism are still only partially clear.

In [46], we report on measurements of polarization profiles obtained by applying a piezoelectrically generated pressure step (PPS) method to films P(VDF-TFE) that were charged in a negative corona discharge under different conditions.

The samples were films from experimental batches of 20 μm thick P(VDF-TFE) consisting of 95% VDF and 5% TFE. The films were extruded from the melt and stretched unilaterally by the supplier (Plastpolymer, Russia) and contained approximately 90% of the ferroelectric β -phase crystals according to the IR spectroscopy measurements. Aluminum electrodes with a diameter of 20 mm and a thickness of 150 nm were deposited at one surface of the samples by thermal evaporation in vacuum. Non-metallised films were also sometimes used.

Poling was carried out in a corona triode [44] with a bare surface of the sample subjected to a negative corona discharge initiated by a sharpened tungsten electrode. The ions and electrons passed through a control grid, which was held at a constant negative potential in relation to the grounded rear electrode. The polarization field was generated by charges adsorbed on the surface of the sample. The grid was made vibrating to allow simultaneous measurement of the surface potential by the Kelvin method and the DC poling current.

Six combinations with three poling parameters were investigated by maintaining the field strength at two levels (50 MV/m and 100 MV/m), temperatures (25 °C and 85 °C), and electrical mode (constant current and constant voltage). Moreover, we conducted

experiments with a multi-layered sample formed from identical films, in which only the lowest film was metallized that was in contact with a positive electrode. Immediately after completion of poling all samples were short-circuited for 15 minutes. The short circuiting was carried out by the non-electrode grounding of the bare sample surface. To do this, polarity of the corona was changed from negative to positive with the simultaneous grounding of the control grid. Thus, the sample was short-circuited, because its upper surface, now bombarded with positive corona discharge ions, received a grid potential equal to the potential of the rear electrode. The duration of the short circuit was long enough to provide a zero field everywhere in the main part of the sample. After the short circuiting, the samples were stored in an open circuit conditions.

Polarization profiles were measured at room temperature using a piezoelectric-induced pressure step (PPS) method. The full description of the method is given elsewhere [32,33], and only its basic principle is described here. The pressure step is generated by an electrically controlled quartz crystal connected to the sample. Pressure waves propagate at a sound speed (~ 2000 m / s) through a sample in the direction of the thickness causing an electrical signal measured by an oscilloscope with a bandwidth of 1 GHz and then digitized for further processing. It was shown [75,118] that the reaction of the short-circuit current to the pressure step provides a direct image of the spatial distribution of the piezoelectricity in the sample. It is also known [6,7,67] that piezoelectric coefficients in ferroelectric polymers are proportional to the level of the residual polarization. Thus, the magnitude of the current at any time was proportional to the residual polarization in the corresponding point of the sample. Therefore, the measured signal was calibrated directly in polarization units. A 23 μm polypropylene film was inserted between the sample and the measuring electrode to reduce the input capacitance. To obtain reliable data, we measured the polarization profiles twice on each sample.

We found that the residual polarization is distributed non-uniformly in P(VDF-TFE) films under constant current conditions, regardless of temperature, as can be seen from Fig. 4.10 and 4.11. The polarization peaks in the samples poled at room temperature are shifted to the positive side leaving almost half of the thickness not polarized (Fig. 4.10). In samples heated to 85 °C, the peak is higher and closer to the positive surface than at room temperatures (Fig. 4.11). Another small peak is observed near the surface bombarded with corona discharge ions in all samples poled by the constant current, as

shown in Fig. 4.10 and 4.11.

Multilayer samples were poled at constant voltage. The field strength was either moderate (50 MV/m) or high (100 MV/m). The first value was close to the coercive field of PVDF [7].

The polarizing field in the multilayered samples was not the same in all films from which the sample was composed. For example, from two films polarized in the average field of 50 MV/m, only the lower one, which was in direct contact with the positive rear electrode, contained the residual polarization (Fig. 4.12). The upper film bombarded by ions and electrons did not show any trace of the residual polarization indicating that the voltage was applied mainly to the lower film.

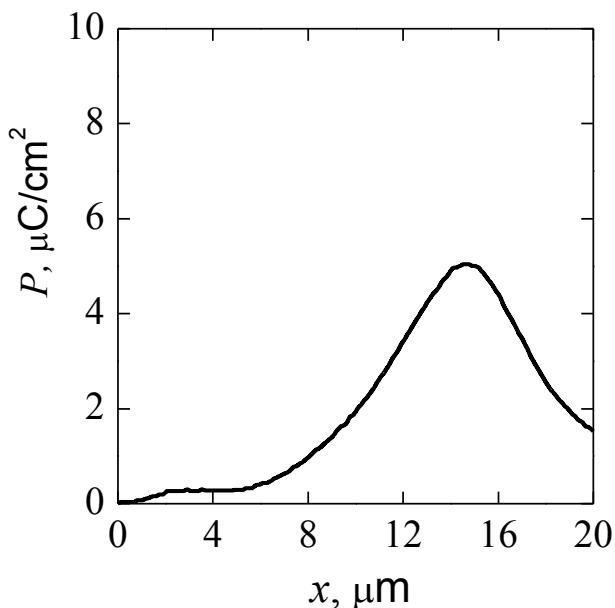


Fig. 4.10. Distribution of polarization in P(VDF-TFE) films after poling at 25 °C and the DC current density of 80 $\mu\text{A}/\text{m}^2$ for 15 min. The field at the end of poling was 100 MV/m. The coordinate $x = 0$ corresponds to the sample surface bombed by negative corona ions.

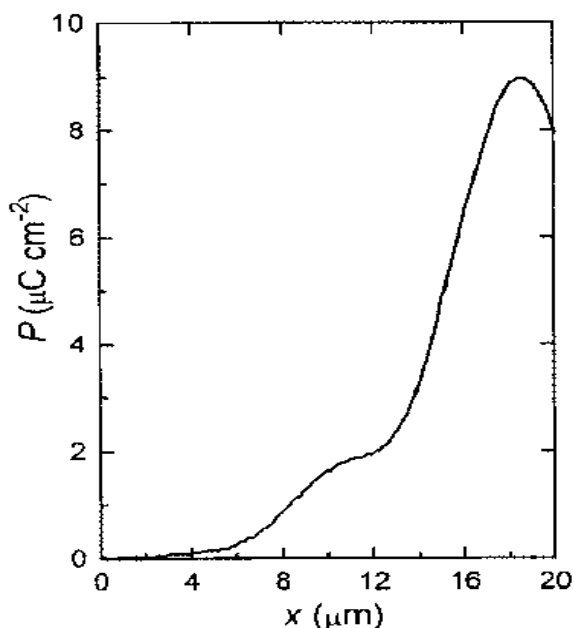


Fig. 4.11. Distribution of polarization in P(VDF-TFE) films after poling at 85 °C and the DC current density of 160 $\mu\text{A}/\text{m}^2$ for 15 minutes and cooled to 25 °C in the applied field of 100 MV/m. The $x = 0$ coordinate corresponds to the negative side of the sample.

However, both films are polarized in case of a high field, as can be seen from Fig. 4.13. The distribution of polarization in the lower ("positive") film is rather uniform (Fig. 4.13 (b)), whereas in the upper film there are two asymmetric peaks with the higher one located near the surface that was bombarded by the corona ions (Fig. 4.13 (a))

Three-layer and four-layer specimens were poled in the average nominal field of 50 MV/m. The results shown in Fig. 4.14 and 4.15 differ significantly from the results obtained on the two-layered samples (Fig. 4.12 and 4.13). Of the three films in the sample, the upper film, which was subjected to the action of ions, was not polarized at all.

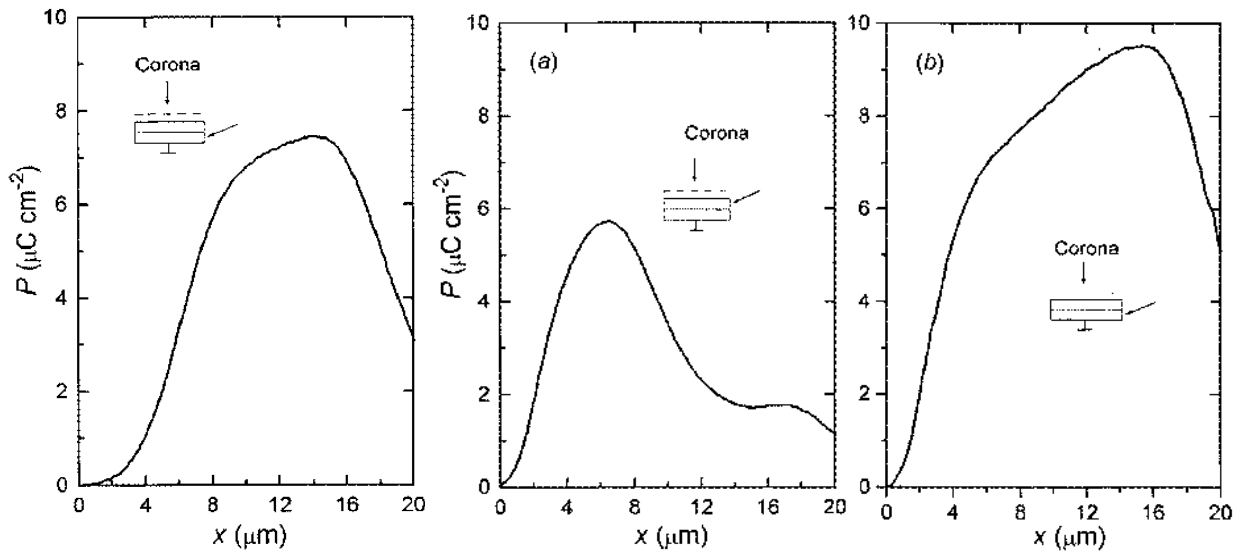


Fig. 4.12. Distribution of polarization in the lower film of a two-layered sample poled at 85 °C in the constant field with the average intensity of 50 MV/m for 15 minutes and cooled to 25 °C in the applied field. Coordinate $x = 0$ corresponds to the negative side of the film. The upper film bombarded by corona discharge ions did not have any residual polarization.

Fig. 4.13 Distribution of polarization in (a) upper and (b) lower films of a two-layer sample poled at 85 °C with the constant average field of 100 MV/m for 15 minutes and cooled to 25 °C in the applied field. Coordinate $x = 0$ corresponds to the negative side of each film.

The distribution of polarization in the film attached to the positive electrode is not uniform and similar to that in case of constant current poling (Fig. 4.10 and 4.11), while in the middle film there are two symmetric peaks separated by a saddle (Fig. 14 (a)) In case of four films, only two films at the positive side of the sample are polarized, but not uniformly (Fig. 4.15). Polarization peaks in both films are shifted to the positive side,

and the magnitude of the polarization is much higher in the film, which directly contacts the electrode, as seen in the Fig. 4.15 (a) and 4.15 (b).

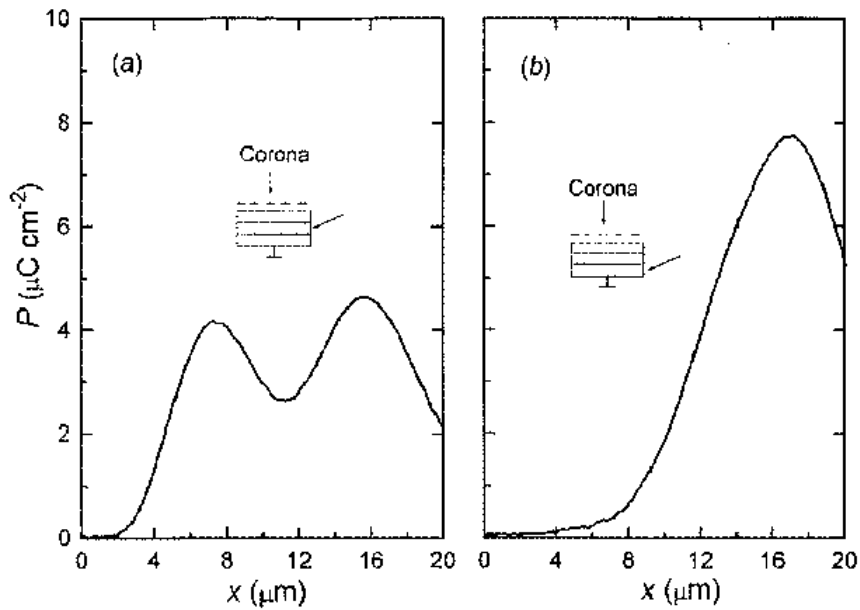


Fig. 4.14. Distribution of polarization in (a) middle and (b) the lowest films of a three-layer sample poled at 85 °C in the average field of 50 MV/m and cooled to 25 °C in the applied field. Coordinate $x = 0$ corresponds to the negative side of each film. The upper film bombarded with corona discharge ions did not have any residual polarization.

From our experiments on multilayer samples, it should also be anticipated that the polarization peak near the positive electrode with a large depleted polarization region near the negative electrode occurs in case of one thick film. A similar phenomenon was observed in corona poled PVDF films with a thickness of 120 μm [75].

Polarization and injection of charges

The heterogeneity of polarization in the direction of thickness in homogeneous specimens may obviously be due to the non-uniform distribution of the applied field. According to the Poisson equation, the inhomogeneity of the field strength $E(x,t)$ is due to the presence of either a real uncompensated charge $\rho(x,t)$ or the polarization charge $dP(x,t)/dx$:

$$\epsilon_o \epsilon \left[\frac{\partial E(x,t)}{\partial x} \right] = \rho(x,t) - \frac{\partial P(x,t)}{\partial x} \quad (4.13)$$

where ϵ is the dielectric constant, ϵ_o is the permittivity of a vacuum, P is the ferroelectric polarization, x is the coordinate in the direction of the film thickness, t is time. Since the polarization P itself depends on the field strength E , the initial heterogeneity of the poling field should be attributed only to the effect of real charges.

There are two main sources of the space charge in a dielectric. It can be caused by the spatial separation of already existing intrinsic positive and negative charge carriers, or by injection of charges to the volume from the outside. To show how to use equation (4.13) to distinguish the effects of injected and internal carriers, we first assume that the external voltage V is applied to a sample of thickness x_o , when the density of the injected charges is much lower than that of the intrinsic carriers.

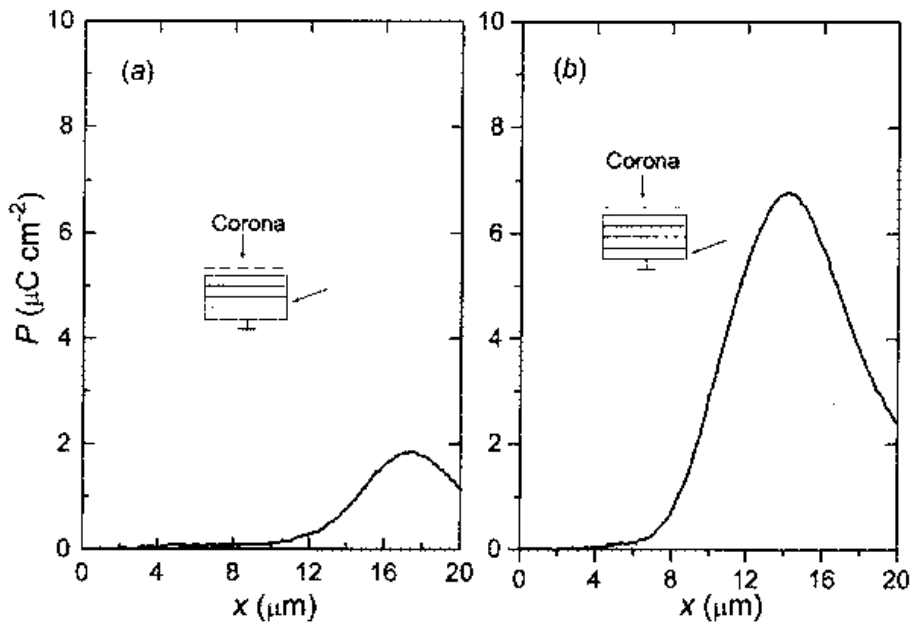


Fig. 4.15. Distribution of polarization in (a) penultimate lowest and (b) the last lowest film of a four-layer sample that was poled at 85 °C in the average field of 50 MV/m for 15 minutes.

Spatial neutrality inside the sample will be distorted due to the predominant movement of positive charges to the negative electrode and vice versa, as shown schematically in Fig. 4.16 (b). From equation (4.13) it follows that the field increases

near both surfaces of the sample and accordingly decreases in the central region. If the applied field $E_p = V/x_o$ is equal to or close to the coercive value E_c , then two peaks of the ferroelectric polarization will appear in front of the electrode sections separated by a non-polarized zone, as shown schematically in Fig. 4.16 (b).

Now suppose that the same voltage V is applied to another sample where monopolar injection of negative carriers takes place, and their density is much higher than that of the intrinsic charges. The injection charge does not affect the average E_p field, but creates heterogeneity of the field, as shown schematically in Figure 4.16 (a). The field at the injecting electrode is almost zero, but it increases in the direction of x in accordance with equation (4.13) until it reaches the E_c value at a certain depth. It is clear that the peak of the residual polarization will be shifted to a positive electrode.

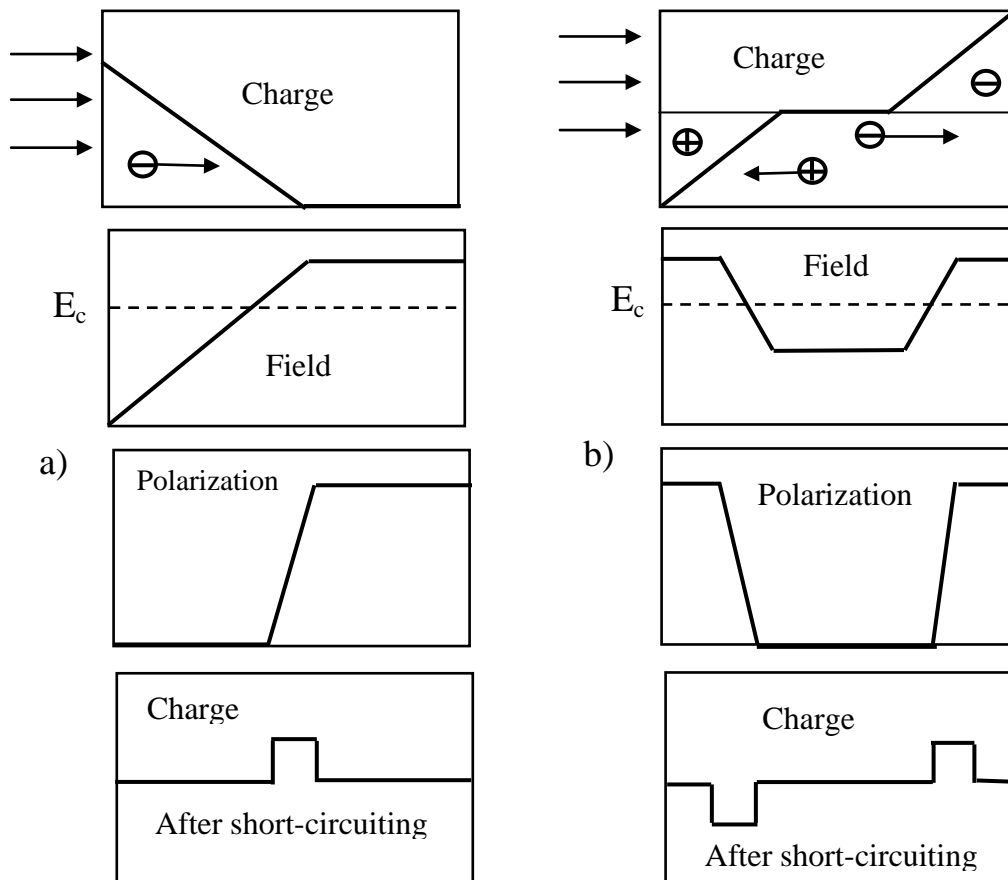


Fig. 4.16. Schematic diagram showing the distribution of volume charge, field strength and ferroelectric polarization during corona poling in case of (a) monopolar injection of negative charges and (b) separation of internal positive and negative charge carriers. The average field strength is equal to the coercive field E_c . Also shown is the distribution of localized charge after completion of poling

and short circuiting of the sample.

Thus, one can determine the dominant phenomenon from the position of polarization peaks. For example, profiles in fig. 4.13 (a) and 4.14 (a) indicate that the level of injection was low in these samples. However, injection of negative charges in many cases is more important than the separation of the intrinsic carriers. The consequence is visible, for example, in Fig. 4.10, 4.11, 4.14 (b), 4.15 (a) and 4.16 (b), in which polarization peaks in all these cases are observed near the positive electrode.

The charges injected during poling do not remain there after a short circuiting. They form a spatial charge that corresponds to the slope of the residual polarization profile, since $dP(x)/dx = \rho(x)$. $E(x) = 0$ under short circuit conditions.

The contribution of the space charge to the measured signal can not be experimentally separated from the residual polarization, but it can be considered as insignificant, since the piezoelectricity in ferroelectric polymers, to which the PPS method is sensitive [75,118] is caused by the residual polarization, but not by the space charge.

Our results obtained for P(VDF-TFE) films are consistent with the data on the polarization profiles observed in case of other ferroelectric polymers that have been poled in a corona discharge. The depletion of polarization near the negative side due to the charge injection was detected in PVDF and P(VDF-TrFE) [72,75,77]. Moreover, a similar phenomenon was observed in ferroelectric polymers, poled by the thermoelectret method [33,75], by direct application of a high field [12,29], and the electron-beam polarization [155].

The charge injection is most likely appears from a virtual electrode formed on a surface bombarded by electrons and ions. Our results show that homogeneity of polarization is more severely distorted by injection, if low or moderate fields are used. For example, the field in case of a constant voltage gradually increases from zero to about 100 MV/m, and the resulting polarization distribution is highly heterogeneous (Figs 4.10 and 4.11). Almost a quarter of the sample thickness is not polarized, since the field in this area is too low for the formation of the ferroelectric polarization. In case of two-layer samples poled in the average field of 50 MV/m, charges are mainly injected into the film under action of the corona that causes increase of the film conductivity. We assume that the conductivity corresponds to the following equation

$$g = e[n(\mu_+ + \mu_-) + n_+\mu'_+ + n_-\mu'_-] \quad (4.14)$$

where e is the elementary charge, n is the density of the carriers, n_+ and n_- are injected charge densities, μ_+ , μ_- , μ'_+ and μ'_- are mobilities of intrinsic and injected carriers (they may be different). This expression implies that the conductivity increases if injection takes place. As a result, the applied voltage is redistributed, so that its main part is applied to a film attached to the positive electrode. The distribution of polarization in such a film is quite homogeneous (Fig. 4.12), although the effect of the negative charge injection is still considered as a thin non-polar layer near the negative side of the sample. The top film was completely unpolarized because there was a very low field. Similarly, one film in a three layer and two films in four-layered experiments are also not polarized.

The results of our measurements on P(VDF-TFE) films coincide with the results obtained from multilayered experiments on PVDF films poled by the thermoelectret method [127,139,160], but the explanation of this phenomenon is different. The increase of the pyroelectric and piezoelectric activities near the positive electrode was attributed [127,139,160] to the effect of the positive charge injection. We believe that, according to the theory of injection currents [110,112], the heterogeneity of the field and hence polarization is due to injection of the negative charges, but not the positive ones, as previously thought [127,139,160].

This is considered normal if the charge is injected either from a real metal electrode, or from a virtual electrode formed on the surface of the sample bombarded by electrons and ions. However, our results indicate that the virtual injecting electrode can also be formed on a surface that was neither metallized nor bombarded by ions. Exhaustion of polarization at the negative side of the samples shown in Fig. 4.12, 4.14 (b), and 4.15 (b) proves that in all these cases, a negative charge is injected.

Transition zones

It is worth analyzing the behavior of the space charge after the completion of poling. Immediately after a short circuiting, the average field in the sample becomes zero, but the local field still exists. Therefore, mobile charges are redistributed under the action of

this field until the field becomes zero at any point of the sample. The characteristic Maxwell relaxation time for this process is given as

$$\tau = \varepsilon_o \varepsilon / g \quad (4.15)$$

where g is the explicit conductivity. Considering the typical values of $g = (10^{-11}-10^{-12}$ Sm/m [151]) for PVDF and its copolymers, we obtain $\tau \approx 10-100$ s. The real value of τ is even lower, since additional carriers are introduced during poling, and the apparent conductivity increases accordingly, as can be seen from equation (4.14).

From equation (4.13) it follows that under conditions of equilibrium ($E(x) = 0$), the spatial charge $\rho(x)$ can be localized only at the boundaries of the polarized zones where the derivative $dP/dx \neq 0$.

$$\rho(x) = dP(x) / dx \quad (t > \tau) \quad (4.16)$$

It is clear from equation (4.16) that thickness of the transition zone where the polarization decreases from its maximum value to zero, depends on the density of the charge, therefore, the higher the density of the charge, the narrower the transition zone.

The thickness of the transition zone can not be measured with a high precision by the PPS method, since its resolution (2 μm) is comparable to the thickness of the zones. However, these values can be estimated by comparing the growth time of the measured electrical signal and the pressure step. The first in all cases was longer than the last, indicating that the transition zones are thicker than 2 microns. For example, the most delicate transition zones (4-5 μm) are shown in Fig. 4.12 and 4.13 (b). The corresponding times of the electrical signal grows and the pressure step are 2-3 ns and 1 ns, respectively.

It is known that any polarization heterogeneity creates a polarization charge with the density of $dP(x)/dx$. This charge creates a depolarizing field, which tends to switch the ferroelectric polarization back to its original state after the completion of poling. The residual polarization can be stable only if the depolarization field is compensated or neutralized [49]. We believe that in case of the ferroelectric polymers, the compensation is carried out by the spatial charge $\rho(x)$ trapped in the transition zones, by which the polarized part of the sample is separated from the unpolarized part. Since the

polarization charge $dP(x)/dx$ and the real charge $\rho(x)$ are equal to each other (according to equation (4.16)), the depolarizing field is completely compensated, so that $E(x) = 0$ everywhere in the sample. We consider the existence of the transition zones in conjunction with compensating spatial charges as a general feature of poled P(VDF-TFE) and, probably, of all other ferroelectric polymers. Presence of the spatial charge in the transition zones is a guarantee of a high stability of the residual polarization.

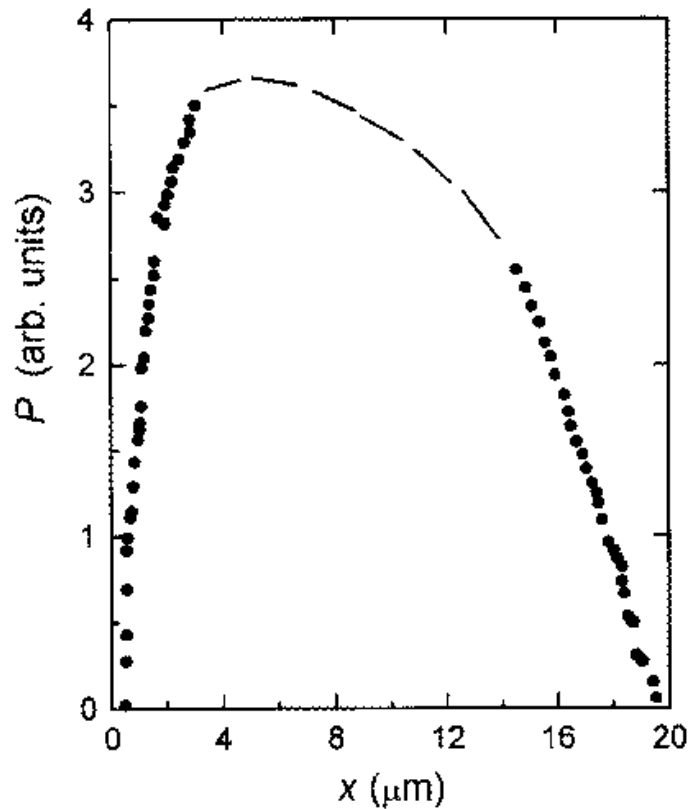
Near-to surface areas

We observed two types of polarization profiles in near-to-surface zones of P(VDF-TFE). The residual polarization was zero to a certain depth, as can be seen in Fig. 4.10, 4.11, 4.14 (b), 4.15 (a) and 4.15 (b) near the negative surface. In other cases $P_r = 0$ near the positive surface, as shown in Fig. 4.10, 4.11, 4.12, 4.13 (b), 4.14 (b), 4.15 (b) or near the negative surface in Fig. 4.12, 4.13 (a), 4.13 (b). It is clear that zones of the first type are created due to the massive injection of negative charges during poling, because the field near the injection surface is reduced and the ferroelectric polarization is not formed. The thickness of the unpolarized zone depends on the depth of the injected carriers penetration. The zones are particularly wide in case of moderate poling fields, as can be seen from Fig. 4.10, 4.11, 4.15 (a) and 4.15 (b). On the other hand, if the polarizing field strength is high, the near-to-surface zones are very narrow if the negative charges are not injected deeply into the volume (Fig. 4.12, 4.13 (a), 4.13 (b), 4.14 (a)).

In some cases, the separation of the intrinsic charge carriers dominates over the external injection. Then there are two polarization peaks at the two sample surfaces. Unpolarized near-to-surface zones are either very narrow or not observed at all (Fig. 4.13 (a) and 4.14 (a)). According to our results, it can be concluded that a certain time is required for the injected charge for deep penetration into the bulk. This can only be done if the pre-poled regions are unpolarized, for example in case of low or moderate electric fields. However, if the ferroelectric polarization is already formed near the surface, as in case of a high field, the injected charge cannot easily pass through a polarized region. It seems that the effective conductivity of the polarized regions is much lower than that of unpolarized ones.

The second type of near-to-surface zones with rather high polarization can be seen

near a metallized surface attached to a positive electrode during poling. The role of a positive electrode in the accumulation and distribution of polarization has been widely discussed since the discovery of the inhomogeneous distribution of piezoelectricity and pyroelectricity in PVDF [127,139,160], and many contradictory explanations of this phenomenon were proposed [152]. Our measurements show that the maximum polarization appears in all metallized samples near the positive electrode. This means that the conditions are favorable both for the rapid development of ferroelectric polarization, and for its stabilization. Positive charges are either not injected or deeply trapped very closely to the surface creating good conditions for compensating the depolarizing field. At the same time, the trapped charges do not allow the attachment of



a highly polarized zone directly to the electrode.

Fig. 4.17. Distribution of polarization measured by the method of the modulated intensity of laser radiation in near-to-surface regions of a nominally well-poled P(VDF-TFE) film. The conditions for poling were the same as for the sample shown in Fig. 4.5. Coordinate $x = 0$ corresponds to the negative side of the film.

The PPS method with a resolution of about $2 \mu\text{m}$ cannot provide more information

about the fine structure of near-to-surface zones, but this can be achieved by using the LImm method [114]. Polarization profiles in uniformly electrified P(VDF-TFE), measured by this method, are presented in Fig. 4.17. We used the same specimens as those for which the results obtained by the PPS method are shown in Fig. 4.13 (b). It is known that the resolution of the LImm method is about 0.1 μm near the illuminated electrode [140].

As can be seen from Fig. 4.17, the polarized zones are not directly attached to the positive and negative surfaces. The transition zones consist of thin layers where the polarization drops from maximum to zero and is supplemented by a completely unpolarized layer of about 0.5 μm thickness.

This can be considered as evidence of a charge injection, since it is known that the field at the injection electrode is either zero or it is very low [110,112]. However, not only electrical properties, but also structural heterogeneity in the near-to-surface zones can contribute to the formation of transitional and unpolarized zones.

Thus, the poling of the P(VDF-TFE) copolymer in a negative corona at room temperature under direct current conditions leads to the inhomogeneous distribution of polarization with a peak near the positive electrode, while the wide zone near the surface that was bombarded by electrons and corona discharge ions remains unpolarized .

The thermal stimulation does not improve the polarization uniformity, but affects the magnitude of the peak. The polarization distribution in moderate poling fields highly affects the injection of negative charge carriers from a virtual electrode formed either on the sample surface or between two bare contacting surfaces (in case of multilayered samples). In most cases, the charge injection predominates over the distribution of the intrinsic carriers.

The applied voltage is distributed non-uniformly between layers in case of multilayered samples poling. Only the film near the positive electrode shows a high and fairly uniform polarization, while the upper films remain unpolarized indicating that the injected charge permeates the entire thickness of the film.

Therefore, to obtain a uniformly polarized P(VDF-TFE) copolymer film in a moderate field, it would be advisable to cover the main sample during poling with another auxiliary film.

In case of high poling fields, the residual polarization is homogeneous, since

injections of charges are suppressed. But even in this case, the polarized part of the volume is separated from the sample surfaces by transition zones where compensating charges are trapped. A thin layer of about 0.5 μm thickness always remains completely unpolarized near the sample surfaces.

4.6 Thermal stability of polarization in P(VDF-TrFE) copolymer

Recently, it has been shown that a high stability of the residual polarization in PVDF and P(VDF-TrFE) is due to interaction of the polarization with the injected charge trapped at the boundaries of crystallites or macroscopic polarized regions [11,58,67,102,108,185].

In both cases the polarization and the space charge form a stable and a self-consistent system in which the latter plays a decisive role. Assuming Debye's approximation for relaxation and the continuous distribution of activation energies for the charge trapping, Eisenmenger et al. received such a distribution for PVDF and P(VDF-TrFE) [108]

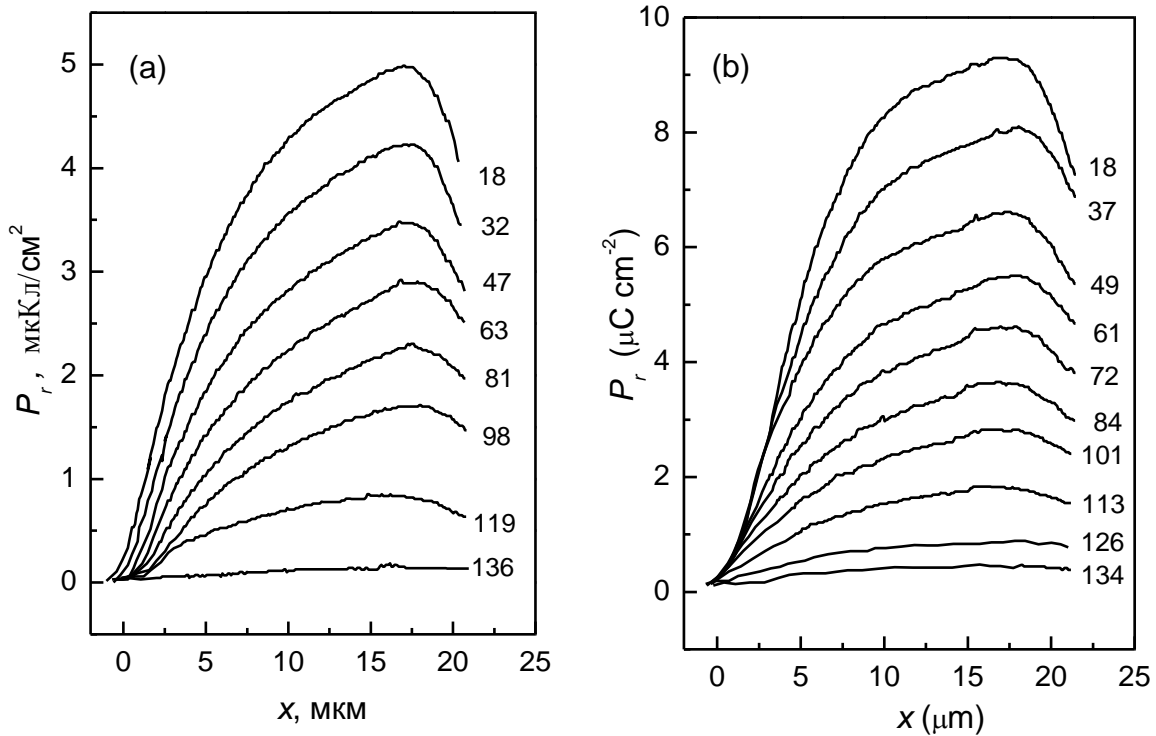


Fig. 4.18. Spatial distribution of polarization at different temperatures in P(VDF-TrFE) films poled (a) by direct application of the high field strength and (b) by the thermoelectret method. Zero on the axis of the thickness corresponds to the negative surface of the sample during processing. Figures indicate the

temperature (in °C).

Our purpose was to find out how the bulk charge affects the thermal stability of the residual polarization in P(VDF-*TFE*) copolymer which also belongs to the class of the ferroelectric polymers [84,126], but is much less studied than PVDF and P(VDF-*TrFE*).

To do this, we measured the polarization profiles in P(VDF-*TFE*) samples as a function of temperature by performing the linear heating from 20 °C to the melting point of crystallites. The activation energy was calculated by applying our experimental data and the theoretical model proposed in [108]. The obtained results were compared with those that are known for PVDF and P(VDF-*TrFE*) copolymer.

The samples were cut from experimental batches of P(VDF-*TFE*) 20 μm thick copolymer films containing more than 90% of the ferroelectric β-forms in the crystalline phase. Aluminum electrodes with a diameter of 4.5 mm and a thickness of 0.15 μm were deposited on both sides of the samples by thermal evaporation in vacuum.

Poling was carried out either by direct application of high voltage (3.2 kV at 20 °C for 2 min) or by thermoelectret method (2.5 kV at 85 °C for 10 min and fast cooling to 20 °C with the switched on applied voltage).

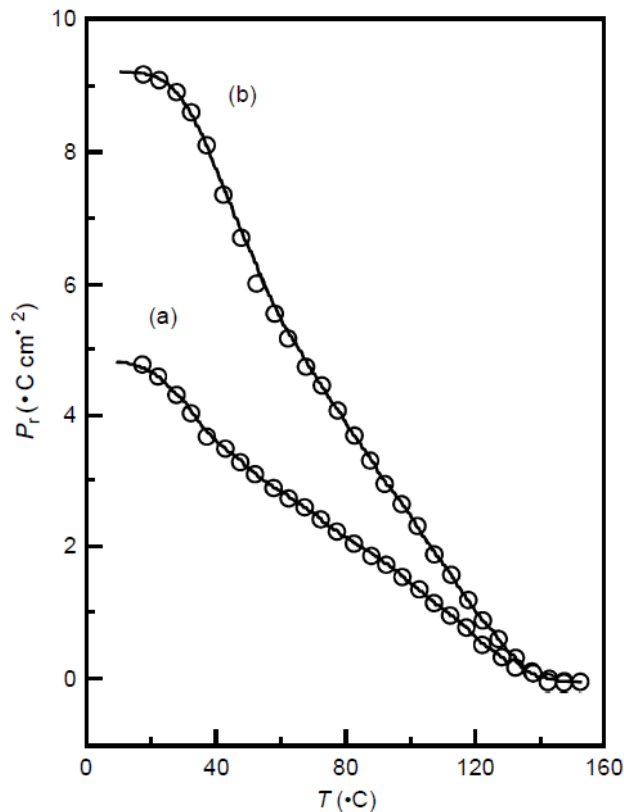


Fig. 4.19. The value of residual polarization in P(VDF-*TFE*) obtained experimentally (points) and

theoretically (solid lines) depending on (a) poling in a high field and (b) the thermoelectret method.

The polarization of the field in both cases was three to four times greater than the coercive field, which is 35-40 MV/m in P(VDF-TFE) [32,89].

The residual polarization profiles in the direction of the sample thickness were measured with a repetition rate of about 100 Hz using the PPS method [165], while the temperature was linearly increased at a rate of 3 K/min from 20 °C to the melting point of the crystallites, which turned out to be 134 ± 2 °C.

It is established that the distribution of polarization in the thickness direction is rather uniform, except for areas close to the electrode zones, where the polarization decreases from the maximum to the low value (Fig. 4.18). The profiles of polarization at all temperatures were slightly asymmetric, with a maximum located near the positive electrode, similarly to that observed in other ferroelectric polymers [11,165,185]. We used these maximum values for evaluating the thermal stability of the residual polarization.

From the data presented in Fig. 4.19, it is clear that the polarization in P(VDF-TFE) breaks down with the temperature throughout the studied range almost linearly decreasing from the maximum at room temperature to zero at a melting point (134 °C). This behavior is significantly different from PVDF and P(VDF-TrFE) [108] where the polarization decreases only when the temperature exceeds 90 °C.

It is known that the residual polarization in conventional inorganic ferroelectrics does not depend highly on temperature below the Curie point [43], but this dependence is higher in the ferroelectric polymers, since they contain about 50% of the amorphous phase and they have residual polarization in crystallites stabilized by trapped charges [11,58,185]. Since the charge can be released by the thermal activation, it should be expected that the stability of the polarization highly depends on the thermal stability of the trapped charges. Reducing the charge will shift the corresponding polarization area so that the equilibrium will be restored again at slightly lower levels of both polarization and spatial charge.

It is advisable to use the Debye approximation for the relaxation of polarization with the temperature dependence of the decay constant corresponding to the Arrhenius law. Then, the current of depolarization $i_a(T)$ in case of one activation energy is [108]:

$$\begin{aligned}
i_a(T) &= -dP/dT = \\
&= [h \cdot f_o \exp(-a/T)] \cdot P_o \exp\left[-h \cdot f_o \int_{T_o}^T \exp(-a/T) dT\right]
\end{aligned}
\tag{4.17}$$

where h is the heating rate, f_o is the proper frequency, P_o is the initial value of polarization at T_o , $a = A/k$, where A is the activation energy, k is Boltzmann's constant.

Taking into account that energy is continuously distributed on the surface of the polarized crystallites [58] surrounded by a disordered amorphous phase, one can conclude that the energy spectrum of traps is, most likely, continuous, rather than discrete. Therefore, the total depolarization current $i(T)$ is a superposition of all relaxation components:

$$i(T) = \int_0^\infty g(a) i_a(T) da \tag{4.18}$$

where $g(a)$ is the distribution function of activation energies. It was shown that the depolarization current $i(T)$ calculated from the experimental curve $P(T)$ is an image of the distribution function $g(a)$:

$$i(T) \propto g(mT) \tag{4.19}$$

where m is a constant value.

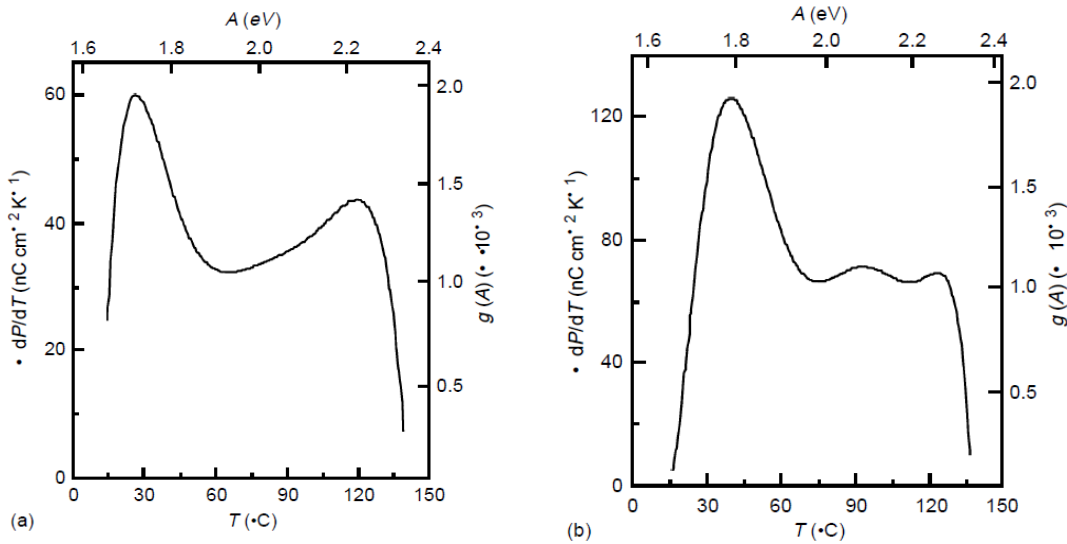


Fig. 4.20. The temperature dependence of the depolarization current $i(T) = dP / dT$ and the distribution function of the activation energy in P(VDF-TFE) calculated depending on (a) poling in a high field and (b) by the thermoelectret method.

The results of calculations based on experimental data of Fig. 4.19 are shown in Fig. 4.20. It is clear that the high-temperature behavior of the P(VDF-TFE) copolymer is regulated by two relaxation processes characterized by significantly expanded energy levels. The low-temperature peak in thermoelectret samples is slightly shifted to lower energy, whereas the high-temperature peak does not affected by the heat treatment. The relationship between the values of the two peaks in P(VDF-TFE) differs from PVDF [108] where the second peak is more advanced than the first one.

Comparing the curves in Fig. 4.20a and 4.20b, one can see that there is no significant difference in the magnitude and distribution of the activation energies in the samples polarized in a high field strength and by the thermoelectret method. This indicates that the residual polarization in P(VDF-TFE) is not thermally frozen, as in case of ordinary polar thermoelectrets, but it is stabilized, most likely, by the field of the trapped charges. P(VDF-TFE) has two components of polarization, namely: a ferroelectric component and an electret component. The first one is concentrated in the crystalline phase, and the second is localized in the amorphous phase. Therefore, the two peaks shown in Fig. 4.20 can be related to the relaxation of these polarization components. A similar behavior was observed in PVDF and P(VDF-TrFE) copolymer [108] indicating that this phenomenon is likely to be common in the whole class of the ferroelectric polymers.

It is known that the ferroelectric polarization is stable only when the depolarizing field is somehow neutralized or compensated [43]. In the ferroelectric polymers, this compensation is performed by trapped charges [11,58,108,185]. Since the charge is deeply trapped and the binding energy is in the range of 1.65-2.35 eV, as can be seen from Fig. 4.20, the spatial charge effectively compensates the depolarizing field in the crystals. This explains the high polarization stability at room temperature. According to our calculations, based on the data of Fig. 4.20, polarization is expected to decrease to 90% of its initial value for about one year.

The model of the continuous distribution of activation energies was verified by calculating the dependence $P(T)$ by using the data given in Fig. 4.20. The results of the calculations shown in Fig. 4.19 by solid lines agree with the experimental data indicating that the thermal stability of the residual polarization in P(VDF-TFE) and, probably, in other ferroelectric polymers, is indeed controlled by the trapped volume charge.

Chapter 5. Thermally stimulated processes in ferroelectric polymers

5.1. Thermally stimulated depolarization (TSD) of ferroelectric polymers

To measure the thermal relaxation of the residual polarization, the measurement of the thermally stimulated depolarization currents (TSD) is the most appropriate. Despite numerous experimental studies, there is still no theory of the TSD current method for the case of poled ferroelectric polymers like PVDF. Therefore, the description and interpretation of measured current peaks are usually qualitative and hypothetical.

To detect the nature of the TSD current peaks, their connection with polarization and pyroelectricity must be taken into account, as well as processes occurring in the amorphous and crystalline phases. Such an attempt was made [145,146] by considering individual contributions to TSD currents of pyroelectric processes, polarization in the amorphous phase, "charge-induced interphase polarization" (called the Maxwell-Wagner effect) and the ferroelectric polarization in the crystalline phase. In qualitative description of the predicted processes, in addition to compensating charges, "injected surplus charges" were taken into account, that is, space charges. Often it is considered as a self-evident that there are polarization in PVDF, compensating charges, and space charges. While there is no doubt about the existence of polarization, the existence of the space charge in addition to compensating charges is questionable, since PVDF has a sufficiently high specific conductivity about $g = 10^{-11}$ Sm/m at room temperature [174,177] and the dielectric permittivity $\varepsilon = 10-20$.

Therefore, any surplus charges will be neutralized with the Maxwell relaxation time of approximately

$$\tau = \frac{\varepsilon_0 \varepsilon}{g} \approx 13 \text{ s} \quad (5.1)$$

This indicates that in the short-circuited sample, after about 40 seconds, any electric field caused by charges (other than compensating charges and polarization charges of the ferroelectric crystals) will disappear.

Homogeneously polarized two-phase materials, like PVDF, consist of ferroelectric crystallites scattered in the amorphous matrix. Compensation of the depolarizing field in

the ferroelectric crystallites is possible only due to the charges localized at two sides of the crystallites. Full compensation by the electrode charges, as in case of single crystals or 100% crystalline materials, is not possible. In PVDF and other biphasic ferroelectric polymers, the accumulation of charge at the boundaries between the crystalline and amorphous phases only occurs to a small extent due to the difference in dielectric constant, and is the most likely due to presence of the ferroelectric polarization. von Seggern and Fedosov proposed a model of a layered structure with alternating ferroelectric and non-ferroelectric layers for the description of initial poling [174,177], switching of polarization [175], short circuiting and the back switching [62] in PVDF.

The theory of the TSD method [23,173] was developed only for electrets with dipole and/or space charge polarization. It is assumed that polarization or space charge is initially thermally frozen, and then it defrosts under linear heating. For application the TSD method to ferroelectric polymers, the theoretical basis has not yet been constructed, since polarization in PVDF is not thermally frozen, but has the ferroelectric nature and can occur in high fields without heating during poling. In addition, in addition to the irreversible relaxation currents, in the TSD experiments on ferroelectric polymers, there are reversible pyroelectric currents, and the separation of these components is not an easy task. However, the TSD method, due to its informative and versatile nature, has been widely used for studying the polymer ferroelectric as well.

The TSD current peak at 50-60 °C was observed by many researchers in a non-ferroelectric α -PVDF and the ferroelectric β -PVDF poled in a wide range of temperatures, electric fields and times [22,42,50,90,96,106,111,133,167,168,170]. The only common feature of all PVDF samples on which these experiments were carried out is the presence of an amorphous phase. Thus, this TSD current peak with high probability can be associated with processes occurring in the amorphous phase of PVDF.

In many cases, it was assumed that the TSD current peak near 50-60 °C is associated with the so-called α_c -process [170,167,133]. However, data on the nature of the α_c -process are still controversial. Moreover, an interrelation between structural transformations and TSD currents should be established, since the TSD currents are the result of electrical, but not always structural processes. Making assumptions about the nature of the TSD currents peaks, it is necessary to take into account not only structural transformations, but also fundamental electrical principles and laws. Otherwise, a

qualitative explanation without the corresponding formulas and equations may be false.

Two high-temperature peaks, in addition to the usual α - and β -processes in PVDF, were found by the TSD method. One of the processes was attributed to charges trapped on the boundary between the nonpolar crystalline α -phase and the amorphous region. The other was assumed to be related to charges on polar β -crystallites. The authors believe that both peaks are due to the positive homocharge injected from the anode, although it is quite probable that they are related to the of the poling temperature.

Eliasson [36], studying the influence of the polarizing field, temperature, and electrode material on TSD currents, believed that the formation of a bulk charge was influenced by injection, although her results did not match with the position and magnitude of peaks in the data of Ieda and others [98]. The picture becomes even more complicated if we compare the data on the TSD obtained by different researchers (Table 5.1). The variety of relaxation processes determined by the TSD method is due to the lack of clear methods for identifying peaks (sometimes they take for relaxation peaks the smallest bends at the TSD current curve). Neagu and others [133] believe that the high influence on the TSD currents has the material of electrodes and the uncontrolled composition of the atmosphere, in particular the presence of oxygen, nitrogen and water vapors.

Table 5.1

Characteristics of the TSD peaks in PVDF films

$T_{max}, ^\circ\text{C}$	Q, eV	Nature of the peak	Main features	The poling method	Samples	Reference
-43	-	Microbrown motion	Glass transition	TE* 40 MV/m, 40-120 °C	35 μm , α -phase	[10]
27-77	0.8	Relaxation of volume charge	The peak shifted to low T with increase in E			[10]
87	1.0	Relaxation of charges at the α - β boundary	The peak appears at $E > 40$ MV/m			[87]

-43	-	Relaxation of dipoles in the β -phase	Increases with the growth of the polarizing field	TE 40 °C	15 μm , β -phase	[10]
80-83	0.7	Relaxation of heterocharge	Relaxation of the displaced ions	TE 120 °C 0.2-12 MV/m	-	[80]
53	-	-	-	TE 50 °C 21 MV/m,	-	[143]
-51	3.2	Reorientation at glass transition	Wide peak	TE, 20 MV/m, 80-110 °C	50 μm	[9]
12		Related to relaxation of the γ -phase	Correlated with the IR spectra	TE, 120 °C 6 MV/m	50-100 μm	[9]
30-55	1.7	The charge relaxation in ion traps	T_{max} increases with aging	25 °C 120 MV/m	6 μm	[186]
35-50	0.7	Micro shifting of charges	T_{max} decreases with increase of E	TE, 60 °C 2-20 MV/m	35 μm	[144]
105-125	0.9	Migration of ions	At $E > 10$ MV/m T_{max} increases	-	-	[144]
80	-	Dipole relaxation	With time the peak is narrowed	-	-	[92]
70-75	-	-	-	-	50 μm	[87]
60	-	Defrosting of dipoles	A small relaxation time	TE	20-300 μm β -phase	[22]
70-130	-	Relaxation of the volume charge	T_{max} coincides with the polarization T			[22]
-40, 70, 95, 160	-	-	Poor reproducibility	TE, 90 °C 10-60 MV/m	20 μm	[180]
0	-	Relaxation of dipoles in β -phase	Peak disappears when orienting the film	TE, 90 °C 100-200 MV/m	20 μm	[180]
52	-	Relaxation at the boundaries of crystallites				[87]

110-120	–	Injection of ions	In dry atmosphere and in vacuum			[87]
50	–	–	–	CD + 20-140 °C	25 μm	[78]
65	–	–	–	CD - 20 °C		
90-94	–	–	–	CD -90°C, 140 °C		
120	–	–	–	CD + and - 140 °C		
50-55	1.2	–	–	CD 5 kV	25 μm	[91]
55	0.9	Relaxation of trapped charges	–	CD	25 μm	[18]
80	1.3	Relaxation in the amorphous phase	Distribution of activation energy			[18]
–45		Exemption of heterocharge	T_{max} increases when extracting the film	TE, 16-93°C 10-45 MV/m		[170]
120-137		Relaxation of volume charge	T_{max} increases when extracting the film	TE, 16-93°C 10-45 MV/m		[170]
10-30		Relaxation on small traps	Relaxation time is small	TE 10-45 MV/m		[170]

*Note: TE is the thermoelectret "sandwich method"; CD is poling in corona discharge.

From the theory of the TSD currents [173] it follows that in a one-component homogeneously polarized dipolar sample, the measured current is equal to the displacement current dP/dt , so that the integral of the TSD current is equal to the value of the initial polarization. As shown by von Seggern and Fedosov [175], the integral of the TSD current is smaller than the residual polarization in case of a two-phase system.

Possibilities of thermally stimulated research methods are extremely wide, since most relaxation processes are thermally activated. At the same time, these possibilities in the study of polymer and composite ferroelectric polymers have not yet been detected and have not been used. This relates to the study of the effective conductivity dynamics in the process of the thermoelectret poling (TEP), the comparison of TEP and TSD

currents, the separation in the ferroelectric polymers of the contribution of the homocharge and heterocharge to the relaxation current, the use of fractional TSD methods for separation of the pyroelectric and the relaxation components of the total current.

5.2. Thermally stimulated depolarization current spectroscopy

In case of thermoelectret poling (TEP), unlike isothermal poling, the sample was initially kept at room temperature at constant voltage for some time necessary to decrease the absorption current to values of the order of 10^{-11} A, and then the temperature was linearly increased to $150\text{ }^{\circ}\text{C}$ at a constant rate ($0.5\text{-}4\text{ }^{\circ}\text{C}/\text{min}$) with continuous measuring of the poling current. After completion of poling, the samples were quickly cooled down without switching off the applied voltage.

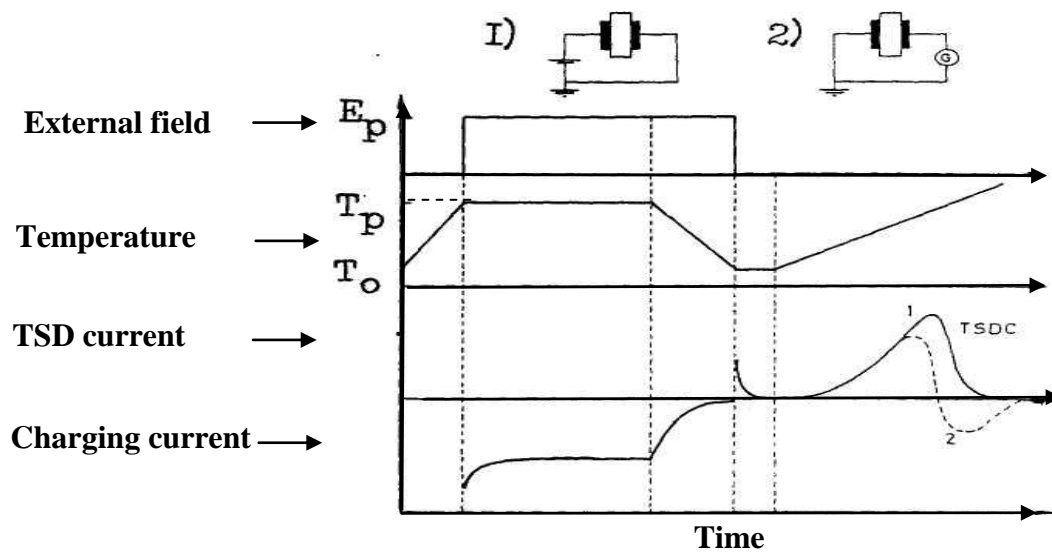


Fig. 5.1. The principle of the thermoelectret poling (1) and depolarization (2) methods.

Since many relaxation processes have the thermally activating nature, the (TSD) method [151,173] was used to predict the space charge and the residual polarization stability and to study the mechanism of their formation. The sample electrodes were connected with each other through the electrometer having a sensitivity of $10^{-14}\text{-}10^{-16}$ A by current and the current recording device. The temperature was raised at a constant rate in the range of $15\text{-}150\text{ }^{\circ}\text{C}$ and measured by a chromel- copel thermocouple. The principle of the current TSD method is shown in Fig. 5.1.

We measured the thermally stimulated decrease in the electret potential by the vibration electrode method (Kelvin's method).

Measurements in the range from -100 °C to +180 °C was carried out by using the relaxation spectrometer Solomat-91000. Studies in the field of low temperatures from -170 to + 40 °C were made using a Kithley-6100 electrometer and the samples were originally cooled in liquid nitrogen.

5.3. Homocharge and heterocharge relaxation and TSD currents

A number of properties of the ferroelectric polymers can be explained within the framework of the modern theory of polar electrets [151] considering relaxation of the homocharge and the heterocharge in a self-consistent regime without taking into account the ferroelectricity in the crystalline phase. We consider the interrelation between the homocharge and the heterocharge taking into account experimental data on thermally stimulated and isothermal relaxation of PVDF films poled in a corona discharge.

Four types of depolarization varieties were used to study the relaxation processes, namely thermally stimulated (T) and isothermal (I) depolarization of short-circuited samples (S) and depolarization in the open circuit mode (O). The modes were denoted as TS, TO, ISO, and IO, where the first letter indicated the temperature mode (thermally stimulated or isothermal), and the second was related to the electrical state (short-circuit or open circuit). Additional experiments on the thermally stimulated electret potential (TP) kinetics were also performed after 24 hours of keeping in the open circuit configuration. A film of polytetrafluoroethylene (PTFE) with a thickness of 10 μm was used as a dielectric gap in TO and IO modes. All thermally stimulated experiments were performed at a constant heating rate of 3 °C/min. In isothermal experiments, the temperature was maintained constant after the required temperature value was achieved by rapid heating. The electret potential in the TP method was measured by the Kelvin method and was continuously recorded.

During poling in a corona discharge, the excess charge is localized on the surface of the sample forming a homogeneous charge σ , which creates a homogeneous field in the sample volume, in which the internal dipolar polarization (heterocharge) is formed characterized by the surface density of the bound charge P . In case of the sample short-circuiting without a gap, only the heterocharge relaxes [173], and the equality $\sigma = P$ and

the zero internal field ($E = 0$) is supported due to the current redistribution in the external circuit. In the presence of a dielectric gap and in the the open circuit mode, the relaxation currents of the homocharge and the heterocharge flow in opposite directions.

In order to find separately components corresponding to the decay of the homocharge σ and the heterocharge P of the full depolarization current in the open circuit mode, we present the current density $i(t)$ and the surface potential $V(t)$ as

$$i(t) = s \left[\frac{dP(t)}{dt} - \frac{d\sigma(t)}{dt} \right], \quad (5.2)$$

$$V(t) = \frac{sx_1}{\varepsilon_o \varepsilon_1} [\sigma(t) - P(t)], \quad (5.3)$$

$$i(t) = - \frac{\varepsilon_o \varepsilon_1}{x_1} \cdot \frac{dV(t)}{dt}, \quad (5.4)$$

where, t is time, ε and x_o are the dielectric constant and the thickness of the sample; ε_l and x_l are similar parameters of the dielectric gap. For the conductivity current density, it is possible to write down

$$i_c(t) = \frac{g}{x_o} V(t) = - \frac{d\sigma(t)}{dt}, \quad (5.5)$$

where $g = g_o \exp(-Q/kT)$ is the specific conductivity, k is Boltzmann's constant, T is temperature, Q is the activation energy of the intrinsic conductivity, g_o is a pre-exponential factor. Integrating (5.4) over time and replacing the variable t by T taking into account the linear heating $T = T_o + \beta \cdot t$ where β is the heating rate, T_o is the initial temperature of the experiment, we obtain from (5.2-5.5) the temperature dependences of the depolarization currents and the electret potential

$$i_1(T) = \frac{d\sigma}{dt} = - \frac{x_1 g_o}{bT_o x_o \varepsilon_o \varepsilon_1} \exp\left(-\frac{Q}{kT}\right) \int_T^\infty i(T') dT', \quad (5.6)$$

$$i_2(T) = \frac{dP}{dt} = \frac{i(T)}{s} + \frac{d\sigma}{dt}, \quad (5.7)$$

$$V(T) = \frac{x_1}{bT_o \varepsilon_o \varepsilon_1} \int_T^{\infty} i(T') dT'. \quad (5.8)$$

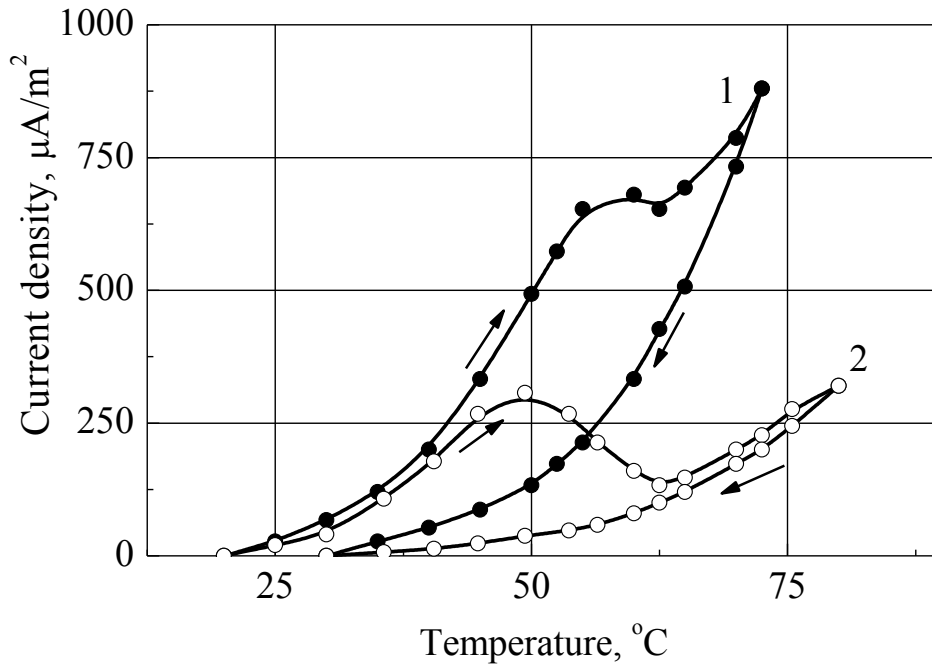


Fig. 5.2. Dependence of current on temperature during thermally stimulated poling in positive (1) and negative (2) corona discharge. Heating rate is 2 °C/min.

All values in the right-hand sides of the equations (5.6-5.8) are known from the experiment. Thus, this technique allows to differentiate processes of homocharge and heterocharge relaxation in different modes of TSD by using experimental $i(T)$ curves.

5.4. Thermoelectret poling of PVDF and P(VDF-TFE) films

The thermoelectret poling method (TEP) has several advantages over isothermal poling, because it allows to obtain additional data on the mechanism of the polarization formation. It is also possible to determine the optimal temperature of poling, as well as to find the temperature, at which the ohmic conductivity becomes significant.

From Fig. 5.2 and Table 5.2 one can distinguish the following features:

1) The TEP curves contain three characteristic areas: a) the growth of the current irrespective of the corona discharge polarity; b) decrease of the current (negative temperature coefficient of conduction); c) increase of the current at high temperatures.

Table 5.2

Effective activation energy during TEP in different temperature ranges (from the inclination of linear parts in $\ln i - 1/T$ curves) [36]

Charge Polarity	Heating			Cooling	
	<u>Activation energy, eV</u> Temperature range °C			<u>Activation energy, eV</u> Temperature range °C	
+	<u>0.87</u> 20-40	<u>0.82</u> 40-50	<u>0.82</u> 50-65	<u>0.92</u> 60-45	<u>1.06</u> 45-25
-	<u>0.87</u> 20-35	<u>1.1</u> 35-45	<u>1.12</u> 65-80	<u>1.19</u> 70-55	<u>0.83</u> 55-35

2) With negative corona discharge polarity, the second region is more pronounced than with positive polarity, and the decrease in conductivity begins at lower temperatures. The difference in the currents of the TB positively and negatively poled samples indicates different injection levels. In a positive corona, it is likely that both positive charges and negative ones (from the rear electrode) are injected. In case of a negative corona, positive charge carriers from the metal electrode are not injected.

3) When thermoelectret poling of PVDF films occurs, the irreversible decrease in the effective conductivity is due to the fact that the value of the thermal current when cooled is much smaller than the current during heating.

In PVDF, the current peak during TEP (Fig. 5.2) cannot be considered to be due to polarization, as in case of linear polar polymers, because its integration gives an unrealistically great value of the polarization. Probably, the conductivity current in TEP ferroelectric polymers is much larger than the polarization component of the current, therefore the graphs in Fig. 5.2 reflect the nature of changing in the films effective conductivity.

The mechanism and nature of conductivity in PVDF are unknown, but presence of

the negative temperature coefficient of conductivity sections in curves Fig. 5.2 suggests that, along with the thermoactivating increase in the number of moving carriers, there is also likely to be a trapping by deep traps, and with certain ratios of field strength and temperature the second process prevails over the first process. The trapped charges play an important role by neutralizing the depolarizing field and contributing to the preservation of the residual polarization.

High polarization in a poled film and a sharp decrease in conductivity (the current passes through the maximum) are probably interconnected. The ferroelectric polarization in crystallites creates conditions for trapping of charges at their boundaries. The field of the trapped charges screens the polarization and contribute to its stabilization. Thus, the processes of the polarization development and the charge trapping are interconnected and interdependent.

At the current curve of TEP from room temperature to 30-40 °C, the dependence $i(T)$ is exponential regardless of the corona polarity. This can be related to the thermal generation of charge carriers in the volume. The further course of the current graphs corresponds to the proposed model for the polarization formation and the charge trapping. There is again increase of the current in the third section that may be due to the internal thermoelectric detrapping of the previously trapped charges with partial destruction of the already formed polarization. If this assumption is valid, then it is an important for practice conclusion that it is impractical to heat PVDF during TEP above the minimum temperature on the current-temperature curve.

Decrease of the current and the effective conductivity in the second section of the TEP curve may be due to the following reasons:

- 1) Depletion of the stock of own carriers due to their migration in the external field and trapping near the electrodes (electrode polarization);
- 2) Irreversible changes at the electrodes or near to them leading to limiting of the charge injection;
- 3) Generation of regions in the volume that do not conduct current, for example, polarized crystallites with layers of the trapped charges;
- 4) Changing the equilibrium between free and trapped charges due to the formation of new traps at the boundaries of the polarized crystallites and macroscopic polarized regions.

The difference between TEP currents in positively and negatively charged samples is

against the migration mechanism causing the reduction in conductivity. The second reason is also unlikely, because due to ionic impurities the field on the electrodes should increase, which together with the effect of the temperature would lead to increase in the injection level. The third reason is more probable, because the ordering in the crystalline phase of the polymers leads to decrease in localized states the density and decrease in conductivity (the band gap width is of the order of 6-9 eV). However, the ordering of the preferred orientation of dipoles in crystallites in the external field cannot substantially change their conductivity, because they already have the spontaneous polarization as the higher degree of the internal ordering.

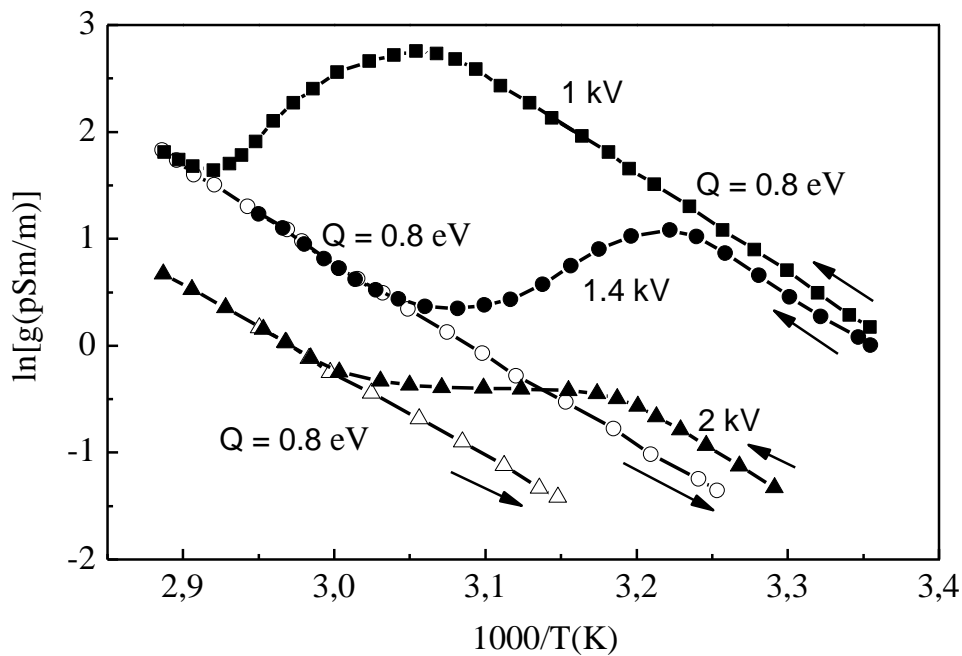


Fig. 5.3. Temperature dependence of the effective conductivity during thermally stimulated poling in a corona discharge under different voltages at a control grid (electret potential).

Most likely, the conductivity of PVDF decreases as a result of the intensive trapping of carriers at the boundaries of polarized crystals and macroscopic polarized regions, which create favorable conditions for localization of the charges. We have found that similar processes at low temperatures and high fields lead to appearance of areas of negative dynamic resistance on volt-ampere characteristics.

If the proposed hypothesis is correct, then there the relationship between the temperature and the field strength must be observed, in which high polarization is formed and the irreversible decrease in conductivity appears. Dependence of the

effective conductivity on temperature in TEP mode at different constant voltages is shown in Fig. 5.3, from which it is seen that the beginning of the negative temperature conductivity section moves to lower temperatures with increasing the polarizing voltage. It is known that the high polarization in ferroelectrics occurs in fields above the coercive one. From the data of Fig. 5.3 it follows that the value of the coercive field decreases with increasing temperature. From Fig. 5.3 and Table 5.2 it is evident that the activation energy that provides the effective conductivity in unpolarized and polarized samples is practically the same. At the same time, the conductivity of the polarized films, and hence the concentration of free carriers in them is almost 100 times smaller than in unpolarized films. Consequently, in the process of poling, there are redistribution of carriers and their additional trapping at the newly created traps.

Let us analyze the shape of the TEP current curve taking into account that the conductivity current I_S is proportional to the concentration of free charge carriers

$$i_c = \mu \cdot n_c e \frac{U}{x_o} \quad (5.9)$$

where μ is the mobility; U is the applied voltage; x_o is thickness of the sample. In the presence of localized states in the forbidden zone, the concentration of trapped charges is determined by the Fermi-Dirac formula [112]

$$n_t = N_t \{1 + (1/g) \exp[-(F - E_t)/kT]\}^{-1}, \quad (5.10)$$

where N_t is the density of localized states; g is their statistical weight; E_t is the localized state energy; F is a quasi-level Fermi based on its own and injected carriers. We assume that the total concentration of carriers and the Fermi level remain constant.

Increase in the density of the localized states with increasing polarization can be represented as a linear function where the polarization P is a function of the field strength E . For ferroelectrics, the function $P(E)$ can be approximated by three rectilinear sections

$$P(E) = \begin{cases} 0, & E < E_c, \\ (E - E_c)P_s / (E_s - E_c), & E_c < E < E_s, \\ P_s, & E_s < E \end{cases} \quad (5.11)$$

where E_c is the coercive field; E_s is the field strength at which polarization reaches saturation. Consider the decrease of the coercive field with increasing temperature

$$E_c = E_o - \gamma \cdot T. \quad (5.12)$$

We will assume that the dynamic permittivity at $E_c < E < E_s$ does not depend on T , that is equivalent to the constancy of the difference $\Delta E = E_s - E_c$. From (5.10) - (5.15), taking into account the made assumptions, we obtain the dependence of the conductivity current on the temperature

$$i_c = (\mu \cdot e \cdot V / x_o) \langle n_o - N_t \{1 + (1/g) \exp[-(F - E_t)/kT]\}^{-1} \rangle, \quad (5.13)$$

where

$$\begin{aligned} N_t &= N_o ; \quad T < T_1 = (E_{co} - V / x_o) / \gamma, \\ N_t &= N_o + \alpha P_s ; \quad T > T_2 = (\Delta E + E_{co} - V / x_o) / \gamma, \\ N_t &= N_o + (\alpha P_s / \Delta E) [(V / x_o) - (E_{co} - \gamma T)], \quad T_2 > T > T_1 \end{aligned} \quad (5.14)$$

From expressions (5.13) and (5.14) it follows that with increasing temperature in the range $T < T_1$ the current i_c increases. N_t begins to increase at $T > T_1$ provided

$$\alpha P_s \gamma / \Delta E > (Q / g k T^2) \exp(-Q / kT), \quad (5.15)$$

where $Q = F - E_t$.

There is a decrease in current i_c despite the increase in temperature. The current increases again, if the saturation of polarization is reached, or if the condition (5.15) is violated,

Reducing of the effective conductivity during TEP indicates the importance of volume-charge processes, since the charge trapped on the boundaries of the polarized

regions compensates the depolarizing field and contributes to the long-term preservation of the residual polarization. A similar relation was established during isothermal poling in high fields [154].

Thus, the increase of temperature and the field strength equally influences on the generation and injection of moving charges, the large concentration of which is a prerequisite for the emergence and development of the high local polarization. As the polarization is formed, the conductivity of ferroelectric polymers is irreversibly reduced due to the trapping of the injected charge carriers at deep traps formed by the polarization of crystallites. These trapped charge carriers stabilize the residual polarization by compensating local depolarizing fields.

5.5 Thermally stimulated depolarization currents in PVDF

Measurement of TSD currents is a powerful tool for studying relaxation processes [173]. Although the theory of TSD currents was developed only for the thermally frozen dipole polarization, this method is widely used to study the ferroelectric polymers [56,133,93,30,95]. In PVDF, two peaks are the most important. One of them, related to the glass transition in the amorphous phase, is always observed at a temperature of about $-45\text{ }^{\circ}\text{C}$ [171,169] and it is well-studied. The nature of the second peak in the range of $50\text{--}80\text{ }^{\circ}\text{C}$ (Fig. 5.4) is not fully understood, although it is clear that several processes, such as the reorientation of dipoles in the amorphous phase, the relaxation of the ferroelectric polarization, the displacement of the space charge, as well as interphase and piezoelectrode processes [41] can be responsible for this peak. It is established that the temperature of about $60\text{ }^{\circ}\text{C}$ is characteristic for PVDF, but its nature is not completely clear. Many researchers associate a peak at this temperature with so called α_c relaxation [167,24,141]. Lacabane et. al. [167,95] explain the appearance of the peak by shrinkage, that is, by a partial restoration after stretching carried out for obtaining the ferroelectric β -phase in PVDF. We believe that this peak is associated with polarization in the amorphous phase.

Ferroelectric polymers have the properties of ordinary polar electrets in addition to the ferroelectricity. Therefore, one can expect the presence of two components of the residual polarization: one associated with the ferroelectricity in the crystalline phase, and another related to the amorphous phase, although there is currently no direct

experimental confirmation of this phenomenon.

Analysis of the relationship between TSD currents in PVDF and pyroelectricity was carried out in the work of von Seggern and Fedosov [175]. They have found that the residual polarization decreases after heating to 60 °C, while the pyrocoefficient remains unchanged. They concluded that the ferroelectric polarization in the crystalline phase is partially offset by localized charges, and partly by polarization in the amorphous phase. Therefore, in the formation of the TSD peak in the ferroelectric polymers, several currents are involved caused by relaxation of the electret and the ferroelectric components of the residual polarization, and associated with the space charge.

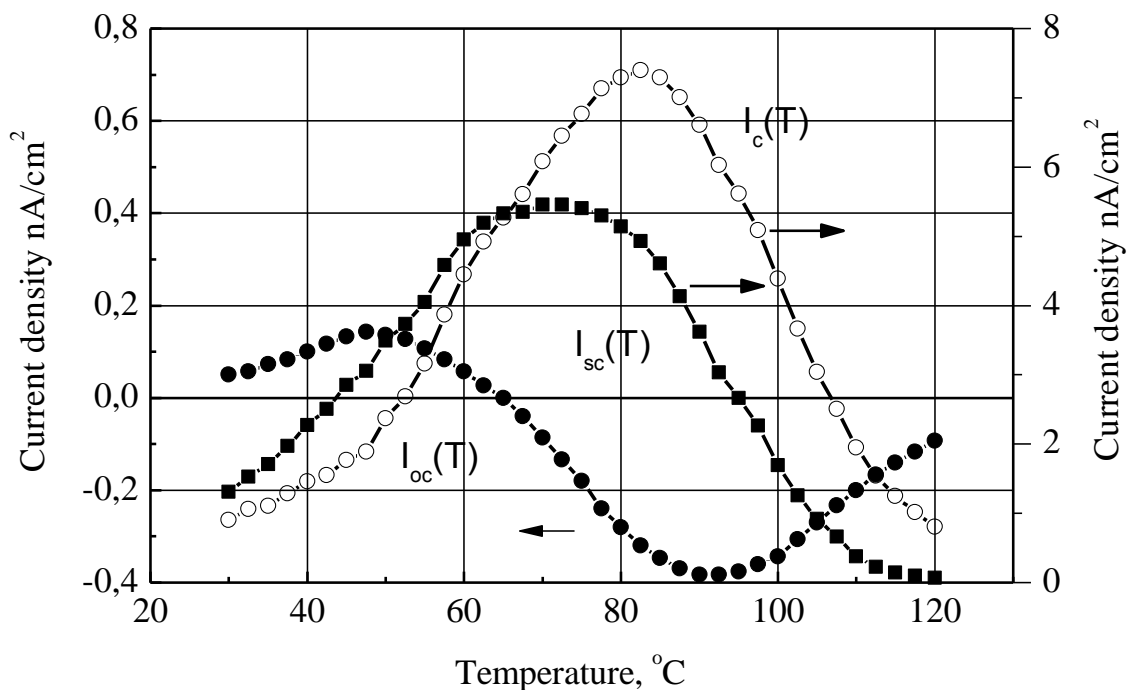


Fig. 5.4. TSD currents $I_{sc}(T)$ and $I_{oc}(T)$ measured on fresh polarized samples in short-circuit and open circuit modes. The curve $I_c(T)$ corresponds to the volume-charge current.

We investigated polarized specimens subjected to TSD either in short-circuit mode or in open-loop with PTFE film as a dielectric gap between the free surface of the sample and one of the electrodes [149]. The period of time after poling to the TSD measurement was either one day or 16 months. The samples were named "fresh" and "old" accordingly.

Similarly to the data reported in other papers [56,167,133,30,95,141], we observed one broad peak in the mode of the short circuit on fresh samples (Fig. 5.4) [47]. The

direction of current at this peak corresponded to the residual polarization relaxation. Because the crystallinity of P(VDF-TFE) is about 50% and most of the molecular dipoles in the crystalline regions are in the ferroelectric β -phase, the contributions of the electret and the ferroelectric components to the formation of this peak in fresh samples can be compared. As for the bulk charging component, it is known that it either does not contribute to the TSD current in the mode of the short circuit, or its direction coincides with the depolarization current component [51].

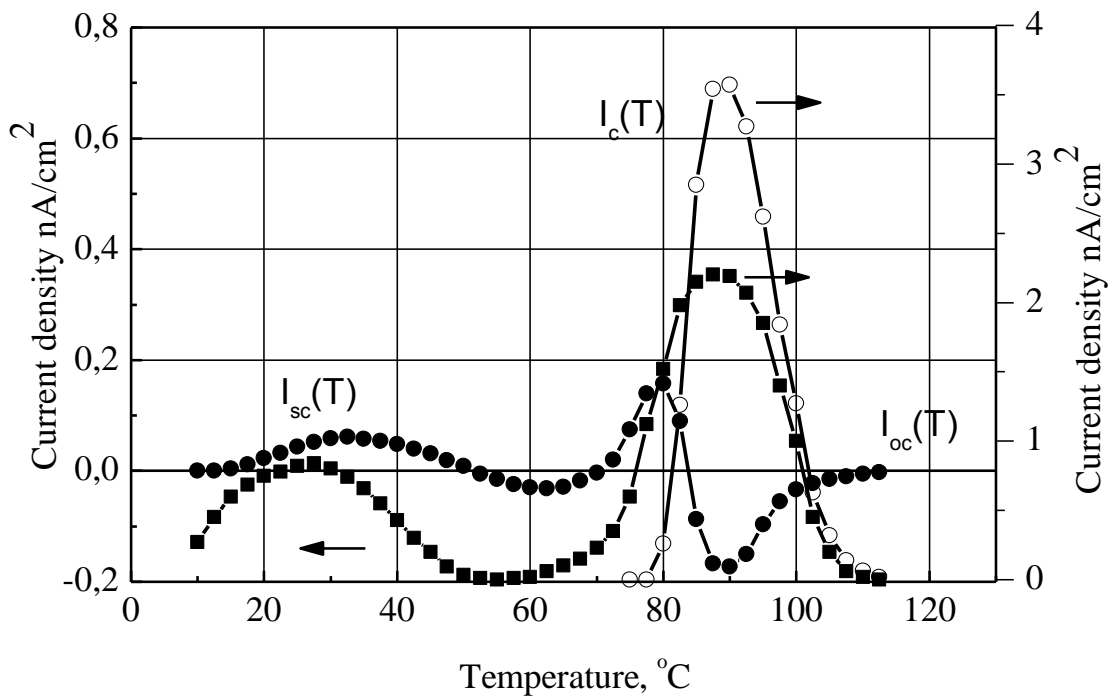


Fig. 5.5. TSD currents $I_{sc}(T)$ and $I_{oc}(T)$ measured in polarized samples in short-circuited and open circuited modes after exposure for 16 months. The curve $I_c(T)$ corresponds to the volume-charge current.

Comparing the TSD currents of fresh and aged polarized samples, we observed a new phenomenon. One broad TSD current peak in the mode of the short circuit was divided during the aging in two narrow peaks completely separated from each other [51]. At the same time, two pairs of the oppositely directed peaks appeared in old samples instead of one pair of peaks typical for fresh samples (Fig. 5.5). This feature is likely to be common to all ferroelectric polymers and does not depend on the polarization conditions, because similar results were also obtained by us on samples

poled by a non-focussed electron beam at the accelerating voltage of 20 kV and in P(VDF-TFE) and PVDF films poled through a lime glass at the voltage of 7 kV [149].

The depolarization current in the open circuit mode remains unchanged, while the TSD current due to the charge changes the direction to the opposite. Therefore, the two peaks shown in Fig. 5.4 can be explained as the result of two partially overlapping and oppositely directed currents arising as a result of the relaxation of polarization and space charge.

In order to separate the depolarization current $I_p(T)$ from the space charge current $I_c(T)$, it is reasonable to assume that the polarization is homogeneous in the direction of the thickness. Since the compensating charges trapped near the surface do not generate any current in the short circuit mode [121], then $I_{sc}(T) = I_p(T)$, where $I_{sc}(T)$ is the experimentally measured TSD current in the short circuit mode. The current $I_c(T)$ can be calculated from the experimental curves $I_{sc}(T)$ and $I_{oc}(T)$ shown in Fig. 5.4

$$I_c(T) = I_{oc}(T) \left[1 + \frac{\varepsilon_1 x_2}{\varepsilon_2 x_1} \right] - I_{sc}(T), \quad (5.16)$$

where ε_1 , x_1 , ε_2 and x_2 are dielectric permittivity and thickness of the sample and the dielectric gap, respectively. In our calculations, we used $\varepsilon_1 = 12$, $\varepsilon_2 = 2.1$, $x_1 = 20 \mu\text{m}$, $x_2 = 25 \mu\text{m}$. It is noteworthy that the peak $I_c(T)$ is at the higher temperature than the peak of the depolarization, indicating that the trapped charges are more stable than the residual polarization [47].

The obtained results can be explained qualitatively taking into account the different nature of the three components of the TSD current. The electret polarization accounting for almost 50% of the residual polarization in fresh samples decays in time faster than the ferroelectric component. That is why the two peaks are overlapped in fresh samples, become completely separated in the old films, as if the slow redistribution of residual polarization is going on for a long time after the completion of poling.

Observed and calculated peaks are difficult to process quantitatively, since there is no TSD currents theory in ferroelectric polymers. However, as evident from the shape of the peaks, all three relaxation processes in P(VDF-TFE) differ significantly from the ideal Debye case, corresponding to the absence of the relationship between the relaxing dipoles. This feature can be taken into account considering that the polarization relaxes

over time in accordance with the law of the expanded exponent

$$P(t) = P_o \exp\left(-\frac{t}{\tau}\right)^\alpha \quad 1 \geq \alpha \geq 0 \quad (5.17)$$

where τ is a time constant, P_o is the initial polarization. If the sample is linearly heated at the rate $\beta = dT/dt$, then

$$P(T) = P_o \exp\left\{-\left[\left(\frac{1}{\beta}\right) \int_{T_o}^T \left(\frac{1}{\tau(T')}\right) dT'\right]^\alpha\right\} \quad (5.18)$$

where T_o is the initial temperature. It is reasonable to assume that the temperature dependence of τ corresponds to the Arrhenius law

$$\tau(T) = \tau_o \exp\left(\frac{A}{kT}\right) \quad (5.19)$$

where A is the activation energy, k is the Boltzmann constant, τ_o is the characteristic time. The expression for the TSD current density is derived from the equations (5.17) - (5.19)

$$i(T) = -\left(\frac{\alpha P_o}{\tau_o}\right) \exp\left(-\frac{A}{kT}\right) [s(T)]^{\alpha-1} \exp\left\{-[s(T)]^\alpha\right\} \quad (5.20)$$

where

$$s(T) = \left(\frac{1}{\beta \tau_o}\right) \int_{T_o}^T \exp\left(-\frac{A}{kT'}\right) dT'$$

The results of computer fitting of the experimentally observed and calculated TSD

peaks in equation (5.20) confirmed our assumptions about the nature and the thermal stability of the relaxation processes. They showed that the depolarization peak in fresh samples where the electret and the ferroelectric components are mixed, is wide ($\alpha = 0.24$), because the two relaxation processes responsible for its formation are very different. The ferroelectric polarization is quite stable ($A = 2.7$ eV), and the TSD peak due to its relaxation is relatively narrow ($\alpha = 0.52$). The parameters of the space charge peaks in the fresh and old samples are completely different, as if there are two types of the space charges, one probably associated with the ferroelectric polarization, and the other one with the electret component. It is also likely that the small peak that occurs near the electret depolarization peak in open mode (Fig. 5.5) is due only to the electret component of the volume charge. Since the glass transition temperature is -45 °C in PVDF, the ordering of the dipoles in the amorphous phase is not thermally frozen, as in the ordinary polar electrets. The dominant orientation of dipoles in these conditions may be supported by the field of the trapped charges [51,60].

Thus, it has been shown that in corona poled films of the ferroelectric polymers, there are two components of polarization, and both components are accompanied by corresponding space charges. The electret-type thermodynamically unstable component relaxes as long as the broad TSD peak observed in fresh polarized samples is not transformed into two completely separated narrow peaks.

The unstable electret component of the residual polarization can be removed by heating the poled sample to a specific temperature (about 60 °C in case of PVDF). Apparently, the trapped charges always accompany the dipolar polarization regardless of its nature.

5.6. Separation of TSD current components in PVDF

Despite the fact that PVDF is considered as a polymer ferroelectric [67], some of its electrical properties can be explained within the framework of the theory of polar electrets. The phenomenological model of Gross-Swan-Gubkin [81,163,83] suggests the presence of two types of charges in the electret, namely, the homocharge $\sigma(t)$, whose sign coincides with the polarity of the electrodes during poling, and the heterocharge $P(t)$ (internal polarization), which is the result of the micro - and macro- displacements of own charges in the dielectric under the field action. In case of PVDF, the

heterocharge is the dipole polarization, and the homocharge is formed by charges trapped on or near the surface [177].

Stability of the electret state in a polar dielectric depends on the mutual relaxation of the homocharge and the heterocharge. Since the heterocharge (polarization) is usually the most important in PVDF, the role of the homocharge has not paid enough attention to the present, although the stabilizing effect of the space charge on the residual polarization has already been discussed [62,177].

Thermally stimulated depolarization (TSD) is a method used to identify relaxation processes in polymer electrets. However, it is very difficult to divide the effect of the homocharge and the heterocharge on TSD currents especially if the corresponding peaks are superimposed on each other in a wide range of temperatures.

We have developed and applied a method for distributing currents of the homocharge and the heterocharge [47] by solving the inverse problem. In addition, it has been shown that the application of various modifications of the TSD method, complemented by isothermal depolarization currents allows us to find such important parameters of relaxation processes as the activation energy, characteristic frequencies and the time constant.

The uniaxially oriented 25 μm thick PVDF films metallised on one side were poled in a corona triode at the control grid voltage of 3 kV at room temperature and a constant poling current density of 90 $\mu\text{A}/\text{m}^2$ for 30 min and then shortened and held at room temperature within 24 hours (except for specimens intended for measuring the electret potential kinetics) [48]. Four modifications of the TSD method were used, namely thermally stimulated (T) and isothermal (I) depolarization of short-circuited (S) and open circuit (O) specimens. Thus, the applied modifications were named TS, TO, IS and IO where the first letter indicates the temperature mode (thermally stimulated or isothermal), and the second indicates the electric state of the sample (short-circuit or open circuit). Additional experiments on the thermally stimulated electret potential (TP) kinetics were performed after 24 hours of being in the open circuit state. As a dielectric layer in TO and IO modifications, PTFE film of 10 μm thickness was used. Thermally stimulated experiments were performed at a constant heating rate of 3 K/min. In isothermal experiments, the temperature was maintained constant after its required value was achieved by rapid heating. The electret potential in TP modifications was measured by the Kelvin method and continuously recorded.

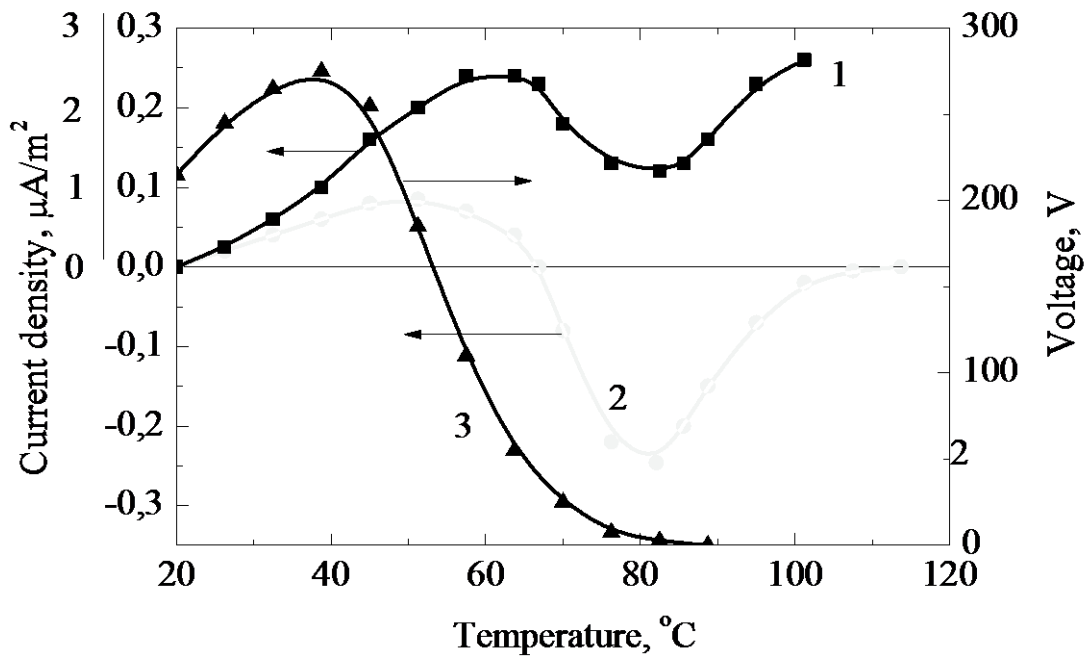


Fig. 5.6. Thermally stimulated currents in the TS modification (1) and in the TO modification (2), as well as the electret potential in the TP modification (3).

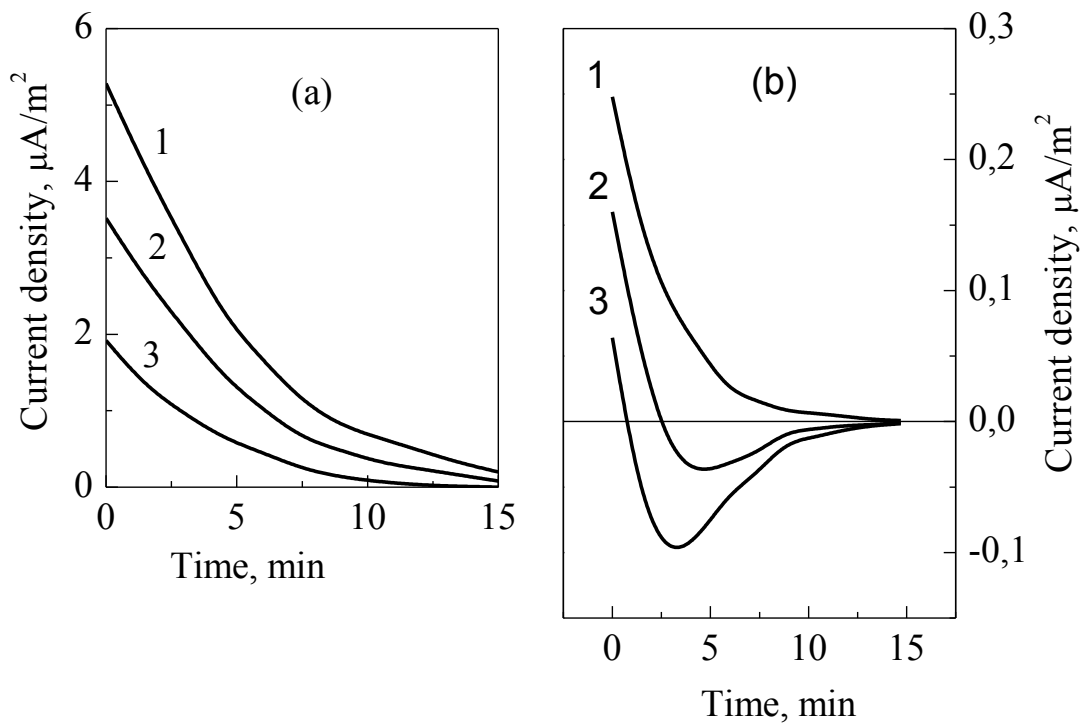


Fig. 5.7. Isothermal transient currents at different temperatures in the IS mode (a) and in the IO mode (b); 1 – 45 °C, 2 – 55 °C, and 3 – 70 °C.

The main features of the experimental curves shown in Fig. 5.6 and 5.7 are as follows:

- The depolarization current in the TS modification forms a broad "non-classical" peak with a maximum of 65 °C;
- There is an inversion of the TSD current in the TO modification, while the current direction coincides with the direction of the current in the TS modification in the initial heating stage;
- The electret potential in TP modification has a maximum at 40 °C.
- The current slowly decreases over time in the IS modification at all temperatures, while the isothermal current changes the direction in IO mode at elevated temperature.

These features can be explained within the framework of the model, which implies existence in the samples of the homocharge and the heterocharge [151,81,163,83]. First, consider the processes of poling and relaxation qualitatively. It is reasonable to assume that negatively charged particles (ions and/or electrons) generated by a corona discharge are adsorbed and thermalized on the surface of the sample due to their low (thermal) energy. Excessive charge in the near-to-surface layer or on the surface forms a homocharge that has a certain superficial density σ and creates a homogeneous field E in the volume of the sample. The high electron affinity of fluorine atoms facilitates the trapping of charges at traps and formation of the stable homocharge.

Homogeneous internal polarization P (heterocharge) is formed as a result of dipoles - $\text{CH}_2\text{-CF}_2$ - orientation in the field created by a homocharge. The formation of polarization is equivalent to the formation of a bound surface charge P , which has a sign opposite to the sign of the homocharge σ . Of all the polarization processes in PVDF, the orientation of the $-\text{CH}_2\text{-CF}_2$ - dipoles is the most significant due to their large dipole moment of 2.1 Debye [151,123].

If the polarization P is zero, then the field is created by a complete superficial charge σ . When P begins to grow, a depolarizing field appears which is "neutralized" by a part of the surface charge. Thus, the field in volume is created by the difference ($\sigma - P$) between the surface charge and the polarization. Consequently, the surface charge σ consists of two parts $\sigma = \sigma_1 + \sigma_2$, the first of which is a charge that provides compensation for the depolarizing field ($\sigma_1 = P$), and the second $\sigma_2 = \sigma - P$ creates the electric field in the volume of the sample.

After the short circuiting of the poled samples (in TS and IS modes), the "excess" charge σ_2 disappears. The equilibrium between the homocharge and heterocharge ($\sigma = \sigma_l = P$), as well as the zero internal field ($E = 0$) are supported by the current in the external circuit, so that the measured current corresponds to the relaxation of the heterocharge.

However, if after the short circuiting and the formation of equilibrium $\sigma = \sigma_l = P$, a non-conductive dielectric insert (in TO and IO modes) is introduced between one of the electrodes and the surface of the sample, then one can observe the relaxation currents both the heterocharge and the homocharge flowing in the opposite directions. The field in the volume is no longer zero, so that the surface charge (homocharge) drifts in its own field through the entire thickness of the sample, or it is slowly neutralized by charge carriers responsible for its own conductivity.

In any case, the relaxation of the heterocharge occurs in a field other than zero and caused by thermal disordering of oriented dipoles [151,173].

We will show that both components of the depolarization current can be found from the dependence of $i(T)$ in the TO mode (Fig. 5.6, curve 2). It is known [151,173] that the TSD current $i(t)$ and the electret potential $V(t)$ in experiments with nonconductive insertion between the surface of the sample and the electrode, depend not only on the relationship between the homocharge and the heterocharge, but also from their derivatives, so

$$i(t) = s \left[\frac{dP(t)}{dt} - \frac{d\sigma(t)}{dt} \right], \quad (5.21)$$

$$V(t) = \frac{sx_1}{\varepsilon_o \varepsilon_1} [\sigma(t) - P(t)], \quad (5.22)$$

$$i(t) = -\frac{\varepsilon_o \varepsilon_1}{x_1} \cdot \frac{dV(t)}{dt}, \quad (5.23)$$

where $s = x_o \varepsilon_1 / (x_1 \varepsilon + x_o \varepsilon_1)$, t is time, ε and x_o are the dielectric constant and the thickness of the sample, ε_1 and x_1 are corresponding values of the dielectric gap, ε_o is the permittivity of a vacuum.

The full component $i_c(t)$ can be represented as

$$i_c(t) = \frac{g}{x_o} V(t) = -\frac{d\sigma(t)}{dt}, \quad (5.24)$$

where $g = g_o \exp(-Q/kT)$ is the own conductivity, k is the Boltzmann constant, T is temperature, Q is the activating energy of its own conductivity, g_o is a pre-exponential factor. Integrating (5.23) and replacing the time t with temperature T in (5.21) - (5.24) according to $T = T_o(1+bt)$, where b is the heating rate, T_o is the initial temperature, we obtain the expressions for the temperature dependences of the homocharge current $i_1(T)$ and the heterocharge current $i_2(T)$, as well as the voltage on the sample (potential) $V(T)$

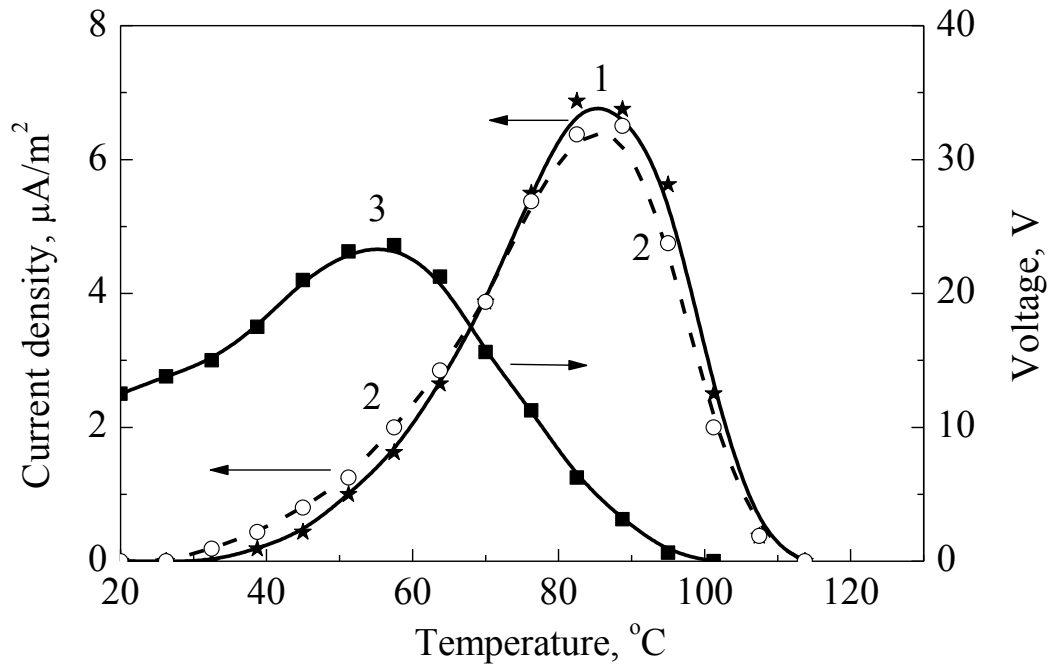


Fig. 5.8. Temperature dependences of the homocharge (1) and heterocharge (2) relaxation currents, as well as of the voltage on the sample (3) calculated according to the model.

$$i_1(T) = \frac{d\sigma}{dt} = -\frac{x_1 g_o}{b T_o x_o \epsilon_o \epsilon_1} \exp\left(-\frac{Q}{kT}\right) \int_T^{\infty} i(T') dT', \quad (5.25)$$

$$i_2(T) = \frac{dP}{dt} = \frac{i(T)}{s} + \frac{d\sigma}{dt}, \quad (5.26)$$

$$V(T) = \frac{x_1}{bT_o \varepsilon_o \varepsilon_1} \int_T^{\infty} i(T') dT'. \quad (5.27)$$

All quantities at the right side of the equations (5.25) - (5.27) are known, or can be obtained experimentally. The results of calculations according to the equations (5.25) - (5.27) based on the data of Fig. 5.6, are shown in Fig. 5.8. The values of the activation energy $Q = 0.76$ eV and the factor $g_o = 0.18$ Sm/m were obtained from constant values of the isothermal poling current and voltage.

As one can see in Fig. 5.8, the homocharge and the heterocharge form two broad peaks with almost identical maxima. The heterocharge relaxes faster in the low-temperature region where the homocharge is relatively stable. This is probably the reason for the initial increase of the thermally stimulated potential (see curve 3 in Fig. 5.6 and curve 3 in Fig. 5.8). The current inversion in TO and IO modes is caused by a change in the ratio between homocharge and heterocharge at high temperatures (curves 1 and 2 in Fig. 5.8) [45].

It is known that the inversion of the TSD current can be caused by the re-polarization, that is, it arises as a result of the appearance of an additional heterocharge in the field of a homocharge, and the voltage in this case should decrease [173]. However, this was not observed in our case (Fig. 5.6). On the other hand, the initial growth of the electret potential during heating can not be caused by increase of the surface charge density σ , since charges in this case would have to move against the electric field created by these charges, which is impossible. Therefore, the first peak of the TSD current and the increase of the electret potential (Fig. 5.6) are due to the faster disintegration of the heterocharge (polarization) compared with the homocharge. It is possible that in PVDF in the first stage of heating, not all polarization is destroyed, but only its least stable part.

Thus, the long-term conservation of the heterocharge in PVDF films is possible only in the presence of a stabilizing field of a homocharge. We believe that many special properties of PVDF are associated with a successful combination of a large dipole moment of $-\text{CH}_2\text{-CF}_2-$ (2.1 D) [67], which contributes to the formation of a heterocharge, and the high electron affinity of fluorine atoms (3.37 eV), which contributes to the creation of the stable homocharge. Although the electret state in the

PVDF is unstable, the self-balanced relaxation of the homocharge and the heterocharge is slowed down due to the stabilizing effect of the homocharge.

In the theory of electrets [81,83,163], it is assumed that the homocharge and the heterocharge decay by the exponential law with the temperature dependent time constants. Therefore, such expressions should be valid for IO and IS modes

$$i_1(t) = -\frac{s\sigma_o}{\tau_1} \exp\left(-\frac{t}{\tau_1}\right), \quad (5.28)$$

$$i_2(t) = -\frac{P_o}{\tau_2} \exp\left(-\frac{t}{\tau_2}\right), \quad (5.29)$$

$$\tau_1(T) = \frac{\varepsilon_o \varepsilon}{g_o} \exp\left(\frac{Q}{kT}\right), \quad (5.30)$$

$$\tau_2(T) = \tau_o \exp\left(\frac{W}{kT}\right), \quad (5.31)$$

where W is the activation energy of the heterocharge relaxation, τ_1 and τ_2 are the corresponding time constants.

Applying the equations (5.28) - (5.31) to the experimental curve in Fig. 5.7, we calculated the following relaxation parameters for the homocharge and the heterocharge: activation energies ($Q = 0.76$ eV and $W = 0.54$ eV), characteristic frequencies ($f_2 = 1/\tau_o = 7.4$ MHz and $f_1 = (g_o/\varepsilon_o \varepsilon) = 1.7$ GHz, time constants at 20 °C ($\tau_1 = 31000$ s and $\tau_2 = 2800$ s). The results indicate that the homocharge is more stable than the heterocharge.

Thus, we have developed a method for separating the depolarization currents of the homocharge and the heterocharge from the measured TSD current, and revealed the relaxation behavior of the both components. Application of various TSD modifications complemented with isothermal depolarization currents allowed to find the most important parameters of the relaxation processes. The developed method allows us to analyze the relationship between the homocharge and the heterocharge not only in PVDF but also in other polar dielectrics. The introduction of polar groups with the

simultaneous creation of deep traps could contribute to increasing of the residual polarization stability in polar polymer dielectrics. Therefore, if there are appropriate conditions for creating a homocharge, then a high level of the residual polarization can also be provided for a long time.

5.7. Isothermal and thermally stimulated processes in composites

Composite materials based on polymers with impurities of ferroelectric ceramics have a number of significant advantages over conventional ferroelectric ceramics, but the possibilities of using composite materials as active elements of piezoelectric and pyroelectric converters are not fully implemented.

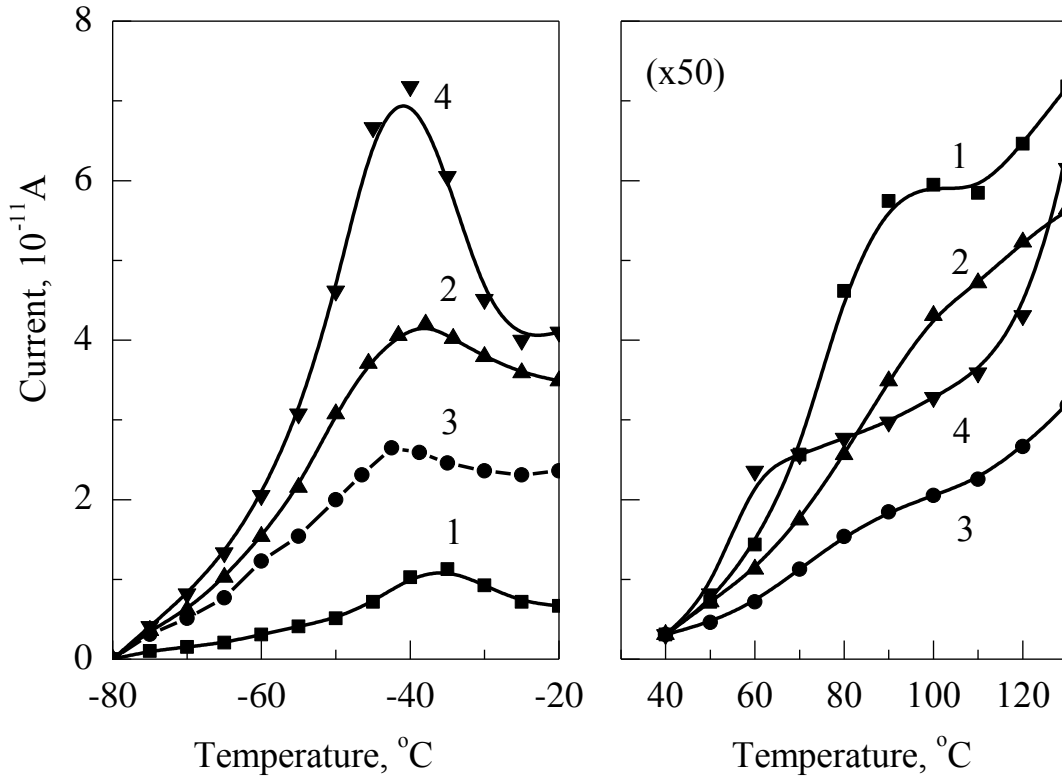


Fig. 5.9. TSD current curves of poled PVDF-BaTiO₃ composites with different content of BaTiO₃: 0% (1), 40% (2), 50% (3) and 70% (4).

It is known that most of the polarization in ferroelectric ceramics immediately switches back to its original state after switching off the applied voltage, and only 25-30% of the domains remain oriented if no special actions are taken [99]. Therefore, the dominant orientation of domains should be somehow fixed. A similar problem exists in

ferroelectric polymers, in which ferroelectric crystallites are distributed in the amorphous phase. This structural similarity between composites and ferroelectric polymers can also determine the similarity of the electrical relaxation processes in these two classes of materials.

We considered the PVDF-BaTiO₃ composite as a model material. The obtained results were compared with PVDF data to verify the applicability of the concepts already proven for the case of the ferroelectric polymers. In addition, concrete data on the parameters of the electrical relaxation in the specified composites were obtained.

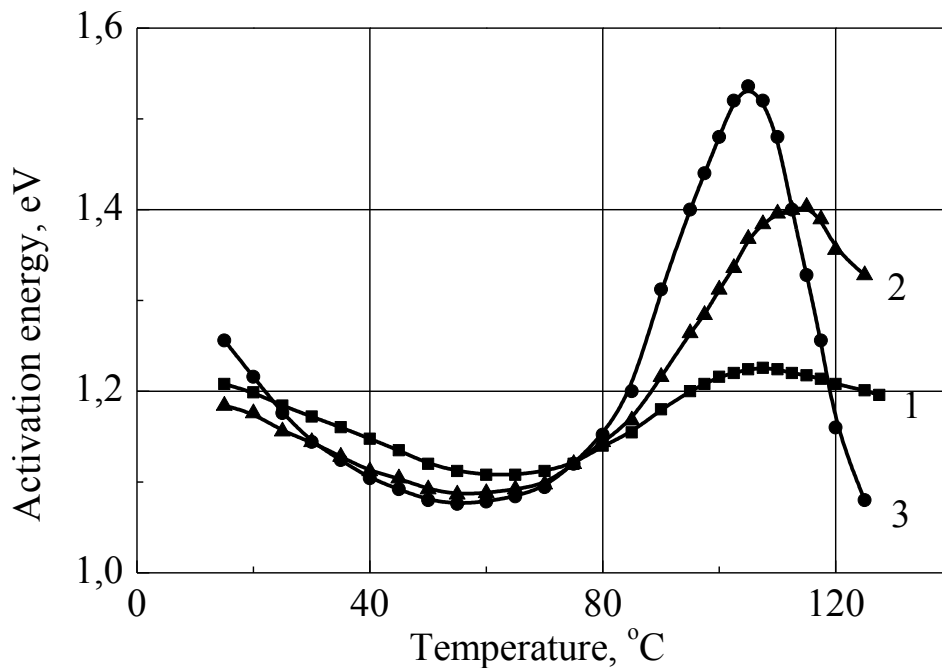


Fig. 5.10. The activation energy of relaxation processes in PVDF-BaTiO₃ composites containing 40% (1), 50% (2) and 70% (3) of BaTiO₃.

Samples of PVDF-BaTiO₃ composites with a thickness of 300 μm containing 0%, 40%, 50% and 70% of BaTiO₃ were obtained by hot pressing of a mixture consisting of PVDF powder and BaTiO₃ particles with an average size of 10 μm. The composites were annealed at 140 °C and examined using a Solomat 91000 spectrometer [55,94] for obtaining a general spectrum of TSD currents in the range from -80 °C to +180 °C (Fig. 5.9).

The samples were prepoled at 150 °C in the electric field of 1.25 MV/m for 15 min, and then cooled to -100 °C without disconnecting the electric field. The samples were then depolarized by heating in a short-circuit mode at the rate of 7 °C/min.

The fractional analysis of relaxation processes was carried out by the method of thermal windows. The polarization temperature increased every time for 5 °C from 20 °C to 150 °C. The equivalent frequency of experiments was about $2 \cdot 10^{-4}$ Hz. From these experiments, the activation energy of the relaxation processes was calculated (Fig. 5.10).

It was found that thermal activation of the polarization process is necessary, since polarization is not formed at room temperature even in high electric fields of about 20 MV/m. This fact is confirmed by the lack of the TSD current after poling of specimens at room temperature. In addition, the VAC at 20 °C was superficial and typical for the space charge limited currents [110], but not *N*-shaped, as in case of PVDF.

In all samples, including PVDF without ceramic additives, well-expressed low-temperature peaks near -40 °C can be seen on TSD curves (Fig. 5.9). This peak is near the glass transition temperature of the amorphous phase in PVDF and is usually attributed to the β -relaxation associated with the micro Brownian motion of molecular chains in amorphous regions. Neither the peak nor its magnitude correlates with the amount of the filler in the composite, which indicates that this peak is associated with the properties of the polymer. The peak in the range 80-120 °C is structurally good only in case of PVDF, but suppressed in composites by an exponentially increasing leakage current of unknown nature. To eliminate the parasitic currents, we periodically included a capacitor in series with the sample [149]. But even in this case, the unambiguous interpretation of the peaks was difficult, because the theory of TSD currents in composites has not yet been developed.

It is assumed that in the thermal windows method each individual peak corresponds to a single Debye relaxation process. Then the peak analysis gives the temperature-dependent relaxation time $\tau(T)$, which can be approximated by the Arrhenius equation

$$\tau(T) = \tau_0 \cdot \exp(Q/kT), \quad (5.32)$$

where τ_0 is the pre-exponential factor; Q is the activation energy; k is Boltzmann's constant.

As can be seen from Fig. 5.10, the activation energy slightly decreases in the range of 20-80 °C from 1.17 eV to 1.09 eV regardless of the samples composition. Then it sharply increases reaching the maximum values of 1.23-1.55 eV at 105-110 °C. The amount of the activation energy correlates with the concentration of the ceramic filler

and equals 1.23 eV at 40%, 1.4 eV at 50% and 1.55 eV at 70% of BaTiO₃ in the composite. In addition, the peak temperature in the Fig. 5.10 is very close to Curie point of BaTiO₃ confirming the fact that relaxation behavior of the composite near this temperature is determined by ceramics.

It was found that the maximum temperature of the thermal window peak was about 15 °C above the polarization temperature for all fractions, regardless of the composition of the sample.

The dielectric constant of the composites increased with temperature and was in a certain ratio with the percentage content of the filler equaling 20-250 at 40%, 30-400 at 50% and 40-1100 at 70% of BaTiO₃ in the composite. It is known that the dielectric constant of pure PVDF was about 10-12, and in BaTiO₃ it was equal to 1500-7000 [99]. The polarization field applied to the composites in the experiments (1.25 MV/m) was higher than the coercive field of pure BaTiO₃ estimated as 0.3 MV/m [99], but it is unclear whether the ferroelectric polarization occurs, because the resistance the polymer matrix is much higher than that of ceramics.

Thus, it was established that the processes of the polarization formation and electrical relaxation in PVDF-BaTiO₃ composites are similar to similar processes in the ferroelectric polymers. This can serve as a prerequisite for the creation of a generalized model that not only explains, but also predicts the electrical behavior of polymer-ceramic composites.

We have established the influence of the polymer matrix conductivity and poling regime on the effective conductivity of the PVDF-PZT composites [55]. The research was carried out on flat plates of PVDF-PZT composite, made by hot pressing of a mixture of PVDF powders and PZT ceramics taken in a volume ratio of 60:40. Two types of the PVDF powder differing in concentration of ionogenic end groups that contribute to dissociation of impurities, and therefore have a specific resistance at room temperature $10^{10} \Omega \cdot \text{m}$ and $10^{12} \Omega \cdot \text{m}$, are used to study the influence of the properties of polymer matrix. Specific resistance of the PZT has an order of $10^{10} \Omega \cdot \text{m}$.

Poling of the samples was carried out by the thermoelectret method. The samples were kept for 50 min at high temperature in the outer field, and then cooled without removal of the field. As changing parameters we used the poling temperature (70-130 °C) and the conductivity of the polymer component.

The problem of the field distribution between phases in a heterogeneous mixture in

case of a double-layer dielectric was considered in [51]. It was assumed that there are different conductivities and dielectric permittivities in the layers. In real ferroelectric polymers the phenomenon of percolation and injection of carriers in volume should be taken into account. From the theory of percolation it is known that for three-dimensional two-phase systems the leakage threshold depending on the structural features of the phases is in the range of 0.05-0.6. In case of conventional ferroelectric polymers with the concentrations of the filler or crystalline ferroelectric phase of the order of 0.4-0.5 it is very likely to find the mixture either in the critical region or in the region where the infinite cluster is formed. Therefore, known formulas for generalized electrical characteristics of mixtures expressed by formulae of Lichteneker, Landauer-Brugemann, Odelevsky and others are unsuitable for ferroelectric polymers and composites because they assume relative proximity of the components properties and the small volume fraction of one of them.

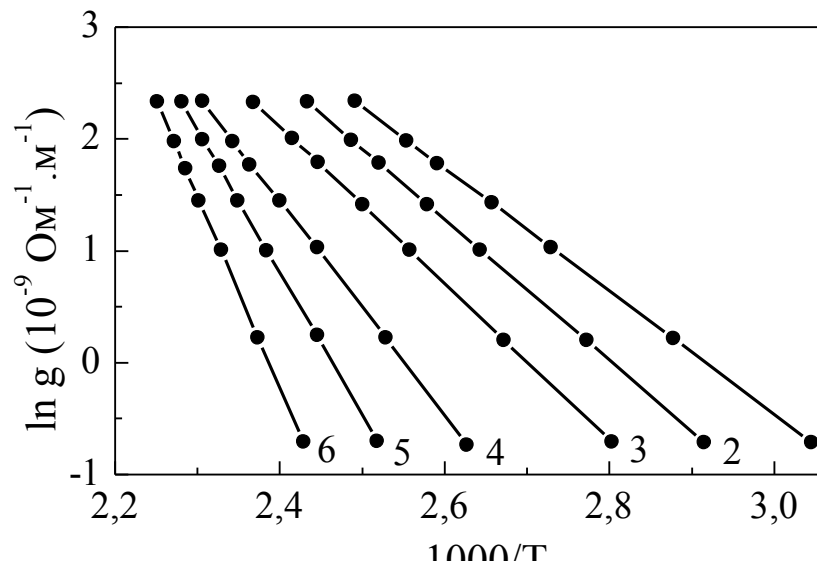


Fig. 5.11. Temperature dependence of the specific conductivity of PVDF-PZT samples poled at 70 °C (1,4), 100 °C (2,5) and 130 °C (3,6). Specific resistance of the polymer is $10^{10} \Omega \cdot m$ (1,2,3) and $10^{12} \Omega \cdot m$ (4,5,6).

It is obvious that in the presence of contacts between particles of crystallites or ceramics, equivalent circuit diagrams should take into account not only sequential combinations of layers, but also parallel ones. Consideration of the injection based on the Poisson equation should lead to the field heterogeneity in the thickness of the sample. The mentioned effects in ferroelectric polymers and composites have not yet

been studied and the theory of these phenomena is absent.

As can be seen from Fig. 5.11, change in the poling temperature affects the temperature dependence of the conductivity. The activation energy increases with increasing temperature both in low-conductive and high-conductive composites, and the value of the conductivity decreases. This corresponds to the proposed hypothesis that explains decrease of the conductivity by trapping a part of the carriers at the boundaries of the polarized crystallites. Indeed, residual polarization increases with increasing temperature and the specific conductivity decreases [55].

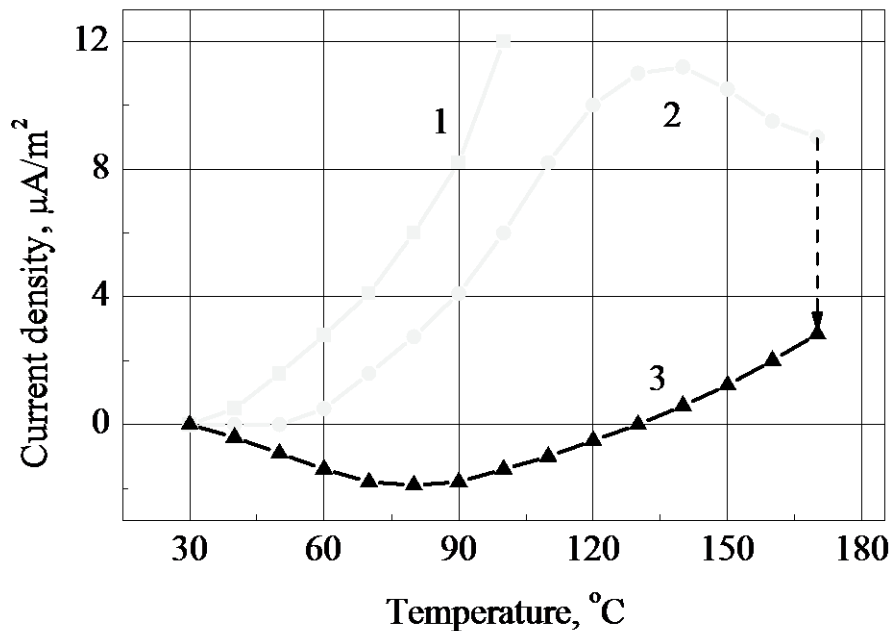


Fig. 5.12. Thermal currents during primary (1) and repeated (2) heating of poled PVDF-PZT composites samples, and also cooling after the reheating (3). The heating rate is 3.5 °C/min. The thickness of the samples is 280 μm. Piezo modulus 8 pC/N.

The degree of the residual polarization and its stability in a ferroelectric ceramic essentially depend on the magnitude of the injected space charge [107] that apparently compensates the depolarizing field occurring when dipoles in crystallites are oriented. Similar processes occur in the ferroelectric polymers. However, in view of the morphological features, the conditions for maintaining the stable polarization in ferroelectric polymers are better than in ferroelectric composites where the incomplete polarization occurs due to boundaries scarcity, mechanical stress and restriction in free volume. Therefore, some of the residual polarization immediately relaxes after removing

the external field. For example, only 53% of 90° reorientations are carried out in PZT, of which 44% remain after the removal of the field [123]. In a ferroelectric polymer, the ferroelectric particles are free that creates favorable conditions for trapping the charge at their borders. Although the particles are in contact with each other, they do not form a rigid grid and easily allow for volume changes during poling. Large-scale potential changes during poling contribute to deep trapping of charges, as well as to reduced molecular mobility in the interphase layer. That is why the piezoactivity of polymer in ferroelectric polymers is higher than that of ceramics used as a filler.

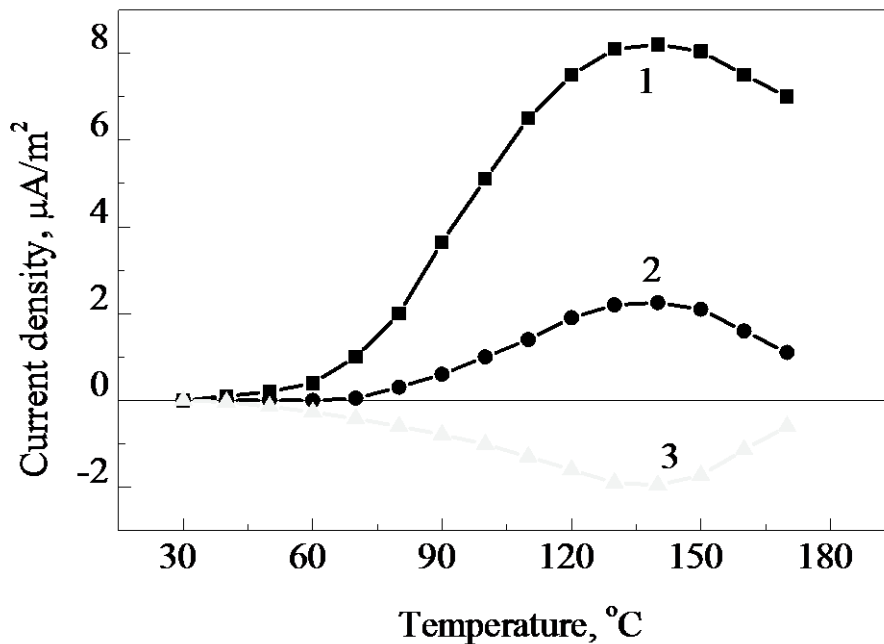


Fig. 5.13. Thermal currents when heated for the first (1) and the third (2) times, and also after cooling after the third heating (3) of PVDF-PZT samples poled by the thermoelectret method. The heating rate is 3.5 °C min. The thickness of the samples is 240 μm, the poling temperature is 100 °C.

In "polymer-ferroceramics" composites as in the ferroelectric polymers, one should not contradict the role of space charge and polarization in the appearance of high pyroactivity, but consider them in a relationship. In the composites like as in PVDF, irreversible relaxation processes and reversible (pyroelectric) are interconnected.

It is known that pyroelectric currents are reversible, that is when switching from heating to cooling they must change the direction to the opposite. However, as can be seen from Fig. 5.12, this is not always observed.

The imbalance of direct and reciprocal current is due to the influence of the

relaxation component, which does not diminish instantaneously to zero with the termination of heating, but it relaxes with the time constant of order of tens and hundreds of seconds [55]. As a result, there is a delay in the pyroelectric current, which is observed in Fig. 5.12.

With repeated heating and cooling of the samples, along with decrease of the current in the forward direction as a result of the relaxation processes annealing, the symmetry of the direct and the reverse current appears for the same reason (Fig. 5.13), which indicates the predominance of the pyroelectric component over the relaxation component.

It is interesting to note that in the polymer-ceramic composite, as in PVDF, the maximum of pyroactivity coincides with the position of the TSD current peak indicating the interrelation of these processes, and possibly also their general nature.

Chapter 6. Pyroelectric effect in ferroelectric polymers

6.1. Nature of the pyroelectricity in ferroelectric polymers

Pyroelectric effect in PVDF films was discovered more than 40 years ago. However, despite the large number of works, the nature of pyroelectricity in PVDF still remains unclear. A series of papers is devoted to the pyroelectric properties of the ferroelectric polymers, the results of which are summarized in reviews of Das-Gupta [25], Kepler and Anderson [102], Fukadu [66], Bauer and Lang [8] and Nalva [132]) that describe the main proposed models of pyroelectricity in PVDF. In the first of the three most popular models assumes that pyroelectricity results from the contribution of electrostriction in 27%, dipole fluctuations 23% and changes in the size 50% with temperature. In the second model, only the change in the dimensions of the sample is considered (47%) and the crystals (53%), while in the third model, 76% of the pyroelectricity is attributed to electrostrictions and 24% to the change in size when temperature changes.

Under the pyroelectric effect, one means the range of phenomena associated with reversible changes in the electric displacement vector (induction) when the temperature changes. In case of a free sample, the pyrocoefficient is determined by the following expression [151]

$$p_i = \left(\frac{\partial D_i}{\partial T} \right)_{H,E} = \left(\frac{\partial D_i}{\partial T} \right)_{U,E} + \left(\frac{\partial D_i}{\partial U_{i,j}} \right) \left(\frac{\partial U_{i,j}}{\partial T} \right)_{H,E}, \quad (6.1)$$

where D_i is the component of the induction vector; $U_{i,j}$ is the deformation tensor; H is the mechanical stress; E is the field strength, $\left(\frac{\partial D_i}{\partial U_{i,j}} \right)$ is the piezo modulus; $\left(\frac{\partial U_{i,j}}{\partial T} \right)$ is the thermal expansion coefficient. The first term in (6.1) corresponds to the primary or true pyroelectric effect measured on the compressed sample, and the second term characterizes the secondary pyroelectric effect being the result of the piezoelectric induction changes due to the thermal expansion.

Since the pyroelectric effect depends both on the internal polarization and on the space charge, in principle, it can be caused by the temperature dependence of both quantities. If we neglect the influence of the space charge, then for the case of a flat short-circuited sample with homogeneous polarization P we obtain

$$p_o = \frac{\partial D}{\partial T} = \frac{\partial P}{\partial T} = \frac{\partial \sigma}{\partial T} = \frac{\partial(q/S)}{\partial T}, \quad (6.2)$$

where q and σ are magnitude and density of the bound surface charge; S is the surface area.

In the experimental conditions, the current $I(T) = \frac{dq}{dt}$ occurring when the temperature change (dT/dt), is measured, and the pyrocoefficient is considered to have the following value

$$p = \frac{1}{S} \frac{dq}{dT} = \frac{1}{S} \frac{I(T)}{dT/dt}. \quad (6.3)$$

Because $p_o \neq p$ there are differences in the values of the theoretically calculated and experimentally measured pyrocoefficients. It has been proved that the pyroelectric effect can only be caused by a nonuniform distribution of the space charge (without taking into account polarization) [94].

Investigating the pyroelectric effect in PVDF, Lines and Glass [123] came to the

conclusion that this is a real pyroelectricity, but not a depolarization effect observed in many polar electrets, because the crystalline phase of PVDF completely corresponds to the definition of a ferroelectric, as a pyroelectric with reversible spontaneous polarization under application of the electric field. A fundamental question was posed that has not been solved for the time being: is the pyroelectricity an equilibrium property of PVDF or a result of non-equilibrium polarization, that is, in some way it is a fixed orientation of dipoles?

In early works on PVDF [131], the effect of volume charge on the pyroelectric effect was considered decisive, but after the proof of the ferroelectric nature of PVDF crystallites, the pyroelectric was more often associated with the spontaneous polarization. So, in the model of Broadhurst and Davies [15] the behavior of rigid dipoles in thin crystalline plates (lamellae) distributed in the amorphous phase is considered. In the model of Wada and Hayakawa [180], the presence of spherical ferroelectric particles scattered in the amorphous phase is assumed. Both models predict the influence of thermal expansion (dimensional effect) on the pyroelectric effect, as well as temperature dependence of the dielectric constant and the spontaneous polarization $P_{sc}(T)$.

At the same time, there is no satisfactory correspondence between calculated and experimental data. Tashiro and others [166] drew attention to the fact that the models of Broadhurst [15,151] and Wada and Hayakawa [180] ignored the contribution of the volume charge to the pyroelectric effect. An attempt to take into account the volume charge leads to a contradiction with the obtained data [151]. Estimated calculation of Lines and Glass [123] showed that the theoretical pyrocoefficient even at 100% orientation of dipoles in PVDF is several times lower than the value measured in the experiment. An attempt to eliminate this contradiction led Kepler and Anderson [102] to the hypothesis of a reversible change in the degree of crystallinity when the sample is heated and cooled, but this assumption has not received an experimental confirmation. Due to the lack of reliable data there is no consensus among scientists about the ratio of primary and secondary pyroelectric effect in the ferroelectric polymers that considering the large spread in the choice of parameter values in the models is estimated from 3:1 [75] to 1:99 [10].

Rollik and others [145] showed that not only the crystalline, but also the amorphous phase contributes the pyroelectricity. Investigating the pyroelectricity in PVDF, Das

Gupta [25] found that there are thermal and electrical components. In another work of the same author [23] it is shown that when a constant displacement is introduced, an additional component of the pyroelectricity associated with the conductivity appears. Takahashi and others [164] reported the effects of electrodes on the pyroelectricity, while Das Gupta [25] has not found the effect of the electrode material. Elling et al [38] found that the pyrocoefficient value is affected not only by the residual polarization, but also by the supramolecular structure on which the mechanical properties of PVDF depend.

In the work of Fedosov and Sergeeva [53] it is shown that one of the components of the pyroelectric effect in the ferroelectric polymers is the electret component, that is, the pyroactivity of PVDF is due to the reversible temperature changes of the residual polarization closely related to those in equilibrium with trapped charges. Fedosov and von Seggern [62,174,177] proved that compensating charges localized on the surface of crystallites are very important in two-component ferroelectric polymers of the PVDF type for obtaining high and stable polarization. With periodic increase and decrease of temperature [53], the pyrocoefficient irreversibly decreases at temperatures much lower than the Curie point indicating the possible effect of charges. It is generally accepted that the pyrocoefficient in PVDF is directly proportional to the value of the residual polarization [67]. However, this relationship is more complicated, because the pyrocoefficient usually increases nonlinearly with increasing temperature, while there is no increase in polarization occurs in this case.

Summarizing the above data we can conclude that the pyroelectricity in PVDF is usually considered in isolation from other processes. However, to understand the nature of this phenomenon, it is of interest to experimentally study the dynamics of its formation and changes simultaneously with other isothermal and thermally simulated processes, such as measurement of volt-ampere characteristics, thermoelectret poling and depolarization.

6.2. Method for measuring the pyroelectric coefficient

The pyroelectric effect is usually investigated in quasi-static or dynamic mode [54]. In the first case, the pyroelectric current is measured during the slow heating of the short-circuited sample, while in the second case, the variable component of the current is

studied during a rapid change of temperature. The main difficulties of the quasi-static method are the separation of the pyroelectric (reversible) component of the thermal shock from the relaxation (irreversible) component in the TSD current.

We measured the pyroelectric dynamic coefficient by the thermal pulse method developed by Collins [21] and used in a number of other papers [9,10,186].

The light pulse of 50 μ s duration was generated using the Metz 45 CT-3 flashlight and was used as a reproduced heat source that penetrates the surface of the poled films. The pyroelectric signal was recorded using a broadband oscilloscope. This method is the dynamic one.

With the help of a highly sensitive pyroelectric sensor it was established that light pulses are characterized by a rather high reproducibility. The average energy scatter in measuring of 200 consecutive pulses was 2.4%. The magnitude of the pyroelectric coefficient was judged by the maximum value of the electric signal, thus the results were obtained in relative units.

Measurement of the pyrocoefficient by a quasi-static method was carried out by linear heating and cooling of polarized samples. Dependence of the pyrocoefficient on temperature was calculated by the following formula

$$p(T) = \frac{I_p(T)}{A\beta_c} \quad (6.4)$$

where $I_p(T)$ is the pyroelectric current measured during cooling, β_c is the cooling rate, which is a derivative of the temperature over time, A is the sample surface area. The heating rate was maintained constant 3 K/min, while the cooling rate depended on time and temperature.

6.3 Pyroelectric activity of PVDF and switching of polarization

Pyroelectric studies of PVDF films have an independent value, since PVDF is widely used in pyroelectric sensors. However, it is interesting to study pyroactivity in conjunction with the residual ferroelectric polarization, because it will allow on one side to clarify the nature of the pyroelectricity in PVDF, and on the other to ensure its stability.

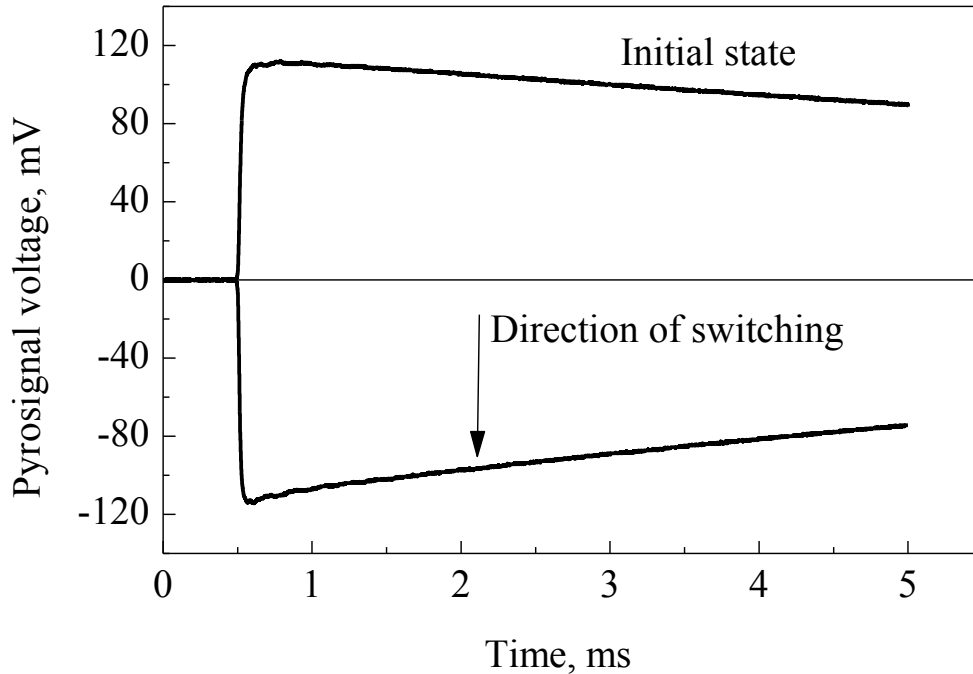


Fig. 6.1. The pyroelectric signal after the polarization switching of PVDF film by applying 2 kV voltage for 50 seconds. Pyroelectricity was measured after 1.5 min after the voltage switching off.

Measurement of the pyroactivity by the Collins method was carried out immediately after the polarization switching. Fig. 6.1 shows how the pyroelectric signal changes when the polarization is fully switched from a fully polarized state. Although the value of the pyrocoefficient can only be judged in relative units, it is evident that the sensitivity of the method is rather high and the signal a completely symmetric after the full switching. In Fig. 6.2 it is shown that full switching occurs only if the voltage pulse duration exceeds 100 s. At a shorter duration of the voltage pulse, there is only a partial switching of polarization judging from the data of Fig. 6.2.

Fig. 6.3 shows the results of four series of experiments, in which the polarization switching was performed at different durations of the voltage pulse, but with the same magnitude in each series. At a voltage of 0.5 kV (Fig. 6.3) that provides a field strength of about 40 MV/m, being in the same order as the coercive field, even with a pulse duration of 50 s, only 6.4% of the polarization is switched, which in principle can be switched, and if the pulse duration is shorter than 50 ms, no switching is practically happening.

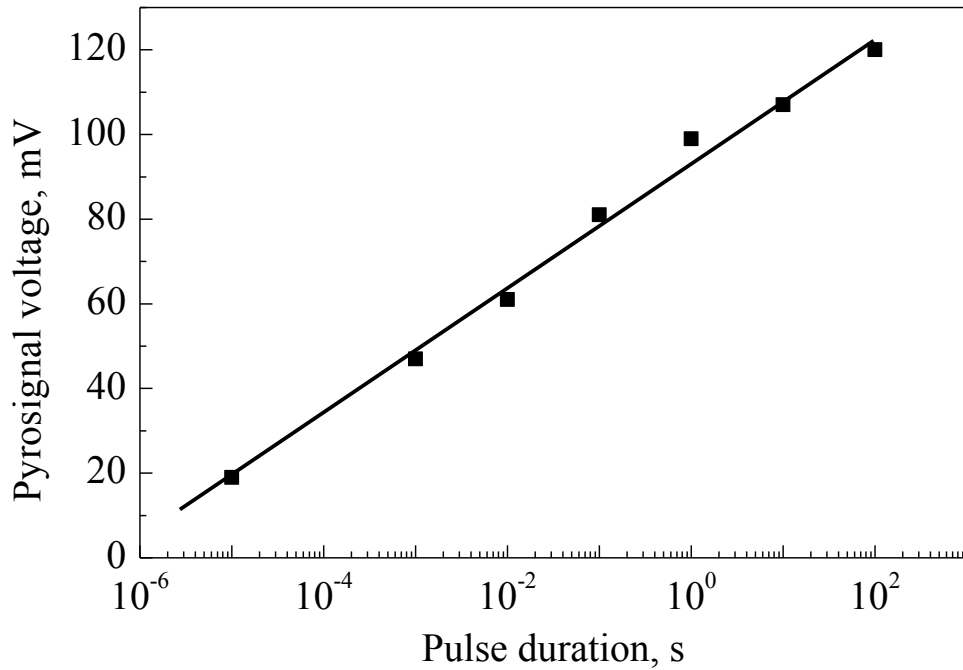


Fig. 6.2. Dependence of the pyroelectric signal on the duration of the polarizing pulse in the range from 10 μ s to 100 s during initial poling of the PVDF film by 2.5 kV voltage.

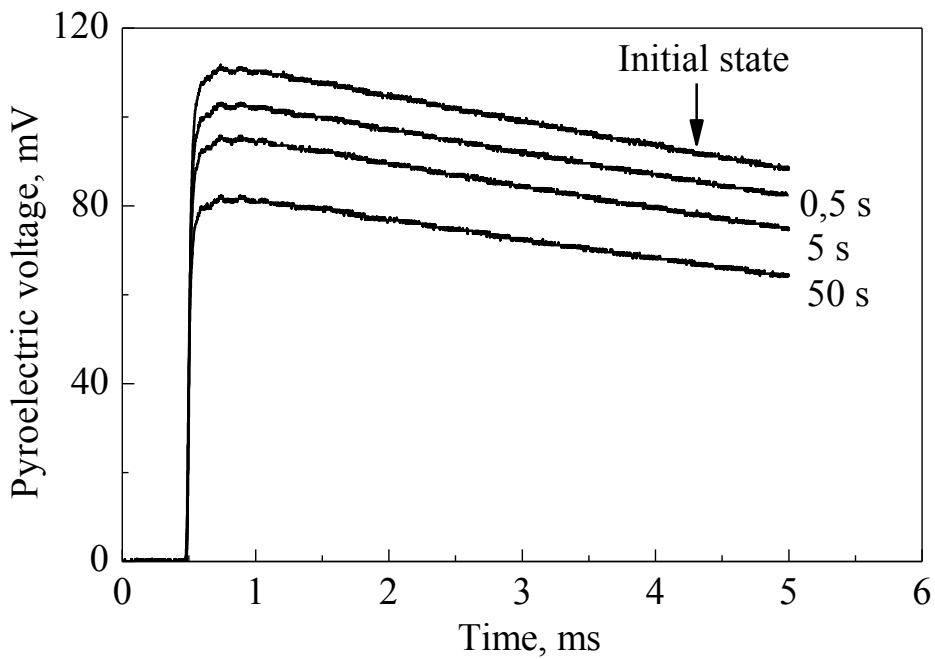


Fig. 6.3. Pyrosignal at sequential polarization switching in PVDF films by pulses of 0.5 kV voltage with duration from 5 ms to 50 s. The duration of the voltage pulse is indicated near the curves.

At a voltage of 1 kV applied for 50 s, 44.4% of the residual polarization is switched, that is, the sample is almost converted to the state with zero mean polarization. At this voltage, the 2.2% polarization is switched even within 50 μ s of the switching voltage application. Increasing the voltage to 1.5 kV leads to the switching of 79.4% of the residual polarization by a 50 s application of voltage. At a voltage of 2 kV for 50 s, the polarization is completely switched [52].

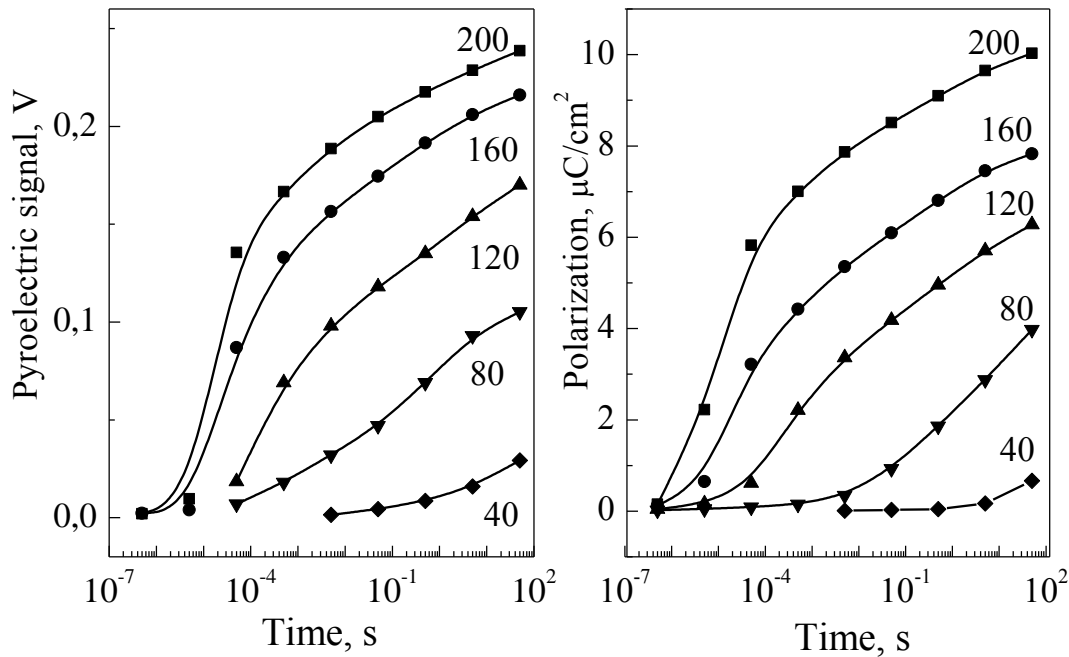


Fig. 6.4. Evolution of pyroelectric activity and stable ferroelectric part of polarization obtained by sequential application of switching voltage pulses with increasing duration from 0.5 μ s to 50 s and at different field strength.

It is interesting to note the specific shape of the pyroelectric signal when switched polarization is more than 50%, that is, when the direction of the average predominant orientation of the dipoles changes to the opposite direction. In the electrode zone, which the thermal pulse passes during $t_o = 0.2$ ms, when the polarity direction changes to the opposite, a non-symmetric in shape pyroelectric signal is formed in relation to the initial one. In the vicinity of the electrode, the direction of the pyro-signal change is maintained during the switching polarization indicating the existence of a near-to-electrode layer of thickness about $x = \sqrt{\lambda t_o}$ where λ is the thermal conductivity of PVDF.

According to the literature data [152], the coefficient of thermal conductivity of

PVDF is $\lambda = 6 \cdot 10^{-8} \text{ m}^2/\text{s}$, thus the thickness of the electrode layer is of the order of $3 \text{ }\mu\text{m}$. We believe that the feature revealed by us is due to the fact that the originally formed polarization in this layer does not switch even in high fields.

It is natural to assume that polarization near the electrode does not increase sharply, but there is some transition layer in which the polarization grows from zero at the electrode to a maximum uniform value in the volume of the film. According to the Poisson equation, inhomogeneous polarization in any layer can be stable only with the presence of a compensating charge in this layer. Apparently, this charge was trapped by deep traps and not released during the polarization switching. The revealed phenomenon is similar to the established by us feature about impossibility of improving the polarization uniformity if its initial formation took place in weak or medium fields.

It was found that polarization switched under the action of several successive short voltage pulses is much smaller than the polarization switched by one pulse of the duration equal to the total time of several short pulses. This indicates that there is some distribution of switching times, i.e. some dipoles are easily switched, while others require more time to be switched. Under the influence of short voltage pulses, only "fast" dipoles are switched, while during the continuous voltage application both "fast" and "slow" dipoles are switched, so the total switched polarization significantly increases.

In conclusion, polarization switching at different time and field strength is compared with the values of the pyrosignal under the same switching conditions (Fig. 6.4). The absolute similarity of the above experimental graphs indicates that there is a direct proportional relationship between the residual ferroelectric polarization and the value of the pyroelectric coefficient. This provision makes it possible to use the technically simple pyrocoefficient measurement to evaluate the polarized state of poled PVDF films, that is, to estimate the magnitude and the direction of the residual polarization.

6.4. Pyroelectric activity of composites based on PVDF

Although the literature has a lot of data on the pyroelectric effect in composites such as PVDF-PZT and PVDF-BaTiO₃, the state of the question about the nature of this

phenomenon can not be considered as satisfactory. It is established that the pyroelectric effect in composites, in contrast to the piezoelectric effect, is "diluted", i.e. the pyrocoefficient of the composite is always smaller than the coefficient in ferroelectric ceramics. The reason is that the temperature changes are caused by external influence and cannot increase in the volume of the composite. If PVDF is used in the composite, then theoretically the overall effect of two ferroelectrics should be weak, since pyroelectric coefficients in ceramics and in PVDF have opposite signs. In the experiment, however, it turned out that the pyroactivity in composites based on PVDF is much higher than in case of using non-polar polymers like polyethylene [135].

The dependence of pyroactivity on the composition of composites has not been studied. It can be assumed that pyrocoefficient increases with increasing concentrations of filler. At the same time, Singh [156] found that the pyrocoefficient maximum in the composites of PVDF-BaTiO₃ corresponds to the concentration of the filler equal to 0.7.

Appearance of a maximum on the $p(E_p)$ dependence may be related to the experiment's technique. For example, if the effective conductivity of the composite in a high field increases due to the Poole-Frenkel effect, so that the resistance of the sample becomes comparable to the internal resistance of the power supply, then because of redistribution of the applied voltage, the sample may be weakly polarized and has a small pyrocoefficient. The same can be said about the extreme dependence of pyroactivity on the temperature of the composite polarization.

Thus, in the field of composites based on PVDF and ferro-ceramics, as well as in pure PVDF, there is no clarity about the nature of the pyroelectric effect; therefore research in this direction should be continued in view of the prospects of these materials practical application.

Conclusion

Important features of formation and relaxation of polarized state in ferroelectric polymers and composites have been experimental revealed that made it possible to formulate the following conclusions:

Application of the developed and applied method of sensing the parameters of relaxation processes by fractional poling in a corona discharge allowed us to reveal the three-stage character of the polarization formation in ferroelectric polymers and to detect

an abnormal increase of the electret potential stability with increase of its value, explained by decrease of the effective conductivity due to the trapping of compensating polarization charge.

It has been shown that a quasi-stationary system consisting of ferroelectric polarization and compensating charges is formed in the process of poling, the mutual influence of which always manifests itself in the significant deceleration of the electrical relaxation processes.

It has been established that for obtaining high and stable residual polarization in polymer ferroelectrics, presence of free charge carriers is required, which compensate the depolarizing field being trapped at the boundaries of the polarized zones, thereby providing the high polarization stability. It was also proved that the spatial polarization inhomogeneity is due to the influence of the volume charge formed as a result of injection and separation of intrinsic carriers in the external field. The effect of the trapped charges is so high that the homogeneous polarization cannot be obtained in films electrified beforehand in weak or medium fields.

It was found that the measurement of the pyroelectric coefficient by the thermal pulse method is a simple and reliable method for sensing the polarized state and its stability in the ferroelectric polymer films. Some abnormal phenomena in ferroelectric polymers, such as increased electret potential stability in highly polarized films, *N*-shaped type of the volt-ampere characteristics, absorption currents and thermoelectret poling curves, were revealed and explained.

The commonality and similarity of electrophysical and polarization processes in ferroelectric polymers and in composites based on PVDF and ferroelectric ceramics was proved to be caused by the two-phase structure of materials and the need to neutralize the depolarizing field by the trapped charges at the interphase boundaries.

Application of the corona triode in most of our studies allowed to make the poling process fully controlled, to optimize the magnitude of the resulting polarization and to perform a virtual short circuiting after the completion of poling. Based on the multifactorial experiment, the best correlations of parameters such as temperature and time of poling, as well as the potentials of the corona electrode and the grid are established. A new technique for studying the relaxation of homocharge and heterocharge processes in the ferroelectric polymers was developed. The technique is developed for separation of the complete electrical displacement components during

PVDF films poling by voltage pulses for allocation and analysis of the polarization components and kinetics of their formation.

When measuring the dynamics of the polarization profile in PVDF by the PPS method, it was established that the polarization heterogeneity formed in the middle fields cannot be eliminated even by applying very high voltage at a later time. At the same time, the homogeneous polarization uniformity is formed during initial poling and polarization switching in high fields.

A detailed analysis of the complete electrical displacement curves allowed to develop and apply a new method for separation of its constituents and the allocation of the polarization components, as well as to measure the effective conductivity of PVDF films, which significantly influences the ferroelectric polarization development.

An experimental study of the polarization switching in PVDF showed that the expected theoretical and actual switching times differ in 10^6 times, which was explained by the influence of slow processes associated with conductivity and charge accumulation at the interphase boundaries. The correctness of the conclusions was evidenced by the higher values of the displaced polarization and its much faster switching in P(VDF-TFE)copolymer, which has a higher crystallinity and almost 100% content of the polar β -phase. From the comparison of the experimental polarization switching curve and the calculated curve, the effective mobility, the characteristic polarization switching time and the activation field strength were found.

The commonality and similarity of electrophysical and polarization processes in ferroelectric polymers and composites have been experimentally proved considering their two-phase structure and the need to neutralize the depolarizing field by trapped charges at the interphase boundaries.

Phenomenological models of the polarized state formation and relaxation processes under different conditions were proposed and calculated taking into account and explaining polarization heterogeneity, nonlinear dependence of polarization on the field and trapping of carriers at the boundaries of polarized regions.

A phenomenological model for the polarized state formation a ferroelectric polymer subjected to constant current poling was developed and analyzed, in which an important role is assigned to injection of charges, which create a heterogeneous distribution of the space charge, the field strength and the residual polarization. Three-stage nature of the poling process of the ferroelectric polymer films is explained. Comparison of

experimental and calculated kinetics of the electret potential showed their high degree of conformity that allowed considering the reasonable assumption about deeply trapped injected charges, on the basis of which the model was constructed.

A model of the polarization switching in PVDF in the mode of the constant applied voltage has been developed that took into account the the following features:

- two-phase structure of the polymer,
- presence of the intrinsic conductivity and injection of charges from the electrodes,
- trapping of charges at the boundaries of polarized crystallites and their release depending on the stage of the process,
- partial recombination of the released charges and their secondary trapping,
- dependence of the polarization switching time on the field strength,
- nonlinear dependence of quasi-stationary polarization in crystallites on the field strength.

A system of differential equations describing the process of the polarization switching was formulated and solved in which the following parameters were used as alternating variables:

- field strength in amorphous and crystalline phases,
- polarization in crystallites,
- effective conductivity and surface charge density at the interphase boundaries.

From comparison of the experimental polarization switching curve with the calculated curve, such parameters as the effective mobility, the characteristic polarization switching time and the activation field are found. Based on the model, the difference between the initial polarization formation in a two-phase polymer ferroelectric and the polarization switching was explained.

A model for explaining polarization profiles in PVDF films in the mode of the constant voltage creating either the middle field close to the coercive field, or the high field substantially exceeding the coercive field was developed and analyzed. The model took into account the monopolar injection of charges from a negative electrode, the nonlinear dependence of the quasi-stationary ferroelectric polarization on the field strength, the Poisson equation on interrelation between charges and the gradient of the field strength. The character of the injected charges front motion was calculated, as well as the time dependence of the field strength in the zone adjacent to the positive electrode. Formation of the inhomogeneous polarization in case of the middle fields was

explained, as well as formation of the deeply trapped charge layer at the boundary of the polarized region. This layer is stable even when the polarization is switched leading to distortion of the polarization uniformity profile and impossibility of its improvement by application of very high fields. It is shown why the uniform residual polarization is formed in case of high applied fields during initial poling.

On the basis of the conducted research, practical recommendations for the modes of ferroelectric polymers and composites poling are developed, which provide high and stable residual polarization.

References

1. Al-Jishi R., Taylor P.L. J. Appl. Phys., **57**, 902 (1985).
2. Arkhipov V.I., Fedosov S.N. *et al.* J. Electrostatics. **22**, 177 (1989).
3. Bae J.-H., Chang S.-H. *Funct. Compos. Struct.* **1** 012003 (2019).
4. Baise A.I., Lee H., Salomon R.E. *Appl. Phys. Lett.* **26**, 428 (1975).
5. Bauer F. *Proc. Int Symp. Electrets.* 647 (1999).
6. Bauer F. *Ferroelectrics.* **115**, 247 (1991).
7. Bauer F. *Ferroelectrics.* **49**, 23 (1983).
8. Bauer S. and Lang S. B. // in *Electrets*, 3rd ed. 252 (1999).
9. Bauer S. *Phys. Rev. B.* **47**, 11049 (1993).
10. Bauer-Gogonea S., Bauer S. *et al.* *Brazilian Journal of Physics*, **29**, 306 (1999).
11. Bihler E., Holdik K., Eisenmenger W. *IEEE Trans. Electr. Insul.* **22**, 207 (1989)
12. Bihler E., Holdik K., Eisenmenger W. *IEEE Trans. Electr. Insul.* **24**, 541 (1989).
13. Bihler E., Neunann G., Eberle G. *et al.* *Annu. Rep. CEIDP.* 140 (1990).
14. Bloss P., Steffen M. *et al.* *IEEE Tr. Diel. El. Insul.* **3**, 182 (1996).
15. Broadhurst M.G., Davies G.T. *Ferroelectrics.* **82**, 177 (1987).
16. Bur A.J. *Annu. Rept. CEIDP., N.Y.* 156 (1992).
17. Burfoot G.C. and Taylor G. W. *Polar dielectrics and their application* (London: The Macmillan Press Ltd).–Ch. 12. (1979).
18. Capellades M.A. *et al.* *Proc. IEEE Intern. Symp. Electr. Insul.,* 554 (1994).
19. Chand S., Mehendru P.S. *J. Phys. D.* **197**, 857 (1986).
20. Chen X., Han X., Shen Q. D. *Adv. Electron. Mater.,* 1600460 18 p (2017)
21. Collins R. E. *J. Appl. Phys.* **51**, 2973 (1980).

22. Dantras E., Ibos L. *et al.* Proc. 12th Int. Symp. Electrets, 329 (2005).
23. Das-Gupta D.K. (ed.) *Ferroelectric polymers and ceramic-polymer composites* – Trans. Publ. 332 p. (2004).
24. Das-Gupta D. K. *Ferroelectrics*. **211**, 165 (2001).
25. Das-Gupta D.K. *Ferroelectrics*. **118**, 165 (1991).
26. Davies G.T., Broadhurst M.G., *et al.* *Ferroelectrics*. **81**, 73 (1987).
27. Davies G.T., McKinney J.E. Broadhurst M.G. *J. Appl. Phys.* **49**, 4998 (1987).
28. Day G.W., Hamilton C.A., Peterson R.L. *Appl. Phys. Lett.* **24**, 456 (1974).
29. De Reggi A.S., Broadhurst M.C. *Ferroelectrics*. **194**, 351 (1997).
30. Eberle G. and Eisenmenger W. *IEEE Trans. Electr. Insul.* **37**, 768 (2002).
31. Eberle G., Schmidt H., Eisenmenger W. // in *Electrets* 3rd ed. 232 (1999).
32. Eisenmenger W., Haardt M. *Sol. State Comm.* **41**, 917 (1982).
33. Eisenmenger W., Haardt M., Holdik K. *IEEE Annual Report CEIDP* 52 (1982).
34. Eisenmenger W., Schmidt H. *Proc. Int. Symp. Electrets*, 635 (1999).
35. Eisenmenger W., Schmidt H., Dehlen B *Brazilian J. of Physics*, **29**, 295 (1999).
36. Eliasson S. *J. Phys. D.: Appl.Phys.***19**, 1965 (1986).
37. Elling B., Danz R. *Proc. Int. Symp. Electrets*. 701 (1999).
38. Elling B., Danz R., Weigel P. *Ferroelectrics*. **56**, 179 (1984).
39. Fan F.R., Tang W. and Wang Z.L *Adv. Mater.* **28**, 4283 (2016).
40. Faria R.M., Gross B. *Proc. 5th Int. Symp. Electrets*. 636 (1995).
41. Faria R.M., Jorge A., Oliveira Jr. O.N. *J. Phys. D: Appl. Phys.* **23**, 2027 (1993).
42. Faria R.M., Neto J.M.G., Oliveira O.N. *J. Phys. D –Appl.Phys.* **27**, 611 (1994).
43. Fatuzzo E. and Merz W.J. *Ferroelectricity*, 240 (1972).
44. Fedosov S.N. *Phys. Stat. Sol (a)*. **115**, 293 (1989).
45. Fedosov S.N., Butenko A.F., Sergeeva A.E. arXiv:0705.0149 6 p. (2007).
46. Fedosov S.N., Sergeeva A.E. *et al.* *J. Phys. D: Appl. Phys.* **29**, 3122 (1996).
47. Fedosov S.N., Sergeeva A.E. *et al.* arXiv:0704.3993 5 p. (2007).
48. Fedosov S.N., Sergeeva A.E. *et al.* *Proc. SPIE Polym. Liquid Crystals*. **4017**, 53 (1999).
49. Fedosov S.N., Sergeeva A E., Marat-Mendes J.N. *Ferroelec.* **294**, 93 (2003).
50. Fedosov S.N., Sergeeva A.E., Zhang H. *Proc. 9th Int. Symp. Electr.* 902 (1996).
51. Fedosov S.N., Sergeeva A.E. *et al.* *Bull. OSU, Phys. & Math.* **8**, 220 (2003).
52. Fedosov S.N., Sergeeva A.E. *et al.* "*Strategiczne Pytania Swiatowej Nauki*",

Przemysl: Nauka i studia. **20**, 28 (2008).

53. Fedosov S.N., Sergeeva A.E. Solid State Physics. **31**, 270 (1989).
54. Fedosov S.N., Sergeeva A.E. *et al.* High-molecular compounds. **41**, 7 (1999).
55. Fedosov S.N., Sergeeva A.E. *et al.* "Comp. Mater. Industry", Yalta, 356 (2007).
56. Fedosov S.N., von Seggern H. J. Appl. Phys. **103**, 014105 (2008).
57. Fedosov S.N. Phys. Stat. Solidi, Ser.A. **114**, 435 (1989).
58. Fedosov S.N. Molec. Cryst. Liquid Cryst. **230**, 61 (1993).
59. Fedosov S.N., Butenko A.F. Proc. 9th Int. Conf. Phys. & Techn. Thin Films, Ivano-Frankivsk. 45 (2007).
60. Fedosov S.N., Butenko A.F. Proc. 2nd Int. Conf. Sensor Electronics and Microsystem Technologies. Odessa: 136 (2006).
61. Fedosov S.N., Sergeeva A.E. J. Electrostatics. **30**, 39 (1993).
62. Fedosov S.N. von Seggern H. J. Appl. Phys. **96**, 2173 (2004).
- 63] Fedosov S.N. *Polarization and space charge in ferroelectric polymers and composites*, DSc Dissertation, Moscow Institute of Steel and Alloys, 416 p. (1989).
64. Fridkin V., Ievlev A., Verkhovskaya K. *et al.* Ferroelectrics. **314**, 37 (2005).
65. Fridkin V.M., Vizdrik G.M., Yudin S.G. Ferroelectrics. **285**, 377 (2003).
66. Fukada E. IEEE Trans. Ultrason. Ferroelec. & Freq. Control. **47**, 1277 (2000).
67. Furukawa T. Phase Trans. Part B. **18**, 143 (1989).
68. Furukawa T. Adv. Colloid Interface Sci. **71**, 183 (1997).
69. Furukawa T. *et al.* Proc. Int. Symp. Electrets, 129 (2005).
70. Furukawa T., Seo N. Jpn. J. Appl. Phys. **29**, 675 (1990).
71. Gaur M. S., Chaturvedi G. C., Singh R. Proc. Int. Symp. Electrets. 374 (2005).
72. Gerhard–Mulhaupt R. IEEE Annual Report CEIDP. 68 (1983).
73. Gerhard–Mulhaupt R. Ferroelectrics. 202, 385 (1997).
74. Gerhard–Mulhaupt R., Gross B., Sessler G.M. // in Electrets, 383 (1988).
75. Gerhard–Mulhaupt R. *et al.* J. Appl. Phys. **55**, 2769 (1984).
76. Gerhard–Mulhaupt R. *et al.* Proc. Int. Symp. Electrets. 404 (2005).
77. Giacometti J. A. and DeReggi A. S. J. Appl. Phys. **74**, 3357 (1993).
78. Giacometti J.A., Fedosov S. and Costa M.M. Braz. J. Phys. **29**, 269 (1999).
79. Giacometti J.A., Campos J.S.C. Rev. Sci. Instr. **70**, 1143 (1999).
80. Goel M. Proc. Int. Symp. Electrets. 435 (2005).
81. Gross B., J. Chem. Phys. **17**, 866 (1949).

82. Gross B., von Seggern H. *et al.* J. Phys. D: Appl. Phys. **18**, 2497 (1986).
83. Gubkin A. N., Electrets, Nauka, Moscow, (1987).
84. Guo Y. *et al.* Jpn. J. Appl. Phys. Part.2, **31**, 1830 (1992).
85. Gusarov B. PhD Thesis, University Grenoble Alpes (2015).
86. Guy I.L., Das Gupta D.K. Polymer International. **27**, 225 (1999).
87. Hahn B., Webdorff J., Yoon D. Y. Macromolecules. **38**, 718 (2005).
88. Hasegawa R., Takahashi Y., Chatani Y. Polym. J. **13**, 600 (1982).
89. Hicks J.S., Jones T.E., Logan J.C. J. Appl. Phys. **49**, 6092 (1978).
90. Hilczer B., Kulek J., Smogor H. Ferroelectrics. **225**, 33 (1999).
91. Hornsby A., Riggs J.H. *et al.* Proc. Int Symp. Electrets. 651 (1999).
92. Huang C. Proc. Int. Symp. Electrets. 396 (2005).
93. Hughes S.T., Piercy A.R. J. Phys. D: Appl. Phys. **30**, 1175 (1997).
94. Ibar J. P. *Fundamentals of thermally stimulated current and relaxation map analysis*. LSP Press, Hew Canaan., 402 p. (2003).
95. Ibos L., Bernès A., Lacabanne C. Ferroelectrics. **320**, 15 (2005).
96. Ibos L., Bernès A., *et al.* Ferroelectrics. **238**, 163 (2000).
97. Ieda M., Mizutani T., Nagata T. Annu. Rept.CEIDP. 162 (1994).
98. Ieda M., Mizutani T., Nagata T. Annu. Rept. CEIDP. 399 (1994).
99. Jaffe B., *et al.* *Piezoelectric ceramics*, Academic Press, 317 p (1971).
100. Karasawa N., Goddard W. A., Macromolecules. **28**, 6765 (1995).
101. Kaura T., Narh R., Perlman M.M. J. Phys. D: Appl. Phys. **24**, 1848 (1991).
102. Kepler R.G., Anderson R.A. Adv. Phys. **41**, 57 (1992).
103. Kochervinskii V.V. Polymer Sci. B. **47**, 75 (2005).
104. Koga K., Ohigashi H.J. Appl. Phys. **59**, 2142 (1986).
105. Koizumi N. Key Eng. Mater. **92**, 161 (1994).
106. Kulek J. and Hilczer B. Ferroelectrics. **184**, 131 (1996).
107. Kurts S.R., Hughes R.C. J. Appl. Phys. **54**, 229 (1992).
108. Kussner B. *et al.* Proc. 8th Int. Symp. Electrets, 594 (1994).
109. Kussner B., Eberle G., Eisenmenger W., Fedosov S.N., Sergeeva A.E. J. Mater. Sci. Lett. **16**, 368 (1997).
110. Kwan C.K. *Dielectric Phenomena in Solids with Emphasis on Physical Concepts of Electronic Processes*. Academic Press, 579 p. (2004)
111. Lacabanne C., Chatain D. *et al.* J. Non-Cryst. Solids, **172**, 884 (1994).

112. Lampert M.A. and Mark P. *Current Injection in Solids*. Academic Press, New York, 354 p. (1970).
113. Lando J.B. and Doll W.W. *J. Macromol. Sci. Phys.* **B2**, 205 (1968).
114. Lang S.B. and Das-Gupta D.K. *J. Appl. Phys.* **59**, 2151 (1986).
115. Lang S.B., Muensit S. *Appl. Phys. A: Mater. Sci. & Proces.* **85**, 125 (2006).
116. Lang S.B. *Ferroelectric Rev.* **2**, 217 (2000).
117. Lang S.B. *Ferroelectrics.* **258**, 297 (2001).
118. Leal Ferreira G.F. and Gerhard-Multhaupt R. *Phys. Rev. B* **42**, 7317 (1990).
119. Leal Ferreira G.F. et al. *J. Phys. D: Appl. Phys.* **29**, 3117 (1996).
120. Leal Ferreira G.L., Figueiredo M.T. *IEEE Trans. Electr. Insul.* **27**, 719 (1992).
121. Legrand J.F. *IEEE Trans. Electr. Insul.* **28**, 336 (1993).
122. Lewis E.L.V., Ward J.M. *J. Polym. Sci. B.* **27**, 1375 (1989).
123. Lines M.E., Glass A.M. *Principles and Applications of Ferroelectrics and Related Materials*, Oxford University Press, Oxford, 680 p. (2001).
124. Lovinger A.J. in *Applied Science Publications*, D. C. Bassett (ed.), 195 (2002).
125. Lovinger A.J., Davis D.D., Cais R.E. *Macromolecules.* **21**, 78 (1988).
126. Lovinger A.J. *et al. J. Appl. Phys.* **56**, 2412 (1984).
127. Marcus M.A. *J. Appl. Phys.* **52**, 6273 (1981).
128. Mizutani T., Ieda M. *IEEE Trans. Electr. Insul.* **21**, 833 (1986).
129. Mopsik F.J., De Reggi A.S. *Appl. Phys. Lett.* **44**, 65 (1984).
130. Moreno R.A. and Gross B. *J. Appl. Phys.* **47**, 3397 (1976).
131. Murayama N., Hashizume H. *J. Polim. Sci.* **14**, 989 (1986).
132. Nalwa H.S. *Ferroelectric Polymers: CRC Press*, 912 p. (1995).
133. Neagu E.R. *et al. J. Phys. D: Appl. Phys.* **35**, 1229 (2002).
134. Neumann G., Bihler E. *et al. Annual Meeting of CEIDP*, 96 (1998).
135. Ng K.L. *et al. IEEE Trans. Ultras. Ferroelec. & Freq. Contr.* **47**, 1308 (2000).
136. Nunes-Pereira J. *et al. Composites B* **72** 130 (2015).
137. Ohigashi H. *Proc. Int. Symp. Electrets.* 615 (1999).
138. Pépin M.P., Wintle H.J. *J. Appl. Phys.* **83**, 5870 (1998).
139. Phelan R.J., Peterson R.L. *et al. Ferroelectrics.* **7**, 375 (1974).
140. Ploss B., Bianzano O. *Proc. 8th Intern. Symp. Electrets.* 211 (1994).
141. Ploss B., Domig A. *Ferroelectrics.* **159**, 263. (1994).
142. Qian X., Wu S. *et al. Polymers and Soft Matter* **5**, 115 (2015).

143. Regado M P., Dirani E.A.T. *et al.* Proc. Int. Symp. Electrets. 441 (2005).
144. Roh Y., et al. IEEE Trans. Ultrason. Ferroel. & Freq. Contr. **49**, 836 (2002).
145. Rollik D., Bauer S., Gerhard-Multhaupt R. J. Appl. Phys. **85**, 3282 (1999).
146. Rollik D., Kunstler W. *et al.* Proc. 10th Int. Symp. Electrets, 51 (1999).
147. Sazhin B.I. et al. Electrical properties of polymers. L.: Chem., 224 p. (1986).
148. Sergeeva A.E., Fedosov S.N. *et al.* Sens. Elect. & Microsyst. Techn. **3**, 4 (2005).
149. Sergeeva A.E., Fedosov S.N. *et al.* "Phys. & technol. thin films", **1**, 382 (2005).
150. Sergeeva A.E. *Formation and relaxation of space charge and polarization in the ferroelectric polymers*, DSc Dissertation, Odessa State University, 438 p. (1995).
151. Sessler G.M. (ed.). *Electrets* – v.1, 3rd ed., Morgan Hill: 437 p. (1999).
152. Sessler G.M., Das-Gupta D.K. *et al.* IEEE Trans. Electr. Insul. **27**, 872 (1992).
153. Sessler G.M., Berraissoul A. Ferroelectrics. **206**, 489 (1997).
154. Sessler G.M., Das-Gupta D.K. *et al.* IEEE Trans. Electr. Insul. **27**, 872 (1992).
- 155-173. Shilling D., Dransfeld K. *et al.* J. Appl. Phys. **65**, 269 (1989).
156. Singh R. et al. Proc. 12th IEEE Intern. Symp. Appl. Ferroelectr. 504 (2004).
157. Sinha D. Proc. 2nd Int. Conf. Conduct. and Breakdown Solids, 227 (2003).
158. Smiths J.G., IEEE Trans.Sonics Ultrason.**23**, 393 (1976).
159. Southgate P.D. Appl. Phys. Lett. **28**, 250 (1976).
160. Sussner H. and Dransfeld K. J. Polym. Sci. Phys. **16**, 529 (1978).
161. Sussner H. Proc. IEEE Ultrasonics Symp. 491 (1989).
162. Sussner H., Dransfeld K. J. Polym. Sci.: Polym. Phys. **26**, 529 (1988).
163. Swann W.F.G. J. Franklin Inst. **255**, 513 (1953).
164. Takahashi Y. Jpn J. Appl. Phys. Part I. **33**, 202 (1994).
165. Tasaka S. and Miyata S. J. Appl. Phys. **57**, 906 (1985).
166. Tashiro K., Todakoro H., Kobayashi M. Ferroelectrics. **152**, 167 (1991).
167. Teyssedre G. and Lacabanne C. Ferroelectrics. **171**, 125 (1995).
168. Teyssedre G., Bernès A., Lacabanne C. Ferroelectrics. **160**, 67 (1994).
169. Teyssedre G., Bernes A., Lacabanne C. J. Polym. Sci. B. **31**, 2027 (1995).
170. Teyssedre G., et al. Proc. 8th Int. Symp. Electrets. 650 (1994).
171. Teyssedre G., Lacabanne C. Polymer. **36**, 3641 (1998).
172. Thakur V.K., Gupta R.K. Chem. Rev. 11674260 (2016).
173. Turnhout van J. *TSD of polymer electrets*. Elsevier, 327 p. (1995).
174. von Seggern H. and Fedosov S. IEEE Trans. Diel. Elect. Insul. **11**, 232 (2004).

175. von Seggern H. and Fedosov S.N. Appl. Physics Letters, **91**, 62914 (2007).
176. von Seggern H. and Wang T.T. Annual Report CEIDP, 431 (1994).
177. von Seggern H. Fedosov S.N. Appl. Phys. Lett. **81**, 2830 (2002).
178. von Seggern H., Fedosov S.N. IEEE Trans. Diel. Electr. Insul. **7**, 543 (2000).
179. von Seggern H., Gross B., Berkley D.A. Appl. Phys. A. **44**, 163 (1994).
180. Wada Y., Hayakawa R. Ferroelectrics. **32**, 115 (1981).
181. Wang H., Zhang Q.M. *et al.* J. Appl. Phys. **74**, 3394 (1993).
182. Wang T.T., Sondhi M.M., von Seggern H. J. Appl. Phys. **62**, 4514 (1987).
183. Wang C, Jun L. and Zonghan W. Proc. Int. Symp. Electrets. 448 (2005).
184. Wisniewski C. *et al.* J. Phys. D: Appl. Phys. **33**, 2483 (2000).
185. Womes M. *et al.* IEEE Trans. Elec. Insul. **24**, 461 (1989).
186. Zhang G.J., Yoshida J., Sugita T. J. Appl. Phys. **88**, 1230 (2000).
187. Zhang R. and Taylor P.L. J. Appl. Phys. **73**, 1395 (1993).
188. Zhu G., D, Xu J., Yan X.J. *et al.* Thin Solid Films. **510**, 181 (2006).